INTEGRAL-OPERATOR ANALYSIS FOR SCATTERING AND COUPLING IN OPEN-BOUNDARY DIELECTRIC WAVEGUIDES

By

Shuhui Victor Hsu

A DISSERTATION

Submitted to
Michigan State University
in partial fulfillment of the requirements
for the degree of

DOCTOR OF PHILOSOPHY

Department of Electrical Engineering and Systems Science

1984

ABSTRACT

INTEGRAL-OPERATOR ANALYSIS FOR SCATTERING AND COUPLING IN OPEN-BOUNDARY DIELECTRIC WAVEGUIDES

By

Shuhui Victor Hsu

Integral-operator analysis is employed to study two classes of commonly encountered problems in open-boundary dielectric waveguides. They are the scattering by obstacles along the waveguide and the coupling between waveguides in a multi-guide system. First, in the scattering treatment, an equivalent polarization current is identified from the contrast of refractive indices between the discontinuity region and the unperturbed background. Exploitation of this current establishes an electric-field integral equation (EFIE) describing the unknown discontinuity field, which, leads to the formulation of scattering coefficients. Various solutions to the EFIE are discussed, including the Fourier transform method, Method of Moments, and iterative sloutions etc. In the treatment of waveguide coupling, a similar procedure yields a system of simultaneous EFIEs describing the coupled system-mode field for each waveguide. Subsequent coupled-mode perturbation approximation yields

modal amplitude coefficients and the coupling coefficients. Applications of the above analysis and solutions are demonstrated via one-dimensional slab waveguides. Merits of various solution approaches are evaluated. Moreover, the correctness of the obtained results are verified; this consequently confirms that the integral-operator analysis provides an alternative to the conventional boundary-value analysis.

... dedicated to

my father, Chin-lin Hsu

my mother, Su-ying Kuo

and my wife, Sufen Susan Hsu
for her patience and years of
tolerance.

ACKNOWLEDGEMENT

The author wishes to gratefully acknowledge several persons, without whom this dissertation could not have been completed. My achievements, great or little, were possible through their participation.

My father taught me a Chinese proverb: "When you drink water, think of its source." Dr. K. M. Chen, a member of my guidance committee, has been fundamental in my achieving the Ph. D. degree at Michigan State. He was instrumental in first bringing me to this university and he has provided many years of caring friendship. I want to give him my special thanks.

Dr. Dennis P. Nyquist has been my academic advisor and the chairman of my guidance committee. He inspired and motivated me through many years of graduate studies, especially in the formulation and development of my research subject. He was extraordinarily patient and persistent in his neverending encouragements. His very positive influence on my personal and technical development will carry forward into my future endeavors. I am forever grateful to him.

Dr. Bong Ho served on my guidance committee and provided valuable assistance in many ways beyond the academic realm. I thank him and the other members of my

committee, Dr. Jes Asmussen and Dr. Byron Drachman. Moreover, I am appreciative of the support and kind assistance received from Dr. John Kreer, Chairman of the Electrical Engineering and Systems Science Department, and from the Department staff: Enid Maithand, Pauline Van Dyke, and Ginny Mrazek. Special thanks go to Dr. S. Mao for his friendship and encouragement, to Joanne Weiss and her family for being my first hosts in the United States, and to Jane Chen and her husband Peter for her typing of the manuscript and their kind hospitality.

These generous people and many others like them whom I haven't mentioned have given very much to me. Being from another part of the world, I can truly recognize that it is they who make this University and this country so great. In meeting the many challenges of the past few years, their help was essential to me. I gratefully thank every one of them.

TABLE OF CONTENTS

LIST OF TABLES

LIST OF FIGURES

Figure(cont'd) Page

CHAPTER I

INTRODUCTION

Open-boundary dielectric waveguides, as opposed to the conventional closed-boundary metallic waveguides, are dielectric structures capable of guiding propagating discrete TE, TM or hybrid modes and radiation modes having a continuous eigenspectrum. In its most elementary form, it consists of a dielectric guiding core which provides a positive contrast of refractive index relative to that of the surrounding medium (cladding) within which the core is immersed. Confined electromagnetic (EM) fields possess the usual complex-exponential propagation dependence along the waveguiding axis, but are characterized by a real exponential decay along the direction normal to and away from the guiding structure. Field confinment in the core is essentially a consequence of the phenomenon of total internal reflection at the core-cladding interface. Such structures therefore also geneally known as "surface waveguides".

Interest in EM propagation along open-boundary dielectric stuctures has existed since the early part of this century [1] and has progressed with a varying degree of intensity from that time [2]. Recent development and

applications of semiconductor lasers in the communication area has stimulated widespread interest in certain classes of dielectric waveguide for guiding light waves, e.g., the "optical fiber" [3]. Together with the expansion of activities from the microwave spectrum into the millimeter wavelength region in the past decade these studies have culminated in a large store of information characterizing such surface waveguides as transmission and circuit system. Yet, according to Kogelnik [4], integrated optics though intriguing, remains in its infancy at the research stage; a similar review for the dielectric waveguide microwave integrated circuits was given by Knox [5].

Taylor and Yariv [6] point out in their review paper that virtually all integrated-optics decvices, i.e., couplers, modulators, switches and filters, depend critically for their operation upon the characteristics of low order surface-wave eigenmodes supported by isolated or coupled systems of integrated dielectric waveguides. Among the class of uniformly-clad, isolated waveguides, exact solutions exist [7,8] only for planar-slab structures or fibers having circular or elliptical cross-section shape, while the only coupled system which permits an exact solution is composed of parallel slabs. Since boundary conditions at the core/surround interface are inseparable for more general core geometries, conventional differential-operator based methods [9,10,11] become ineffective for such guides. They have, however, provided approximate

solutions to these problems as demonstrated by Marcatile [12] and Goell [13]. The integral-operator description [14-16], related to Katsenelenbaum's [17] polarization integral equation, for uniformly-clad, open-boundary dielectric waveguides, provides a conceptually-exact formulation for propagation modes supported by the waveguiding system having any number of graded-index cores with arbitrary cross-section shape.

This dissertation, consisting of two parts, describes the integral equation formulation as an alternative to the conventional boundary-value analyses in the areas of surface wave research where knowledge of basic phenomena and accurate solutions remain relatively incomplete. This research includes the scattering of surface waves by obstacles along the cladded dielectric waveguide [18,19] in Part I, and the modal coupling phenomena in a multi-waveguide system [15] in Part II.

The most comprehensive available treatments for discontinuities along open dielectric waveguides are those by Marcuse [20] which deal with the abrupt junction between two dissimilar guides and the interaction of surface waves with small, distributed surface irregularities. Among all discontinuities which have been studied, approximate analyses [20-23] of the abrupt junction between dissimiliar (primarily planar slab) waveguide sections have predominated. Rigorous treatments [24,25] of output coupling from a planar, solid state hetero-junction laser

have been advanced, as well as a Green's function approach to scattering from periodic discontinuities in a planar DFB laser [26]. The only rigorous analysis for ensembles of step discontinuities along planar-slab waveguides is evidently Rozzi's [27,28] investigation based on a two-dimensional integral-equation formulation for the fields in transverse discontinuity planes. Vassalo [29] has provided a large-scale, scattering-coefficient, circuit formulation for discontinuities along open waveguides. Mode conversion as a result of scattering was investigated by Lewin [24] for a heterojunction laser.

Surface-wave-mode coupling between adjacent, uniformly-clad dielectric waveguides has been studied by a number of investigators [31-33]. The most complete study of coupled mode theory was given by Miller [34] for conducting waveguides and, for integrated configurations, Marcatili's [12] approximate analysis of coupling between rectangular waveguides remains the primary work. Most conventional differential-operator based treatments [31,35,36] are approximate in nature. Their application is limited to weakly guided or degenerately coupled systems where accurate solutions are possible. To obtain more accurate results for non-degenerate coupling, Kuester and Chang [33] presented a variational approach [38], assuming that coupled guides are well separated. The only exact treatment was given by Jones [39] for coupling of parallel fibers. There, a surface dyadic Green's function including contributions by the

continuous spectrum was considered. However, subsequent treatment was based upon a set of coupled differential equations converted from integral equations initially formulated for the transverse cross-sectional plane of a coupled waveguide configuration.

In Chapter II of Part I, the discussion on scattering of surface waves along dielectric waveguides begins with the recognition of index contrast between the discontinuity region (or obstacle) and the waveguiding region. This leads to the identification of equivalent induced polarization current in the discontinuity region. The fundamental electric-field integral equation (EFIE) for the unknown electric field in the discontinuity region is developed in terms of the electric dyadic Green's function. The nature of the imbedded source point singularity in this EFIE is pointed out as well as the effects of the depolarizing dyad which results from the associated principal-value integration. Scattering coefficients (both reflection and transmissions) are subsequently formulated in terms of the solution for that unknown discontinuity field. Mode conversion from an incident principal mode to higher propagation modes in the scattering process are discussed. Applications of the above EFIE are presented in Chapter III with specialization to a slice gap discontinuity along a one-dimensional slab waveguide. Several solution technigues are discussed, including: i) approximate closed-form radiationless solution, ii) approximate solution including

the radiation contribution, iii) Moment-Method numerical solution and iv) iterative solution in the spatial domain.

Part II discusses the coupling between multiple dielectric waveguide systems. In Chapter IV, following the identification of an equivalent polarization current which arises due to the index contrast between the guiding core and its surround cladding, the formulation of an integral-operator description for a single dielectric waveguide is first presented. This EFIE is subsequently generalized to describe the EM field supported by a coupled system of N waveguides. These EFIEs are subsequently specialized to describe the natural, guided, axially-propagating, coupled surface-wave modes supported by the systems. A perturbation analysis based upon the isolated guide's modal field, and the EFIE which it satisfies, is developed and subsequently applied to a system of two coupled waveguides. The system mode propagation constant, which depends upon the degree of coupled-guide interaction, is obtained for a weakly coupled system. Furthermore, this conceptually-exact formulation with perturbation approximation is shown to recover the results of the standard differential-operator based coupled mode theory. Application of this integral-operator-based coupled mode theory is demonstrated in Chapter V. When a coupled slab-waveguide system is considered, Fourier transform solution to the coupled EFIE's are shown to recover the well known characteristic equation for a two guide system. This confirms the correctness of

the integral-operator approach. Numerical calculations for phase constant shift $\Delta\beta$, due to coupling, are studied using the perturbation approximation for two coupled slab waveguides, both degenerate and non-degenerate cases. Results are compared with the exact solutions obtained by other researchers.

CHAPTER II

INTEGRAL-EQUATION FORMULATION FOR SCATTERING BY DIELECTRIC DISCONTINUITIES ALONG OPEN-BOUNDARY WAVEGUIDE

In practice, a surface waveguide is only the interconnecting component of a complex network which consists of both active and passive wave processing devices such as modulator, amplifier, and directional coupler etc. It is therefore commonplace to encounter some kind of discontinuities at these device interfaces in addition to any imperfections which arise from wall irregularities, inadverdent bends, etc. of the guide sturcture itself. And, when a surface wave is incident upon these discontinuities, it is subsequently scattered, i.e., reflected, transmitted and radiated.

There have been several treatments on the subject of the scattering of surface-wave modes in a dielectric waveguide by obstacles such as step discontinuity [21,28], or the losses due to waveguide tapers and random wall perturbations [44]. Most of the approaches are either variation method or mode matching technique. This chapter presents an analytical formulation [18,19] to calculate the amplitude of scattered waves through the application of a polarization integral equation [45,46]. Such that, the

advantage of digital computation could then be utilized for any arbitrarily-shaped discontinuity as often the case of pratical concern.

Consider an arbitrarily-shaped discontinuity region V_d of permittivity $\varepsilon(\bar{r})$ along an open-boundary dielectric waveguide of permittivity ε_g imbedded in a surrounding cladding medium of permittivity ε_c (Figure 2.1). We can immediately identify a contrast of permittivity between the discontinuity region and the unperturbed waveguide system. This contrast gives rise to an equivalent polarization current, which in turn maintains the scattered field. An integral equation is formulated for the unknown electric field, which is proportional to the equivalent polarization current within the discontinuity region. By solving for this unknown field, the amplitudes of the reflected, transmitted and radiated fields are readily calculated. Also to be discussed in this chapter is the conversion of modal fields due to scattering by the discontinuity in a dielectric waveguide capable of supporting multi-mode propagation.

2.1 Equivalent Current Description for the Discontinuity Region

Referring to Figure 2.1, let $\varepsilon_u(\bar{\rho})$ be the permittivity profile of the unperturbed, axially-uniform ($\bar{\rho} = \hat{x}x + \hat{z}z$ = 2-d position vector) dielectric waveguide with the following decomposition

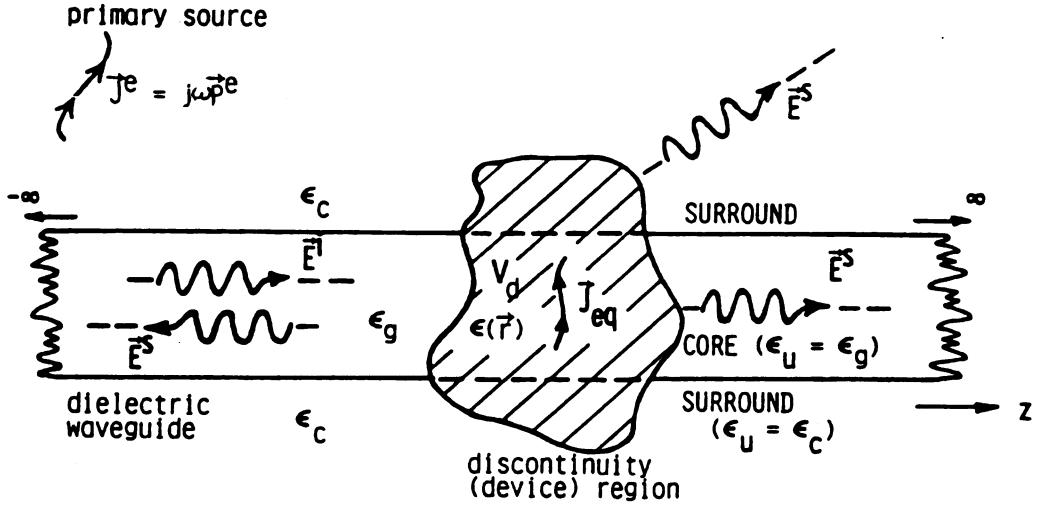

Figure 2.1 Scattering (reflection and radiation) of an incident surface-wave mode by a heterogeneous device-discontinuity region along an open-boundary dielectric waveguide of arbitrary cross-section shape.

$$\varepsilon_u(\bar{\rho}) = \begin{cases} \varepsilon_g(\bar{\rho}), & \text{at points in the graded-index waveguide core} \\ \varepsilon_c(\bar{\rho}), & \text{at points in the surround.} \end{cases}$$

Note that in general the surround need not be homogeneous; in the case of integrated-optics system, it could be a layered dielectric system with substrate covered by film and overlay dielectric regions. The discontinuity region V_d has a complex permittivity of $\varepsilon(\bar{r})$, where $\varepsilon(\bar{r})$ differs from $\varepsilon_g(\bar{\rho})$. Incident wave $\bar{E}^i$ induces an equivalent polarization distribution in V_d, and the latter polarization excites the scattered field $\bar{E}^s$. It is the sum of the impressed field $\bar{E}^i$, due to remote sources with the discontinuity absent, and $\bar{E}^s$, the scattered field excited by the discontinuity, results in the total field $\bar{E}$ anywhere inside the discontinuity region as

$$\bar{E}(\bar{r}) - \bar{E}^s(\bar{r}) = \bar{E}^i(\bar{r}) \tag{2.1.1}$$

We can identify the equivalent polarization current from the Amphere's Law of the Maxwell equations by adding and substracting to it the displacement current of the unperturbed waveguide $j\omega\varepsilon_u(\bar{\rho})\bar{E}$ (harmonic time dependence $e^{j\omega t}$ implied but suppressed throughout) to obtain

$$\nabla\times\bar{H}(\bar{r}) = \bar{J}^e(\bar{r}) + j\omega\left[\varepsilon(\bar{r}) - \varepsilon_u(\bar{\rho})\ \bar{E}(\bar{r})\right] + j\omega\varepsilon_u(\bar{\rho})\bar{E}(\bar{r})$$

$$= \bar{J}^e(\bar{r}) + \bar{J}_{eq}(\bar{r}) + j\omega\varepsilon_u(\bar{\rho})\bar{E}(\bar{r})$$

$$= \bar{J}_t(\bar{r}) + j\omega\varepsilon_u(\bar{\rho})\bar{E}(\bar{r}) \qquad (2.1.2)$$

where

$\bar{J}^e$ = impressed electric current which maintains impressed incident field $\bar{E}^i$,

$$\bar{J}_{eq} = j\omega\bar{P}_{eq} \qquad (2.1.3)$$

= equivalent induced polarization current which describes discontinuity region V_d and maintains scattered field $\bar{E}^s$, with

$$\bar{P}_{eq} = \left[\varepsilon(\bar{r}) - \varepsilon_u(\bar{r})\right]\bar{E}(\bar{r})$$

$$= \varepsilon_0\left[n^2(\bar{r}) - n_u^2(\bar{r})\right]\bar{E}(\bar{r})$$

$$= \varepsilon_0\delta n^2(\bar{r})\bar{E}(\bar{r}) \qquad (2.1.4)$$

= a polarization density in terms of the contrast of refractive index $\delta n^2(\bar{r})$, and

$$\bar{J}_t = \bar{J}^e + \bar{J}_{eq} \qquad (2.1.5)$$

= the total effective current

The induced current $\bar{J}_{eq}$, which is proportional to the contrast of refractive index nonvanishing only in discontinuity region V_d, is now expressed in terms of total field in that region as

$$\bar{J}_{eq}(\bar{r}) = j\omega\epsilon_0 \delta n^2(\bar{r})\bar{E}(\bar{r}) \ . \tag{2.1.6}$$

2.2 Formulation of EFIE for the Unknown Field in the Discontinuity Region

Since the scattered field $\bar{E}^s(\bar{r})$ is induced by polarization current $\bar{J}_{eq}$ of (2.1.6), which is proportional to the unknown field $\bar{E}(\bar{r})$, equation (2.1.1) is rearranged to

$$\bar{E}(\bar{r}) - \bar{E}^s(\bar{r}) = \bar{E}^i(\bar{r}) \ . \tag{2.2.1}$$

Such that both terms on the left-hand side of the above equation depend upon unknown total field $\bar{E}(\bar{r})$. When $\bar{E}^s$ is expressed as an integral operation on $\bar{E}(\bar{r})$, equation (2.2.1) subsequently leads to the fundamental integral equation which describes unknown discontinuity field $\bar{E}(\bar{r})$.

We proceed to expand scattered field $\bar{E}^s$ in the complete set of eigenfunctions (both discrete and continuous) of the unperturbed dielectric waveguide. Solving for the amplitude spectrum of these spectral components (eigenfunctions) will then yield a complete description of the scattered field. Let $\bar{E}_n^{\pm}(\bar{r})$ be the n'th discrete surface-wave mode and $\bar{E}_c^{\pm}(\bar{r},\bar{\xi})$ be a spectral component of the continuous eigen-spectrum having a two-dimensional spectral frequency $\bar{\xi} = \hat{x}\xi_x + \hat{y}\xi_y$. The upper and lower signs of the superscrip '$\pm$' represent the

wave travelling in +z and -z directions respectively. Then

$$\bar{E}^s(\bar{r}) = \sum_n a_n^{\pm} \bar{E}_n^{\pm}(\bar{r}) + \iint_{-\infty}^{\infty} A^{\pm}(\bar{\xi}) \bar{E}_c^{\pm}(\bar{r},\bar{\xi})\, d^2\xi \qquad \text{for } z \gtrless z' \quad (2.2.2)$$

where z' locates an element of polarization current with $\xi=\sqrt{\xi_x^2+\xi_y^2}$ while $a_n^{\pm}$ and $A^{\pm}(\rho)$ are, respectively, the amplitude coefficients of the discrete eigenmodes and continuous eigen-spectrum. The modal eigenfields propagating in the $\pm z$ directions are

$$\bar{E}_n^{\pm}(\bar{r}) = \bar{e}_n^{\pm}(\bar{\rho}) e^{\mp j\beta_n z} = \left[\bar{e}_{tn}(\bar{\rho}) \pm \hat{z} e_{zn}(\bar{\rho})\right] e^{\mp j\beta_n z}$$

$$\bar{E}_c^{\pm}(\bar{r},\bar{\xi}) = \bar{e}^{\pm}(\bar{\rho},\bar{\xi}) e^{\mp j\beta(\xi) z} = \left[\bar{e}_t(\bar{\rho},\bar{\xi}) \pm \hat{z} e_z(\bar{\rho},\bar{\xi})\right] e^{\mp j\beta(\xi) z} \quad (2.2.3)$$

where β_n is the phase constant of the discrete n'th surface-wave mode while $\beta(\bar{\xi}) = [k_c^2-\xi^2]^{1/2}$ is the phase constant of the continuous spectral component with spatial frequency $\bar{\xi}$.

Amplitudes of discrete surface-wave modes and their orthogonality properties are well known [9,41,42]. Through the application of Lorentz Reciprocity Theorem, these properties have also been established in a general manner for the continuous radiation-mode spectral components [43]. These normalization and orthogonality relations for the transverse field components $\bar{e}_t(\bar{\rho})$ and $\bar{h}_t(\bar{\rho})$, which apply

over the infinite transverse cross-sectional plane of the dielectric waveguide, are

$$\int_{CS} \hat{z} \cdot \left[\bar{e}_{tm}(\bar{\rho}) \times \bar{h}_{tn}(\bar{\rho}) \right] dS = \frac{\delta_{mn}}{2} \tag{2.2.4}$$

for discrete surface-wave modes, and

$$\int_{CS} \hat{z} \cdot \left[\bar{e}_{t}(\bar{\rho},\bar{\xi}) \times \bar{h}_{t}(\bar{\rho},\bar{\xi}') \right] dS = \frac{\delta(\bar{\xi} - \bar{\xi}')}{2} \tag{2.2.5}$$

for spectral components of continuous radiation mode.

With the above normalizations, the amplitude coefficients are then obtained [42,43] as

$$a_n^{\pm} = -\int_{V_d} \bar{E}_n^{\mp}(\bar{r}) \cdot \bar{J}_{eq}(\bar{r}) dV \text{ , and} \tag{2.2.6}$$

$$A^{\pm}(\bar{\xi}) = -\int_{V_d} \bar{E}_c^{\mp}(\bar{r},\bar{\xi}) \cdot \bar{J}_{eq}(\bar{r}) dV \text{ .} \tag{2.2.7}$$

Substitution of $a_n^{\pm}$ and $A^{\pm}(\bar{\xi})$ into (2.2.2) for scattered field $\bar{E}^s$ leads to

$$\bar{E}^s(\bar{r}) = -\sum_n \left[\int_{V_d} \bar{E}_n^{\mp}(\bar{r}') \cdot \bar{J}_{eq}(\bar{r}') dV' \right] \bar{E}_n^{\pm}(\bar{r})$$

$$-\iint_{-\infty}^{\infty} \left[\int_{V_d} \bar{E}_c^{\mp}(\bar{r}',\bar{\xi}) \cdot \bar{J}_{eq}(\bar{r}') dV' \right] \bar{E}_c^{\pm}(\bar{r},\bar{\xi}) d^2\xi$$

$$= \int_{V_d} \Big[-\sum_n \bar{E}_n^{\mp}(\bar{r}')\bar{E}_n^{\pm}(\bar{r}) - \iint_{-\infty}^{\infty} \bar{E}_c^{\mp}(\bar{r}',\bar{\xi})\bar{E}_c^{\pm}(\bar{r},\bar{\xi})\,d^2\xi \Big] \cdot \bar{J}_{eq}(\bar{r}')\,dV'. \tag{2.2.8}$$

Scattered field $\bar{E}^s$ can therefore be represented by the following integral operator

$$\bar{E}^s(\bar{r}) = \int_{V_d} \bar{\bar{G}}(\bar{r}|\bar{r}') \cdot \bar{J}_{eq}(\bar{r}')\,dV' \ , \tag{2.2.9}$$

i.e., $\bar{E}^s(\bar{r})$ maintained by equivalent volume polarization current $\bar{J}_{eq}$ is expressed in terms of electric dyadic Green's function $\bar{\bar{G}}(\bar{r}|\bar{r}')$. This Green's function has been constructed from (2.2.8) as

$$\bar{\bar{G}}(\bar{r}|\bar{r}') = \bar{\bar{G}}_d(\bar{r}|\bar{r}') + \bar{\bar{G}}_r(\bar{r}|\bar{r}') \qquad \text{with}$$

$$\bar{\bar{G}}_d(\bar{r}|\bar{r}') = -\sum_n \bar{E}_n^{\pm}(\bar{r})\bar{E}_n^{\mp}(\bar{r}') \tag{2.2.10}$$

= contribution by discrete surface-wave modes, and

$$\bar{\bar{G}}_r(\bar{r}|\bar{r}') = -PV\iint_{-\infty}^{\infty} \bar{E}_c^{\pm}(\bar{r},\bar{\xi})\bar{E}_c^{\mp}(\bar{r}',\bar{\xi})\,d^2\xi + \bar{\bar{L}}\delta(\bar{r} - \bar{r}') \tag{2.2.11}$$

= contribution by continuous radiation-mode spectrum.

To obtain the component forms of $\bar{\bar{G}}_d(\bar{r}|\bar{r}')$ and $\bar{\bar{G}}_r(\bar{r}|\bar{r}')$, we substitute expressions (2.2.3) into (2.2.1Ø) and (2.2.11) such that

$$\bar{\bar{G}}_d(\bar{r}|\bar{r}') = -\sum_n^N \left[\bar{e}_{tn}(\bar{\rho}) \pm \hat{z}e_{zn}(\bar{\rho})\right] \left[\bar{e}_{tn}(\bar{\rho}') \mp \hat{z}e_{zn}(\bar{\rho}')\right] e^{\mp j\beta_n(z-z')} . \tag{2.2.12}$$

It is noted that $\exp[\mp j\beta_n(z-z')] = \exp[-j\beta_n|z-z'|]$ because, for an element of polarization current at z', $z \geq z'$ for forward scattered waves and $z \leq z'$ for backward scattered waves, resulting in

$$\bar{\bar{G}}_d(\bar{r}|\bar{r}') = -\sum_n^N \left[\bar{e}_{tn}(\bar{\rho}) \pm \hat{z}e_{zn}(\bar{\rho})\right] \left[\bar{e}_{tn}(\bar{\rho}') \mp \hat{z}e_{zn}(\bar{\rho}')\right] e^{-j\beta_n|z-z'|} . \tag{2.2.13}$$

Similarly

$$\bar{\bar{G}}_r(\bar{r}|\bar{r}') = -PV\iint_{-\infty}^{\infty} \left[\bar{e}_t(\bar{\rho},\bar{\xi}) \pm \hat{z}e_z(\bar{\rho},\bar{\xi})\right] \left[\bar{e}_t(\bar{\rho}',\bar{\xi}) \mp \hat{z}e_z(\bar{\rho}',\bar{\xi})\right] \times e^{-j\beta(\xi)|z-z'|} d^2\xi + \bar{\bar{L}}\,\delta(\bar{r}-\bar{r}') . \tag{2.2.14}$$

The principal-value notation PV in $\bar{\bar{G}}_r(\bar{r}|\bar{r}')$ indicates that the integration over the discontinuity region V_d should be taken in a manner which excludes the source-point singularity when $\bar{r}'$ passes through field point $\bar{r}$, i.e., $\bar{r}-\bar{r}'=0$. Furthermore, a depolarizing dyadic quantity is found necessary in $G_r(\bar{r}|\bar{r}')$ to evaluate the contribution from this source-point singularity [40,47,48]. Depolarizing dyad $\bar{\bar{L}}$ is identified and evaluated in the following section

as appropriate for the case of dielectric waveguides.

From equation (2.2.9), the scattered field $\bar{E}^s$ can be written in terms of its source polarization current $\bar{J}_{eq}=j\omega\varepsilon_0\delta n^2(\bar{r})\bar{E}(\bar{r})$ as

$$\bar{E}^s(\bar{r}) = \int_{V_d} \bar{\bar{G}}(\bar{r}|\bar{r}') \cdot \bar{J}_{eq}(\bar{r}')dV'$$

$$= j\omega\varepsilon_0 \int_{V_d} \delta n^2(\bar{r}')\bar{\bar{G}}(\bar{r}|\bar{r}') \cdot \bar{E}(\bar{r}')dV' \ . \qquad (2.2.15)$$

With the above integral operator for $\bar{E}^s(\bar{r})$, relation (2.2.1) becomes an electric field integral equation (EFIE) for the unknown total field $\bar{E}(\bar{r})$ within V_d

$$\bar{E}(\bar{r}) - \frac{jk_0}{z_0}\int_{V_d} \delta n^2(\bar{r}')\bar{\bar{G}}(\bar{r}|\bar{r}') \cdot \bar{E}(\bar{r}')dV' = \bar{E}^i(\bar{r}) \qquad \text{for all } \bar{r} \in V_d \qquad (2.2.16)$$

Where $k_0=\omega\sqrt{\mu_0\varepsilon_0}$ is the free-space wave number and $z_0=\sqrt{\mu_0/\varepsilon_0}$ is the associated intrinsic impedance. EFIE (2.2.16) constitutes the fundamental mathematical model which charaeterizes the fields of discontinuity region in a dielectric waveguide. It is normally assumed in the following discussions that a remote source $\bar{J}^e$ which maintains an impressed field $\bar{E}^i$ consisting of single surface-wave mode in the

region of interest, such that solutions to the EFIE for $\bar{E}^i$ excited in V_d by $\bar{E}^i$ lead subsequently to the scattered field interior to V_d through expression (2.2.15).

2.3 Depolarizing Dyad for Electric Dyadic Green's Function

The dyadic Green's function $\bar{\bar{G}}_r(\bar{r}|\bar{r}')$ of (2.2.14), which is the contribution due to the continuous radiation spectrum, has a $\frac{1}{|\bar{r} - \bar{r}'|}$ singularity at $\bar{r} = \bar{r}'$, the source point. Therefore, expression (2.2.11) for the scattered field $\bar{E}^s$ possesses a non-integrtable singularity and the integral does not exist unless an infinitesmal volume δV, the principal volume, surrounding $\bar{r} = \bar{r}'$ is excluded as shown in Figure 2.2. Mathematically, the integral of $\bar{\bar{G}}_r(\bar{r}\,|\,\bar{r}')$ is carried out in this principal value sense such that the spatial frequency integral in $\bar{\bar{G}}_r$ is rendered convergent; however, physically the exclusion of δV interrupts the equivalent current (proportional to electric field) of the discontinuity region. As a result, a non-physical polarization charge layer is created on the surface of δV. Consequently, the effect of the surface charge due to the exclusion of δV, which is built into the principal-value integral, should be substracted in order to obtain a correct result [49]. It is the purpose of this section to demonstrate that the charge density on the principal volume does maintain a finite value of electric field at its center as δV approaches zero in the limit.

Consider a principal volume δV which is cylindrical in shape with height 2a and radius 2b such that $a/b \ll 1$ as

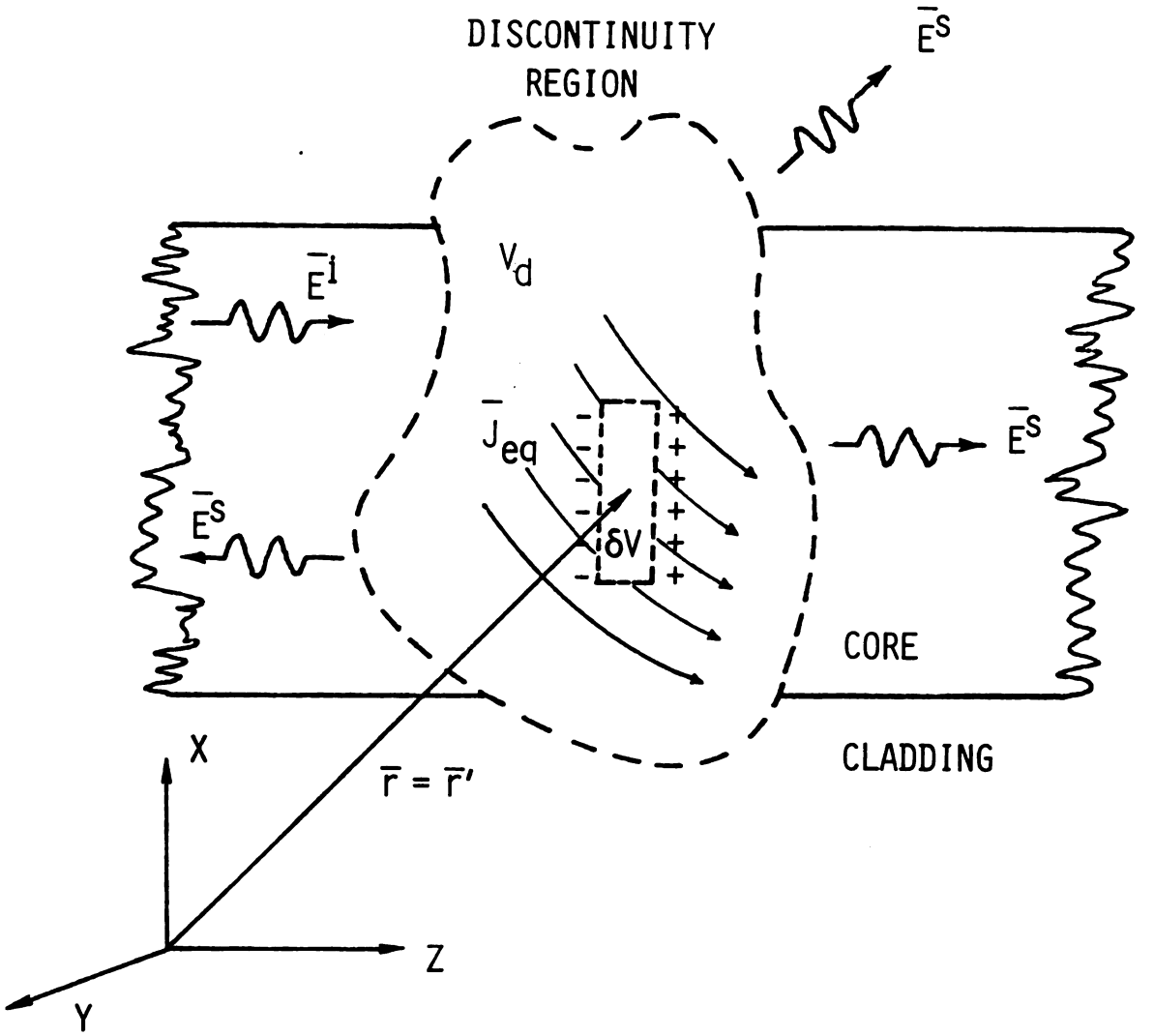

Figure 2.2 Surface charge layer created by the interruption of equivalent polarization current due to the exclusion of principal volume $\underline{\delta}V$ around the source-point singularity at r=r'.

shown in Figure 2.3. A coordinate system is chosen so that its origin coincides with the field point; δV is oriented with its axis parallel with the principal axis of propagation z. Since δV is a small volume, with quasi-static approximation, the electric field $\bar{E}$ at the center of δV can be expressed in terms of scalar and vector potentials as

$$\bar{E} = -\nabla\phi - j\omega\bar{A}$$

$$\cong \frac{1}{4\pi\varepsilon}\int_{\Delta S}\hat{R}\,\frac{\eta dS}{R^3} \qquad (2.3.1)$$

where ε is the local value of permittivity and R is the distance between the source point and field point. Although not shown in (2.3.1), the volume integral involving vector potential $\bar{A}$ vanishes in the limit as δV approaches zero. η ,the surface charge density over ΔS, is equal to $-(\hat{n}\cdot\bar{J})/j\omega$ from the equation of continuity, $\hat{n}$ is the surface normal of ΔS as shown in Figure 2.3.

In the limit as δV approaches zero, the surface integral (2.3.1) over $\Delta S=\Delta S_1+\Delta S_2+\Delta S_3$, sum of top, side and bottom surfaces of δV, is reduced to

$$\bar{E} = \frac{\hat{z}(\hat{z}\cdot\bar{J})}{j\omega\varepsilon}\lim_{\delta V\to 0}\left[1-\frac{a/b}{\sqrt{(a/b)^2+1}}\right]$$

$$= \frac{\hat{z}(\hat{z}\cdot\bar{J})}{j\omega\varepsilon}\,. \qquad (2.3.2)$$

It is observed from the above expression that, as long as $a/b<<1$, the contribution to the electric field at center of

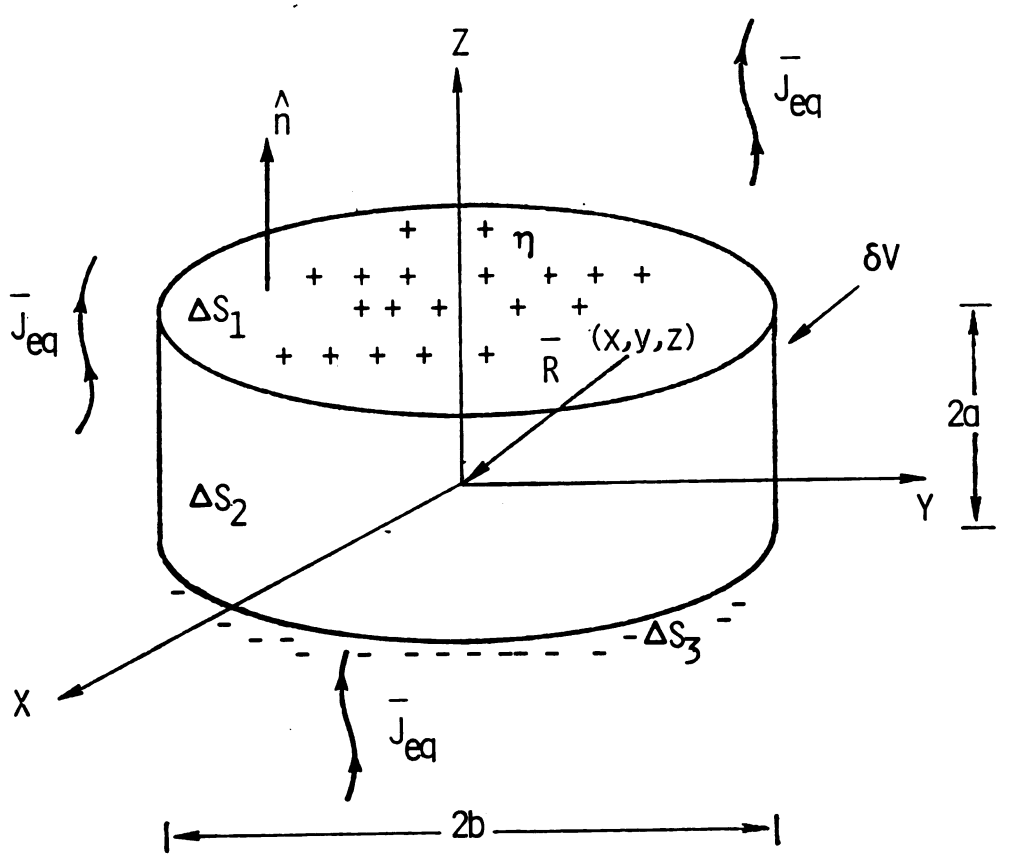

Figure 2.3 Cylindrical principal volume δV with a<<b, centered at field point (the origin), having its axis parallel with the principal axis of propagation z.

δV is insensitive to the shape of its cylindrical cross section.

To further enhence the above observation, a rectangular pillbox of sides a, b and c, centered at origin, is shown in Figure 2.4. Assume that c/a<<1 and c/b<<1, then given the same procedures as before, electric field at the center of δV can be obtained as

$$\bar{E} = \lim_{\delta V \to 0} - \frac{2\eta \hat{z}}{\pi \epsilon} \tan^{-1} \left[\frac{ab}{c\sqrt{a^2 + b^2 + c^2}} \right]$$

$$= \frac{\hat{z}(\hat{z} \cdot \bar{J})}{j\omega\epsilon} \quad . \tag{2.3.3}$$

Note that in (2.3.3), if a=b=c, i.e., a rectangular cube was given instead, then a well known result is obtained:

$$\bar{E} = \frac{\hat{z}(\hat{z} \cdot \bar{J})}{3j\omega\epsilon} \quad . \tag{2.3.4}$$

Hence, the induced charges on the surface of δV, although artificially created, do produce a finite electric field at the singular source point. However, the magnitude of this electric field which is essentially the value of the depolarizing integral involving the depolarizing dyad

$$\bar{\bar{L}}(\bar{r}|\bar{r}') = \frac{\hat{z}\hat{z}}{j\omega\epsilon} \tag{2.3.5}$$

will vary, depending upon the shape of δV [48,49] which is chosen to best suit the geometry of the source region.

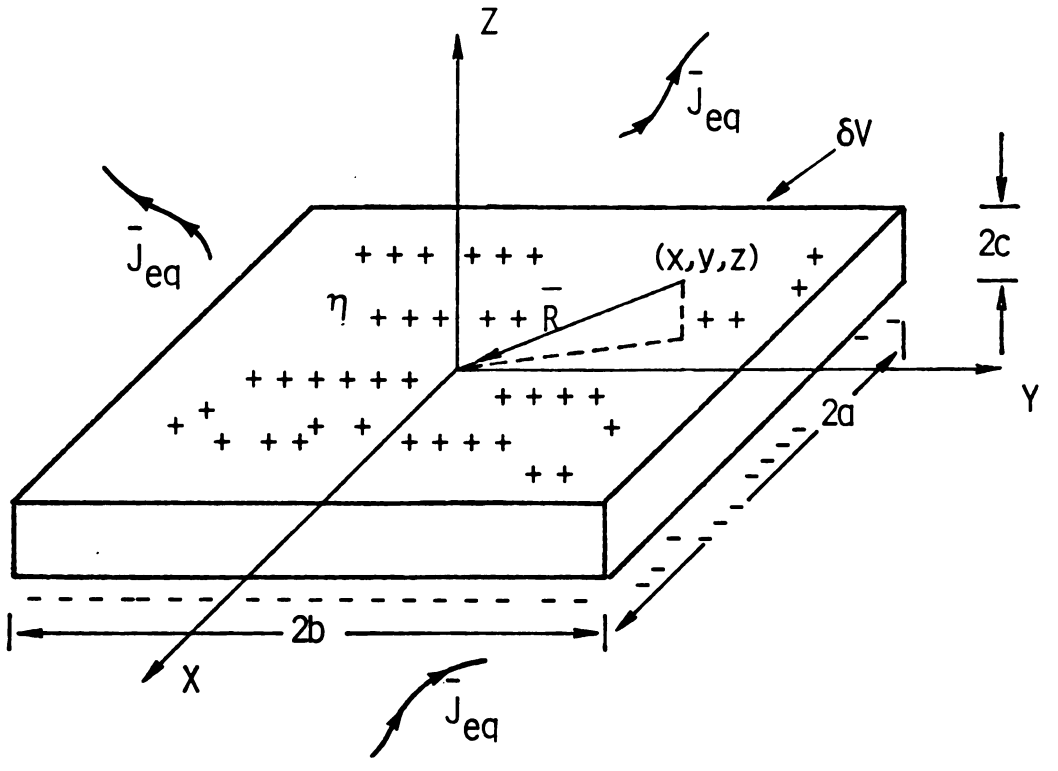

Figure 2.4 Rectangular pillbox as principal volume with c<<a, c<<b, centered at field point (the origin), having it axis parallel with the principal axis of propagation z.

2.4 Scattering Coefficients and Mode Conversion

Consider a multi-mode waveguide which has a transverse dimension large enough to support the propagation of more than a single surface-wave mode. Scattering of an incident surface-wave mode by discontinuities along such a guide results in the excitation of additional discrete and radiation modes in the scattered field. This mode conversion phenomenon is usually undesirable, since energy is radiated through coupling to the continuous spectrum or just simply carried away by non-principal guiding modes. It is therefore of practical interest to calculate these scattering coefficients.

Using the configuration as indicated in Figure 2.5, let the region of discontinuity be bounded by two reference planes, i.e., $z=z_1$, the input terminal plane and $z=z_2$, the output terminal plane. Assuming that a single surface-wave mode of m'th order propagates down the open boundary waveguide and is subsequently scattered by the discontinuity. We define the reflection coefficient at $z=z_1$ as the amplitude ratio of the back-scattered n'th surface-wave mode to the incident m'th surface-wave mode

$$R_{mn} = \frac{a_n^- e^{+j\beta_n z_1}}{E_0 e^{-j\beta_m z_1}} \tag{2.4.1}$$

where a_n^- is the surface-wave mode amplitude of the normalized backward scattered n'th mode while E_0 is the normalized amplitude for the incident wave. Similarly the

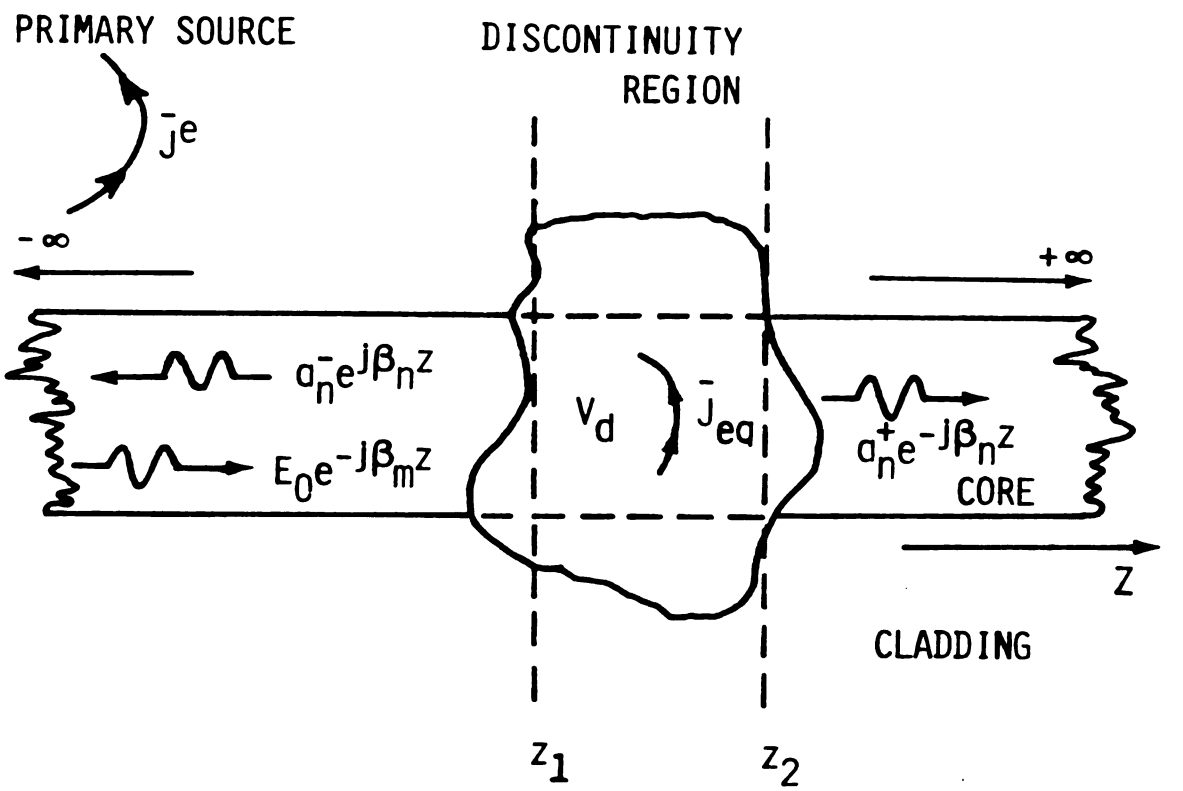

Figure 2.5 Locations of input ans output terminal planes at z_1 and z_2 for the definition of reflection and transmission coefficients appropriate for the incident m'th surface-wave mode and the scattered n'th surface-wave mode.

transmission coefficient T_{mn} at $z=z_2$ is defined as amplitude ratio of total transmitted n'th surface-wave mode, i.e., including both incident and scattered wave, to the incident m'th surface-wave mode at $z=z_1$,

$$T_{mn} = \frac{(E_0\delta_{mn} + a_n^+)e^{-j\beta_n z_2}}{E_0 e^{-j\beta_m z_1}} \tag{2.4.2}$$

where a_n^+ is the surface-wave amplitude of the normalized forward scattered n'th mode; $E_0\delta_{mn}$ represents the contribution of the incident field at the exit plane, it is nonzero only if n=m, as would be the case in mono-mode waveguide.

Both a_n^+ and a_n^- can be obtained from $\bar{E}^s$ of (2.2.9) which, in mono-mode waveguide, has the discrete component

$$\frac{jk_0}{z_0}\int_{V_d} \delta n^2(\bar{r}')\bar{\bar{G}}_d(\bar{r}|\bar{r}') \cdot \bar{E}(\bar{r}')dV'. \tag{2.4.3}$$

The finite sum in the discrete Green's dyad is specialized to extract the contribution by the n'th surface-wave mode, $\bar{\bar{G}}_{dn}$. When $\bar{\bar{G}}_{dn}$ is expressed in terms of its tranverse and longitudinal components as

$$\begin{aligned}\bar{\bar{G}}_{dn}(\bar{r}|\bar{r}') &= -\bar{E}_n^{\pm}(\bar{r})\bar{E}_n^{\mp}(\bar{r}') \\ &= -\left[\bar{e}_{tn}(\bar{\rho}) \pm \hat{z}e_{zn}(\bar{\rho})\right]\left[\bar{e}_{tn}(\bar{\rho}') \mp \hat{z}e_{zn}(\bar{\rho}')\right] \\ &\quad \times e^{-j\beta_n|z-z'|} \\ &\qquad \ldots \text{ for all } \bar{r} \in V_d,\end{aligned} \tag{2.4.4}$$

it is clear that the transverse component field in the reflection coefficient R_{mn} is produced by

$$\bar{e}_{tn}(\bar{\rho})\left[\bar{e}_{tn}(\bar{\rho}') + \hat{z}e_{zn}(\bar{\rho}')\right]e^{+j\beta_n(z-z')} \quad . \tag{2.4.5}$$

Notice that the lower sign of superscript '$\mp$' in equation (2.4.4) is selected for the backward travelling wave, this is because z is to the left of the input terminal plane, such that $z \leq z_1 \leq z'$. By substituting (2.4.5) into (2.4.3), the discrete portion of the scattered field, we then obtain the backward scattered wave for the n'th mode as

$$a_n^- \bar{e}_{tn}(\bar{\rho})e^{+j\beta_n z} =$$

$$-\left(\frac{jk_0}{z_0}\right)e^{+j\beta_n z}\bar{e}_{tn}(\bar{\rho})\int_{V_d}\delta n^2(\bar{r}')\left[\bar{e}_{tn}(\bar{\rho}')+\hat{z}e_{zn}(\bar{\rho}')\right]\cdot\bar{E}(\bar{r}')e^{-j\beta_n z'}dV'. \tag{2.4.6}$$

Following the same procedure, the total field for the n'th mode to the right of exit plane $z=z_2$ is expressed as the sum of the transmitted and forward scattered waves as

$$(E_0\delta_{mn} + a_n^+)\bar{e}_{tn}(\bar{\rho})e^{-j\beta_n z}$$

$$= E_0\delta_{mn}\bar{e}_{tn}(\bar{\rho})e^{-j\beta_n z}$$

$$-\left(\frac{jk_0}{z_0}\right)e^{-j\beta_n z}\bar{e}_{tn}(\bar{\rho})\int_{V_d}\delta n^2(\bar{r}')\left[\bar{e}_{tn}(\bar{\rho}')-\hat{z}e_{zn}(\bar{\rho}')\right]\cdot\bar{E}(\bar{r}')e^{+j\beta_n z'}dV'. \tag{2.4.7}$$

By substituting the transverse field amplitudes obtained from equations (2.4.6), (2.4.7) and the transverse component amplitude of incident m'th surface-wave mode from

$$\bar{E}^{i}_{tm}(\bar{r}) = E_0 \bar{e}_{tm}(\bar{\rho}) e^{-j\beta_m z}$$

into definitions of scattering coefficients given by (2.4.1) and (2.4.2), we obtain R_{mn} and T_{mn} at the corresponding input and output planes as

$$R_{mn} = \frac{-jk_0 e^{j(\beta_m+\beta_n)z_1}}{E_0 Z_0} \int_{V_d} \delta n^2(\bar{r}') \bar{E}^{+}_{n}(\bar{r}') \cdot \bar{E}(\bar{r}') dV' \tag{2.4.8}$$

and

$$T_{mn} = e^{-j(\beta_n z_2 - \beta_m z_1)} \left[\delta_{mn} - \frac{jk_0}{E_0 Z_0} \int_{V_d} \delta n^2(\bar{r}') \bar{E}^{-}_{n}(\bar{r}') \cdot \bar{E}(\bar{r}') dV'\right]. \tag{2.4.9}$$

Use was made of the normalization relation (2.2.5) for $\bar{e}_{tn}$, the transverse wave component, over the infnite cross section of the waveguide.

For the case of a mono-mode dielectric waveguide, i.e., a waveguide that supports only single dominant-mode propagation, there is no excitation of higher-order discrete surface-wave modes in the scattering process. However, mode energy is lost through backscattering, radiation coupling to the continuous radiation mode spectrum and increased dielectric loss due to the existence of standing wave, etc. Equations (2.4.8) and (2.4.9) can be specialized for the mono-

mode dielectric waveguide by letting m=n to obtain

$$R_m = \frac{-jk_0 e^{2j\beta_m z_1}}{E_0 Z_0} \int_{V_d} \delta n^2(\bar{r}') \bar{E}_m^+(\bar{r}') \cdot \bar{E}(\bar{r}') dV' \tag{2.4.10}$$

and

$$T_m = e^{-j\beta_m(z_2-z_1)} \left[1 - \frac{jk_0}{E_0 Z_0} \int_{V_d} \delta n^2(\bar{r}') \bar{E}_m^-(\bar{r}') \cdot \bar{E}(\bar{r}') dV' \right] . \tag{2.4.11}$$

Finally, it follows from the conservation of energy, the relative radiation loss as a result of scattering is

$$\frac{\text{Power radiated}}{\text{Incident power}} = 1 - |R_m|^2 - |T_m|^2 . \tag{2.4.12}$$

2.5 Solutions to Electric Field Integral Equation

This section describes various closed-form and numerical approaches to approximate solutions of EFIE (2.2.16). Without loss of any generality, the dielectric waveguide considered here is assumed to support only dominant mode propagation and the incident field consists of a single surface-wave mode.

First to be discussed is the case of a small discontinuity such that contributions from radiation spectrum can

be neglected; solution for the total electric field which has a longitudinal dependence of exp ($\pm j\beta_0' z$), is then obtained by the Fourier Transform Method. This longitudinal dependence with phase constant β_0' is again assumed for with unknown amplitude coefficients to implement an appoximate radiating solution. Subsequent exploitation of this total field $\bar{E}(\bar{r})$ in (2.2.16), complete with the continuous radiation component in the Green's function, yields these unknown coefficients after enforcing the EFIE at interior points of the discontiniuty region. Hence, radiated power, though negligible for small perturbations, can be quantified to confirm the results obtained otherwise.

Numerical approaches, involving manageable matrix sizes, are often utilized in solving integral equations to obtain solutions of higher accuracy. Therefore, it is appropriate to describe the Method of Moments in the case where discontinuity is of resonant size or smaller. Alternative solution based upon iterative process is then pursued for discontinuities of larger dimensions.

2.5.1 Approximate Radiationless Solution to EFIE

For a small axially-invariant discontinuity (described by $\delta n^2(\bar{\rho})$, i.e., not necessarily uniform) extending from z = $-\ell$ to ℓ, an approximate closed-form solution can be obtained for the field in the discontinuity region if radiation is neglected. This result provides limiting reflection and transmission coefficients which can be used to confirm more

accurate MoM numerical solutions, as well as the zeroth-order discontinuity field required to initiate an iterative solution.

Neglecting radiation from the discontinuity $\delta n^2(\bar{\rho})$ in region $|z| < \ell$ along a monomode (single 0'th surface-wave mode with phase constant β_0) dielectric waveguide leads to the approximate electric Green's dyadic

$$\bar{\bar{G}}(\bar{r}|\bar{r}') \cong - \bar{e}_0^{\pm}(\bar{\rho})\bar{e}_0^{\mp}(\bar{\rho}')e^{-j\beta_0|z-z'|} \quad . \tag{2.5.1}$$

If reduced dyadic (2.5.1) is exploited in EFIE (2.2.16), an approximate IE for unknown E is obtained as

$$\bar{E}(\bar{r}) + \frac{jk_0}{z_0}\int_{-\ell}^{\ell} e^{-j\beta_0|z-z'|}dz' \int_{CS_d} \delta n^2(\bar{\rho}')e_0^{\pm}(\bar{\rho})e_0^{\mp}(\bar{\rho}') \cdot \bar{E}(\bar{r}')dS'$$

$$\cong E_0\bar{e}_0(\bar{\rho})e^{-j\beta_0 z} \qquad \text{... for } |z| \leq \ell,\ \bar{\rho} \in CS_d \ , \tag{2.5.2}$$

where CS_d denotes the transverse cross section of the discontinuity region. In the case of a principal mode well above cutoff, the transverse components predominate over longitudinal components [12]; consequently, only satisfication of the transverse components of IE (2.5.2) is enforced to obtain

$$\bar{E}_t(\bar{r}) + \frac{jk_0}{Z_0}\,\bar{e}_{t0}(\bar{\rho}) \int_{-\ell}^{\ell} e^{-j\beta_0|z-z'|}\,dz' \int_{CS_d} \delta n^2(\bar{\rho}')\, e_0^{\mp}(\bar{\rho}')\cdot\bar{E}(\bar{r}')\,dS'$$

$$\cong E_0\bar{e}_{t0}(\bar{\rho})e^{-j\beta_0 z} \qquad \text{... for } |z| \le \ell,\ \bar{\rho} \in CS_d\ ,$$

(2.5.3)

The preceding expression leads to

$$\bar{E}(\bar{r}) \cong \bar{E}_t(\bar{r}) \cong \bar{e}_{t0}(\bar{\rho})\psi(z)$$

(2.5.4)

where longitudinal wave function $\psi(z)$ satisfies the 1-d IE from (2.5.3)

$$\psi(z) + jk_0 C \int_{-\ell}^{\ell} \psi(z')e^{-j\beta_0|z-z'|}\,dz' \cong E_0 e^{-j\beta_0 z}$$

$$\text{... for } |z| \le \ell,$$

(2.5.5)

where C is defined as

$$C = \frac{\int_{CS_d} \delta n^2(\bar{\rho})\bar{e}_{t0}(\bar{\rho}) \cdot \bar{e}_{t0}(\bar{\rho})\,dS}{2\int \frac{Z_0}{Z_W(\bar{\rho})}\,\bar{e}_{t0}(\bar{\rho}) \cdot \bar{e}_{t0}(\bar{\rho})\,dS}\ ,$$

(2.5.6)

with $Z_W(\bar{\rho})$, the wave impedance of the surface-wave mode $\bar{e}_{t0}(\bar{\rho})$. It is observed that C is independent of normalization chosen for $\bar{e}_{t0}$.

A closed-form solution to approximate IE (2.5.5) can be obtained by exploiting a Fourier-Exponential transform for $\psi(z)$ as

$$\psi(z) = \frac{1}{2\pi}\int_{-\infty}^{\infty} \tilde{\psi}(\eta) e^{j\eta z} d\eta \ . \tag{2.5.7}$$

Substitute (2.5.7) into (2.5.5) to obtain

$$\frac{1}{2\pi}\int_{-\infty}^{\infty} \tilde{\psi}(\eta)\left[e^{j\eta z} + jk_0 C \int_{-\ell}^{\ell} e^{-j\eta z'} e^{-j\beta_0|z-z'|} dz'\right] d\eta$$
$$= E_0 e^{-j\beta_0 z} \ .$$

By selecting the field point z, such that $-\ell \leq z \leq \ell$, the above integration over z' can be carried out and terms of common functional dependence are collected as follows:

$$\int_{-\infty}^{\infty} \tilde{\psi}(\eta)\left[1 - \frac{2j\beta_0 k_0^2 C}{\eta^2 - \beta_0^2}\right] e^{j\eta z} d\eta = 0 \ , \tag{2.5.8}$$

$$- jk_0 C e^{-j\beta_0 \ell} \int_{-\infty}^{\infty} \tilde{\psi}(\eta) \frac{e^{-j\eta\ell}}{j(\eta + \beta_0)} d\eta = 2\pi E_0 \ , \tag{2.5.9}$$

$$\int_{-\infty}^{\infty} \tilde{\psi}(\eta) \frac{e^{j\eta\ell}}{j(\eta - \beta_0)} d\eta = 0 \ . \tag{2.5.10}$$

Since $\tilde{\psi}(\eta) \neq 0$, expression (2.5.8) leads (after invoking the Fourier Transform theorem) to discrete values of allowable spectral frequency

$$\eta = \pm \beta_0' = \pm\sqrt{\beta_0^2 + 2\beta_0 k_0 C} \quad . \tag{2.5.11}$$

The transform solution therefore consist of the discrete spectrum

$$\tilde{\psi}(\eta) = 2\pi A\delta(\eta + \beta_0') + 2\pi B\delta(\eta - \beta_0') \tag{2.5.12}$$

with the corresponding wave function

$$\psi(z) = Ae^{-j\beta_0' z} + B\, e^{j\beta_0' z} \quad . \tag{2.5.13}$$

Substituting (2.5.13) into (2.5.9) and (2.5.10) results in

$$A = \frac{(\beta_0' - \beta_0)E_0 e^{-j(\beta_0'-\beta_0)\ell}}{k_0 C(1 - \rho^2)} \tag{2.5.14}$$

$$\rho = \frac{B}{A} = \frac{\beta_0' - \beta_0}{\beta_0' + \beta_0}\, e^{-2j\beta_0'\ell} \tag{2.5.15}$$

where ρ is defined as the reflection coefficient for the longitudinal wave function $\psi(z)$.

Since $\bar{E}(\bar{r}) = \bar{e}_{t0}(\bar{\rho})\ \psi(z)$, if input and output terminal planes are defined at $z = \mp\ell$, scattering coefficients R_{00} and T_{00} of (2.4.8) and (2.4.9) become

$$R_{00} = -j2\rho\, \frac{e^{j(\beta_0'-\beta_0)\ell}}{1 - \rho^2}\left[\sin\,(\beta_0' + \beta_0)\ell + e^{-2j\beta_0'\ell} \sin\,(\beta_0' - \beta_0)\ell\right],$$

$$T_{00} = e^{-j2\beta_0 \ell}\left\{1 - \frac{j2e^{-j(\beta_0'-\beta_0)\ell}}{1-\rho^2}\left[\sin(\beta_0'-\beta_0)\ell + \rho^2 e^{2j\beta_0'\ell} \times \sin(\beta_0'+\beta_0)\ell\right]\right\} . \tag{2.5.16}$$

2.5.2 Approximate Solution to EFIE for Radiating Discontinuity

The preceding approximate radiationless solution was based upon the assumption that the radiation contribution to the Green's dyadic is negligible. When it is desired to consider such effects, the following Green's function should be employed

$$\bar{\bar{G}}(\bar{r}|\bar{r}') = -\bar{e}_0^{\pm}(\bar{\rho})\bar{e}_0^{\mp}(\bar{\rho}')e^{-j\beta_0|z-z'|} - PV\iint_{-\infty}^{\infty}\bar{e}_0^{\pm}(\bar{\rho},\bar{\xi})\bar{e}_0^{\mp}(\bar{\rho}',\bar{\xi})e^{-j\beta(\xi)|z-z'|}d^2\xi + \bar{\bar{L}}(\bar{r}|\bar{r}')\delta(\bar{r}-\bar{r}') . \tag{2.5.17}$$

Again, in a simplified situation as described in Section 2.5.1, with only a principal mode supported (negligible axial field components) the field in the discontinuity region can be approximated as

$$\bar{E}(\bar{r}) \cong \bar{e}_{t0}(\bar{\rho})\left[a_1 e^{-j\beta_0'z} + a_2 e^{j\beta_0'z}\right] \tag{2.5.18}$$

where β_0' is that obtained in (2.5.11) and a_1, a_2, are the associated unknown amplitude coefficients when radiation effects are considered.

Recall the integral equation (2.2.16) as

$$\bar{E}(\bar{r}) - \frac{jk_0}{Z_0}\int_{V_d} \delta n^2(\bar{\rho}')\bar{\bar{G}}(\bar{r}|\bar{r}') \cdot \bar{E}(\bar{r}')dV' = \bar{E}^i(\bar{r}) \tag{2.5.19}$$

where $\bar{E}(\bar{r})$ is now approximated by (2.5.18). Then, the IE above has two unknown constants a_1 and a_2, therefore in order to reduce it into two algebrac equations to solve for these amplitude coefficients, an integral-operator with weighting function $\bar{w}_p$ is used to pre-dot multiplying into above IE and integrate over the discontinuity region V_d as

$$\int_{V_d} \bar{w}_p \cdot \{\quad\} \, dV, \; p = 1,2 \; . \tag{2.5.20}$$

For the purpose of simplicity, if delta-function is chosen for $\bar{w}_p$ such that

$$\bar{w}_p = \hat{u}_p \delta(\bar{r} - \bar{r}_p) \tag{2.5.21}$$

where $\hat{u}_p$ is a unit vector, subsequent operation of (2.5.20) upon (2.5.19) with the above delta-function weighting yields a matrix equation with p=1 and 2 as

$$\sum_{\ell=1}^{2} C_{p\ell} a_\ell = b_p \tag{2.5.22}$$

where the matrix elements $C_{p\ell}$ and b_p are

$$C_{p1} = \hat{u}_p \cdot \bar{e}_{t0}(\bar{r}_p) e^{-j\beta_0' z_p}$$

$$- \frac{jk_0}{z_0} \int_{V_d} \delta n^2(\bar{\rho}') \hat{u}_p \cdot \bar{\bar{G}}(\bar{r}_p | \bar{r}') \cdot \bar{e}_{t0}(\bar{r}') e^{-j\beta_0' z'} \, dV' ,$$

$$C_{p2} = \hat{u}_p \cdot \bar{e}_{t0}(\bar{r}_p) e^{+j\beta_0' z_p}$$

$$- \frac{jk_0}{z_0} \int_{V_d} \delta n^2(\bar{\rho}') \hat{u}_p \cdot \bar{\bar{G}}(\bar{r}_p | \bar{r}') \cdot \bar{e}_{t0}(\bar{r}') e^{+j\beta_0' z'} \, dV' ,$$

$$b_p = \hat{u}_p \cdot \bar{E}^i(\bar{r}_p) \, . \qquad (2.5.23)$$

2.5.3 Moment-Method Numerical Solution for Discontinuity Field

The integral-operator method described above for scattering by a discontinuity along a dielectric waveguide is particularly suitable for numerical solution, especially when the region of discontinuity is heterogeneous in nature, i.e. $\delta n^2 = \delta n^2(\bar{r})$, and arbitrary in shape. In this scetion, EFIE (2.2.16) is reduced to a matrix equation by Method of Moments (MoM) technique [50]. In this method, the unknown field $\bar{E}(\bar{r})$ is first expanded in an appropriate basis set (expansion functions); then, subsequent to taking the term-by-term inner product with an appropriate set of weighting functions (testing functions), the EFIE is discretized to a matrix equation.

To begin, a volumetric pulse-function basis set is selected because the resulting MoM matrix-element computation is simplified (numerical matrix fill-time minimized); the pulse function expansion for $\bar{E}$, the unknow field, is therefore

$$\bar{E}(\bar{r}) = \sum_{\nu=1}^{3} \sum_{q=1}^{N} \hat{x}_\nu a_{\nu q} P_q(\bar{r}) \tag{2.5.24}$$

with

$$P_q(\bar{r}) = \begin{cases} 1 \ \ldots \text{ for } \bar{r} \in \Delta V_q \\ \emptyset \ \ldots \text{ for } \bar{r} \notin \Delta V_q \end{cases}$$

$$= \text{volumetric pulse function spanning q'th volume element } \Delta V_q \text{ for } q = 1,2, \ldots, N$$

where V_d is partitioned into N volume elements ΔV_q. Use of this expression in EFIE (2.2.16) leads to

$$\sum_{\mu=1}^{3} \sum_{q=1}^{N} a_{\nu q} \left[\hat{x}_\nu P_q(\bar{r}) - \frac{jk_0}{Z_0} \int_{\Delta V_q} \delta n^2(\bar{r}') \bar{\bar{G}}(\bar{r}|\bar{r}') \cdot \hat{x}_\nu dV' \right] = \bar{E}^i(\bar{r})$$

$$\ldots \text{ for all } \bar{r} \in V_d. \tag{2.5.25}$$

Expression (2.5.25) is discretized, to obtain an MoM matrix equation for the $a_{\nu q}$, by operating term-by-term with the δ-function integral testing operator ($\bar{r}_p$ at the center of ΔV_p)

$$\sum_{\mu=1}^{3} \sum_{p=1}^{N} \int_{V_d} \delta(\bar{r}-\bar{r}_p) \ \hat{x}_\mu \cdot \{ \ \} \, dV \tag{2.5.26}$$

which provides

$$\sum_{\nu=1}^{3} \sum_{q=1}^{N} (A_{\mu\nu})_{pq} a_{\nu q} = E_{\mu}^{i}(\bar{r}_p)$$

$$\text{. . . . for } \mu = 1,2,3 \text{ and}$$

$$p = 1,2, \ldots, N, \qquad (2.5.27)$$

a 3N by 3N matrix equation for unknown $a_{\nu q}$, or

$$3N\left\{\underbrace{\begin{bmatrix} & & \\ & (A_{\mu\nu})_{pq} & \\ & & \end{bmatrix}}_{3N}\right\}\begin{bmatrix} a_{xq} \\ a_{yq} \\ a_{zq} \end{bmatrix} = \begin{bmatrix} E_x^i(\bar{r}_p) \\ E_y^i(\bar{r}_p) \\ E_z^i(\bar{r}_p) \end{bmatrix} \qquad (2.5.28)$$

where the MoM matrix elements are

$$(A_{\mu\nu})_{pq} = \delta_{\mu\nu}\delta_{pq} - \frac{jk_0}{z_0} \int_{\Delta V_q} \delta n^2(\bar{r}')\hat{x}_{\mu} \cdot \bar{\bar{G}}(\bar{r}_p|\bar{r}') \cdot \hat{x}_{\nu} dV' \ . \qquad (2.5.29)$$

By applying standard matrix methods, the numerical solution of MoM matrix equation (2.5.28) for $a_{\nu q}$ leads to field $\bar{E}$ in the discontinuity region through expansion (2.5.24).

2.5.4. Iterative Solution to EFIE

Since the polarization EFIE

$$\bar{E}(\bar{r}) = \bar{E}^i(\bar{r}) + \frac{jk_0}{z_0}\int_{V_d} \delta n^2(\bar{r}')\bar{\bar{G}}(\bar{r}|\bar{r}') \cdot \bar{E}(\bar{r}')dV' \tag{2.2.16}$$

is essentially a linear Fredholm integral equation of the second kind, it leads naturally to iterative solutions [51] for the total electric field $\bar{E}(\bar{r})$. This approach provides an alternative to the MoM solution, which remains feasible when the discontinuity region exceeds resonant size. If $\bar{E}$ is the field of the ℓth iteration, then EFIE (2.2.16) provides

$$\bar{E}_{\ell+1}(\bar{r}) = \bar{E}^i(\bar{r}) + \frac{jk_0}{z_0}\int_{V_d} \delta n^2(\bar{r}')\bar{\bar{G}}(\bar{r}|\bar{r}') \cdot \bar{E}_\ell(\bar{r}')dV' \ . \tag{2.5.30}$$

The iteration series provided by the above relation converges if $\| E_{\ell+1} - E \| \to 0$ for large ℓ. Convergent rate depends strongly upon the initial selection for $\bar{E}_0$, the field of the 0'th iteration, which might be estimated as

$$\bar{E}_0(\bar{r}) \approx \begin{cases} \bar{E}^i(\bar{r}) & \text{...for small discontinuities, or} \\ \text{approximate "radiationless" solution for} & \\ \text{"Simple" discontinuities where } \delta n^2 = \delta n^2(\bar{\rho}). & \end{cases} \tag{2.5.31}$$

Choice of $\bar{E}_0 = \bar{E}^i$ leads to the classical Neumann series and the associated resolvent kernel [51]. Due to the complexity

of Green's function $\bar{\bar{G}}$, a practical iterative field solution will require adequate convergence after only serveral iterations; an accurate choice for the 0'th-order field of the first iteration $\bar{E}_0$ is consequently important.

CHAPTER III

APPLICATION TO SCATTERING BY SLICE GAP DISCONTINUITY IN A DIELECTRIC SLAB WAVEGUIDE

3.1 Introduction

The one-dimensional slab waveguide considered in this chapter for the applications is shown in Figure 3.1. The slab extends infinitely in both directions of y and z with a width of 2d. A discontinuity region V_d, being both y and z invariant, occupies the longitudinal cross section of V_d; it is centered at origin and consists of a dielectric material of refractive index of $n_3(x,z)$ which provides a contrast with those of the slab and the surround which are n_1 and n_2 respectively. Single dominant TE surface-wave mode incidence from $z<<0$ with amplitude E_0 is assumed. The infinite dimension along y insures the y-invariance for all the field quantities, i.e., $\partial / \partial y = 0$. Scattering by the discontinuity is interpreted as arising from the equivalent polarization current induced within the discontinuity and proportional to the index contrast $\delta n^2 = n_3^2(x,z) - n_1^2$.

For a planar, step-index symmetric slab waveguide, the well known characteristic equation [42] for eigenvalues of natural TE surface-wave modes is

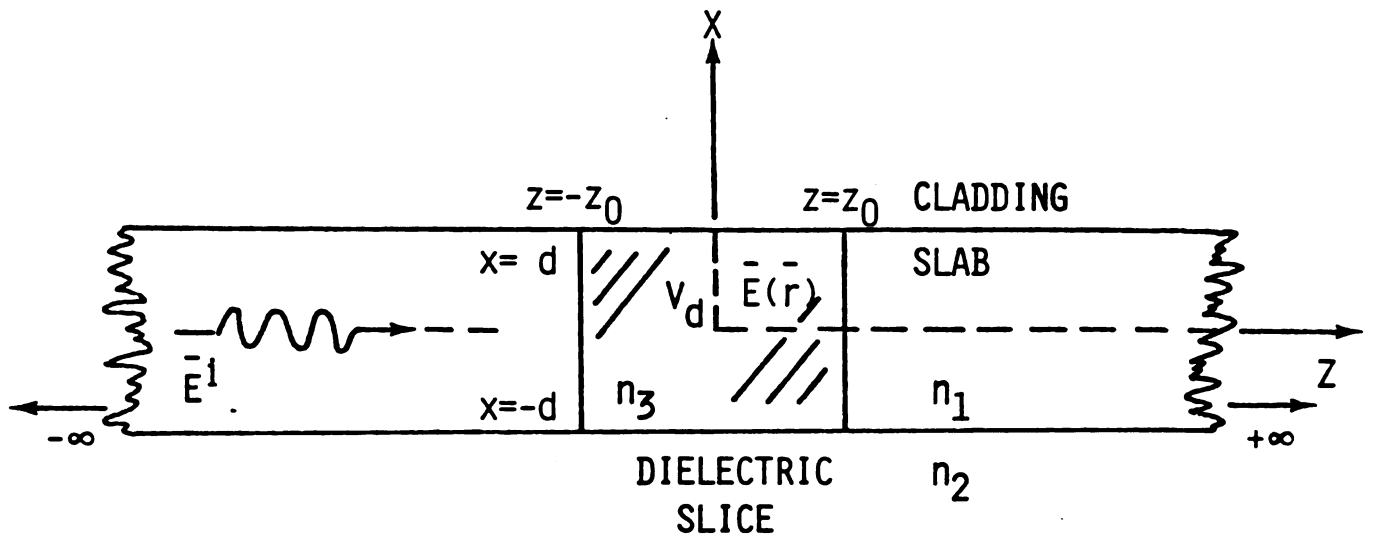

Figure 3.1 Slice discontinuity region V_d of length $2z_0$, width 2d along an one-dimensional slab waveguide having refractive index $n_3(x,z)$.

$$\tan(\kappa t) = \frac{2\gamma\kappa}{(\kappa^2 - \gamma^2)}$$

where t is the thickness of the slab. The characteristic transverse phase constants κ and γ are related to longitudinal phase constant by the definitions $\kappa^2=k_1^2-\beta^2$ and $\gamma^2=\beta^2-k_2^2$, where k_1, k_2 are wavenumbers of the slab and surround respectively with $k_1=n_1k_0$ and $k_2=n_2k_0$. A graphical solution to that eigenvalue equation is shown in Figure 3.2 for a slab waveguide with $n_1=1.6$, $n_2=1.0$. As illustrated in Figure 3.2a for TE even modes and Figure 3.2b for TE odd modes, the later exhibits a lower cutoff frequency while the principal TE even mode does not. It is evident that only a finite number of discrete modes are allowed as contrast with the infinite number of eigenmodes in conventional closed-boundary metallic waveguides. This particular characteristic allows us to vary the waveguide dimensions such that either mono-mode or multimode fields are excited in the scattering process. It is the purpose of this chapter to demonstrate the use of various solutions discussed in the last chapter. Relative merits of each technique are evaluated and qualitative conclusions are drawn regarding scattering phenomena associated with discontinuities along a dielectric slab waveguide.

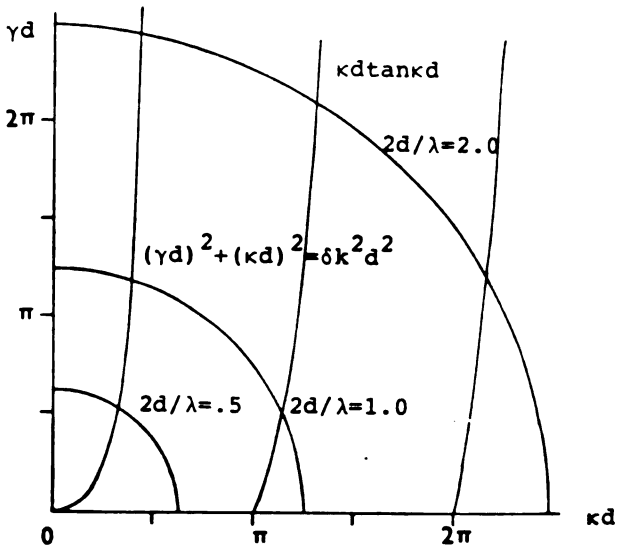

(a). TE even modes.

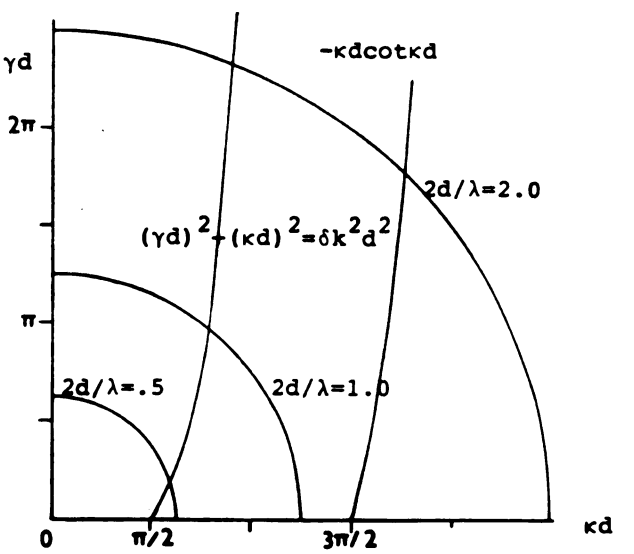

(b). TE odd modes.

Figure 3.2 Graphical solutions to eigenvalue equation for even and odd symmetric-slab surface-wave modes for case of n_1=1.6, n_2=1.0, thickness of slab t=2d.

3.1.1 TE Propagation Mode for Slab Waveguide and Their Normalization

DISCRETE SURFACE-WAVE MODES

Since the TE surface-wave mode fields are of the form

$$\hat{y}e_{yn}(x)e^{\mp j\beta_n z}$$

(where subscript "n" in $e_y(x)$ and β denote the n'th discrete mode) i.e., a travelling wave in the axial direction $\pm z$ with phase constant β_0, its corresponding transverse electric and magnetic fields are

$$\begin{aligned}\bar{e}_{tn}(\bar{r}) &= \hat{y}e_{yn}(x)\\ \bar{h}_{tn}(\bar{r}) &= \frac{1}{Z_{TE}}(\hat{z}\times\bar{e}_{tn}) = -\hat{x}e_{yn}(x)/Z_{TE}\\ &= \hat{x}h_{xn}(x)\end{aligned} \qquad (3.1.1)$$

where $Z_{TE}=\omega\mu_0/\beta_n=Z_0k_0/\beta_0$, $Z_0=\sqrt{\mu_0/\varepsilon_0}$, the wave impedance with wavenumber $k_0=\omega\sqrt{\mu_0\varepsilon_0}$. From (2.2.4) of Chapter 2, the assumed normalization for $e_{yn}(x)$ is

$$-\int_{-\infty}^{\infty}e_{yn}(x)h_{xn}(x)\,dx = \frac{1}{Z_{TE}}\int_{-\infty}^{\infty}e_{yn}^2(x)\,dx = \frac{1}{2} \qquad (3.1.2)$$

It is well known that the tranverse electric field $e_{yn}(x)$ for the slab waveguide can be written as [28]

$$e_{yn}(x) = \begin{cases} A \cos(\kappa x) & \ldots |x| \leq d \\ Ae^{\gamma(d-|x|)} \cos(\kappa d) & \ldots \infty \geq |x| \geq d \end{cases} \tag{3.1.3}$$

where it shows, in the transverse plane, there exists a standing wave inside the waveguide and a rapidly decaying wave outside. The amplitude coefficient A is obtained by exploiting (3.1.3) into (3.1.2),

$$A = \left[\frac{k_0 Z_0}{2\beta_n d\left(1 + \frac{\sin 2\kappa d}{2\kappa d} + \frac{\cos^2 \kappa d}{\gamma d}\right)} \right]^{1/2} \tag{3.1.4}$$

CONTINUOUS RADIATION MODES

From (2.2.5) of Chapter 2, the normalization for continuous radiation modes in slab waveguide is given by

$$\int_{-\infty}^{\infty} d\xi' \int_{-\infty}^{\infty} \hat{z} \cdot \left[\bar{e}_y(x,\xi) \times \bar{h}_x(x,\xi')\right] dx$$

$$= 4 \int_{-\infty}^{\infty} \frac{\delta(\xi - \xi')}{Z_{TE}(\xi')} d\xi' = \frac{4}{Z_{TE}(\xi)} \tag{3.1.5}$$

with $Z_{TE} = Z_0 k_0 / \beta(\xi)$. Similary, the continuous radiation fields inside and outside the slab can be written as [28]

$$e_y(x,\xi) = \begin{cases} \sqrt{\frac{2}{\pi}}\,\frac{1}{c}\cos(\sigma x) & \ldots\ |x| \le d \\ \sqrt{\frac{2}{\pi}}\left[\cos\xi(x-d)+\alpha\right] & \ldots\ |\infty| \ge |x| \ge d \end{cases} \tag{3.1.6}$$

Amplitude coefficient c is obtained by exploiting (3.1.6) into (3.1.5)

$$c = \left[1 + \left(\frac{\upsilon}{\xi}\right)^2 \sin^2\sigma d\right]^{1/2} \tag{3.1.7}$$

where σ, α and υ are defined by the following relations:

$$\alpha = \tan^{-1}\left[\frac{\sigma}{\xi}\tan(\sigma d)\right]$$

$$\sigma^2 = k_1^2 - \beta^2,\ \xi^2 = k_2^2 - \beta^2\ .$$

$$\upsilon^2 = k_1^2 - k_2^2 = \kappa^2 + \gamma^2 = \sigma^2 - \xi^2\ ,$$

3.1.2 Scalar EFIE for TE Mode Scattering along Slab Waveguide

For the one-dimensional slab waveguide in Figure 3.1, equation (2.2.16) of Chapter 2 can be expressed as

$$\bar{E}(x,z) - \frac{jk_0}{z_0}\int_{LCS}\delta n^2(x')\bar{\bar{G}}(x,z\,|x',z')\cdot\bar{E}(x',z')dx'dz'$$

$$= \hat{y}E_0 e_{yn}(x)\exp(-j\beta_n z) \tag{3.1.8}$$

where LCS denotes the longitudinal cross section of the arbitrarily-shaped discontinuity region along the slab waveguide. By carrying out the dyadic dot product of $\bar{\bar{G}}\cdot\bar{E}$ in the integral above, we obtain the following component

form scalar equations for (3.1.8).

x component:

$$E_x(x,z) - \frac{jk_0}{z_0}\int_{LCS}\delta n^2(x')\Big[G_{xx}(x,z|x',z')E_x(x',z') + G_{xy}(x,z|x',z')E_y(x',z') + G_{xz}(x,z|x',z')E_z(x',z')\Big]dx'dz' = 0 \qquad (3.1.9)$$

y component:

$$E_y(x,z) - \frac{jk_0}{z_0}\int_{LCS}\delta n^2(x')\Big[G_{yx}(x,z|x',z')E_x(x',z') + G_{yy}(x,z|x',z')E_y(x',z') + G_{yz}(x,z|x',z')E_z(x',z')\Big]dx'dz' = E_0 e_{yn}(x)\exp(-j\beta_n z) \qquad (3.1.10)$$

z component:

$$E_z(x,z) - \frac{jk_0}{z_0}\int_{LCS}\delta n^2(x')\Big[G_{zx}(x,z|x',z')E_x(x',z') + G_{zy}(x,z|x',z')E_y(x',z') + G_{zz}(x,z|x',z')E_z(x',z')\Big]dx'dz' = 0 \qquad (3.1.11)$$

It is observed that due to the y-invariant property of the slab waveguide, its Green's function, specifically, the dyadic elements $G_{xy}(x,z|x',z')$, $G_{yx}(x,z|x',z')$, $G_{yz}(x,z|x',z')$ and $G_{zy}(x,z|x',z')$ are equal to zero aided by the fact that $\bar{\bar{G}}(x,z|x',z')$ is constructed from electric field eigenfunctions (both discrete and continuous) consisting of TE modes with only y component or TM modes with only x and z components, and the TE and TM modes are orthogonal. Therefore, (3.1.9), (3.1.10) and (3.1.11) can be reduced to

$$E_x(x,z) - \frac{jk_0}{z_0}\int_{LCS}\delta n^2(x')\left[G_{xx}(x,z|x',z')E_x(x',z') + G_{xz}(x,z|x',z')E_z(x',z')\right]dx'dz' = 0 \qquad (3.1.12)$$

$$E_y(x,z) - \frac{jk_0}{z_0}\int_{LCS}\delta n^2(x')G_{yy}(x,z|x',z')E_y(x',z')dx'dz' = E_0 e_{yn}(x)e^{(-j\beta_n z)} \qquad (3.1.13)$$

$$E_z(x,z) - \frac{jk_0}{z_0}\int_{LCS}\delta n^2(x')\left[G_{zx}(x,z|x',z')E_x(x',z') + G_{zz}(x,z|x',z')E_z(x',z')\right]dx'dz' = 0 \qquad (3.1.14)$$

A study of the above expressions reveal that the x and z component equations (3.2.12) and (3.2.14) couple E_x and E_z but are uncoupled from E_y; furthermore, zero forcing function in both implies there exists only trivial solution such that $E_x=E_z=0$. The y component-equation (3.1.13) is independent in E_y with a non-zero forcing term in the right hand side, therefore $E_y\neq 0$. The TE mode only problem is then reduced to that of solving the y-component integral equation:

$$E_y(x,z) - \frac{jk_0}{z_0}\int_{-z_0}^{z_0}\int_{-d}^{d}\delta n^2(x')G_{yy}(x,z|x',z')E_y(x',z')dx'dz' = E_0 e_{yn}(x)e^{-j\beta_n z} \quad \text{... for all } (x,z)\in V_d \tag{3.1.15}$$

This is a specialized EFIE for unknown $E_y(x,z)$ in the discontinuity region due to scattering of incident TE_n surface-wave mode. In this IE, electric Green's function G_{yy} consists of both the discrete and continuous radiation component fields:

$$G_{yy}(x,z|x',z') = \sum_n - e_{yn}(x)e_{yn}(x')e^{-j\beta_n|z-z'|} - \frac{1}{4}\int_0^{\infty} Z_{TE}(\xi)e_y(x,\xi)e_y(x',\xi)e^{-j\beta(\xi)|z-z'|}d\xi \tag{3.1.16}$$

The absence of principal value evaluation in (3.1.16) above is evident from the fact that TE mode propagation in this

slab waveguide does not support any currents in the z direction. Hence, there is no contribution to the correction term $\bar{\bar{L}}$ for the otherwise would be present source point singularity in the continuous spectrum integral of $G_r(x,z|x',z')$ of G_{yy}.

3.2 Approximate Treatment for Scattering along Slab Waveguide

3.2.1 Analytical Solution without Radiation Contribution

A closed-form solution was obtained for $\bar{E}(\bar{r})$, the field inside the discontinuity region, from Section 2.5.1, by neglecting the continuous radiation in a mono-mode waveguide, as

$$\bar{E}(\bar{r}) \cong \bar{e}_{t0}(\bar{\rho})\psi(z) = e_{y0}(x)\psi(z)\hat{y}$$
$$= \hat{y}Ae_{y0}(x)\left[e^{-j\beta_0' z} + \rho e^{j\beta_0' z}\right] \qquad (3.2.1)$$

where A and ρ are given by (2.5.14) and (2.5.15). The constant C given by (2.5.6) is evaluated here for TE_0 mode field under the assumption that the discontinuity region is of homogeneous nature, i.e., $n_3(x,z)=n_3$, a constant, such that

$$C = \frac{j(n_3^2 - n_1^2)k_0}{Z_0}\int_{-d}^{d} e_{y0}^2(x')dx'$$
$$= \frac{\frac{j(n_3^2 - n_1^2)k_0^2}{2\beta_0}(\kappa d + \frac{\sin 2\kappa d}{2})}{\frac{\kappa}{\gamma}\cos^2 \kappa d + (\kappa d + \frac{\sin 2\kappa d}{2})} \qquad (3.2.2)$$

Then, β_0', the phase constant of $\bar{E}(\bar{r})$, has the following eigenvalue

$$\beta_0' = \sqrt{\beta_0^2 + 2\beta_0 k_0 C}$$

which depends upon the values of $\delta n^2 = n_3^2 - n_1^2$, the dielectric contrast, through the definition of C above.

Shown in Figure 3.3 is $\beta_0' t$, the normalized propagation constant, as a function of the value of $\delta n^2 = n_3^2 - n_1^2$. Figure 3.4 displays the relationship between $\beta_0' t$ and the values of refractive indicies of the discontinuity region, n_3.

Amplitudes of the reflection and transmission coefficients |R| and |T| thus calculated from (2.5.16) are shown separately in Figure 3.5 and 3.6. These coefficients are plotted as a function of n_3 with parameter z_0/d(i.e., length of the discontinuity region is normalized w.r.t. the width of slab) having the values of 0.1, 0.5 and 1.0. It is noted from these results that as the contrast of refractive index increses, the discontinuity presents itself as a better and better reflector. Furthermore, oscillatory nature in the obtained values of |R| and |T| shown in these figures due to larger value of z_0/d certainly agrees with the intuition that the "strength" of the discontinuity is becoming "stronger", this can also be verified from the axial field distribution in the MoM solution to be presented in the following section.

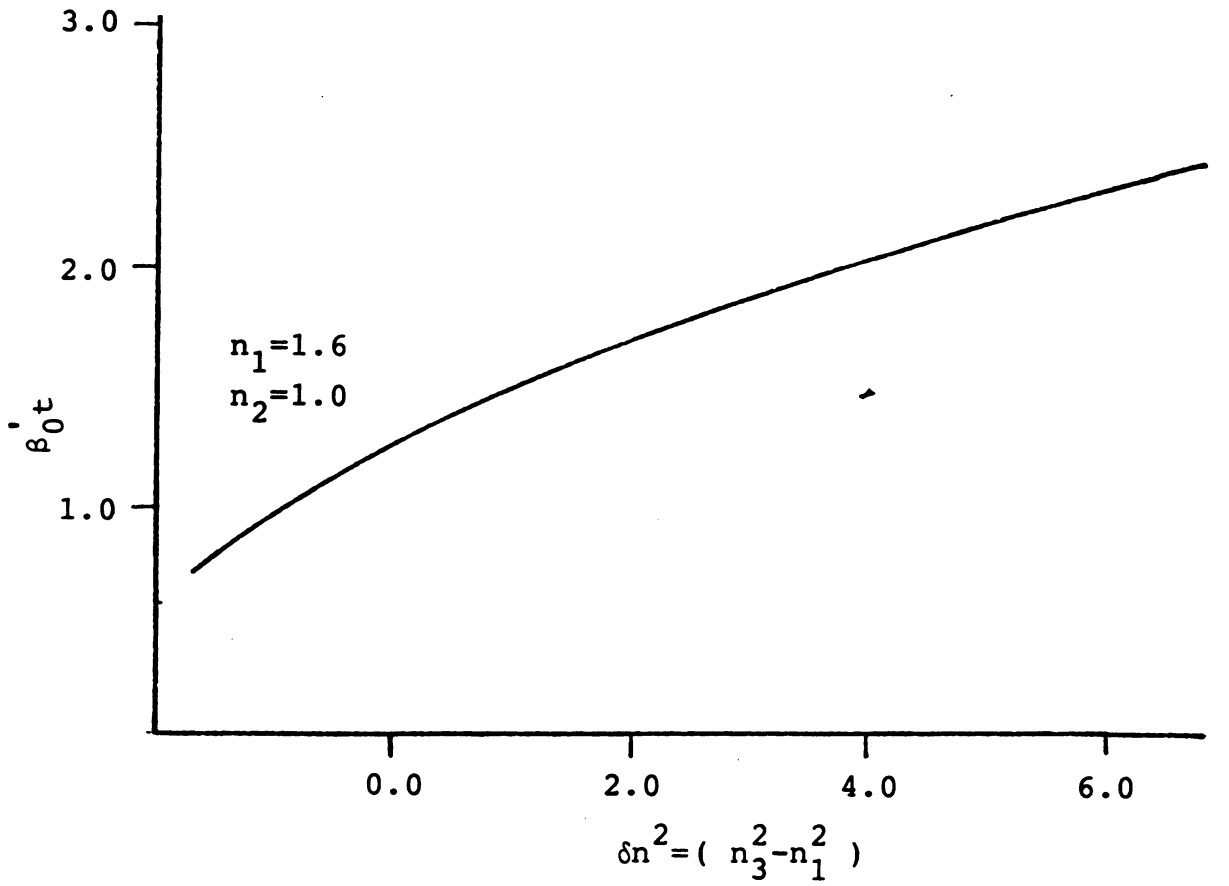

Figure 3.3 Normalized phase constant as a function of index contrast for the axial propagation in the slice-discontinuity region of a slab waveguide.

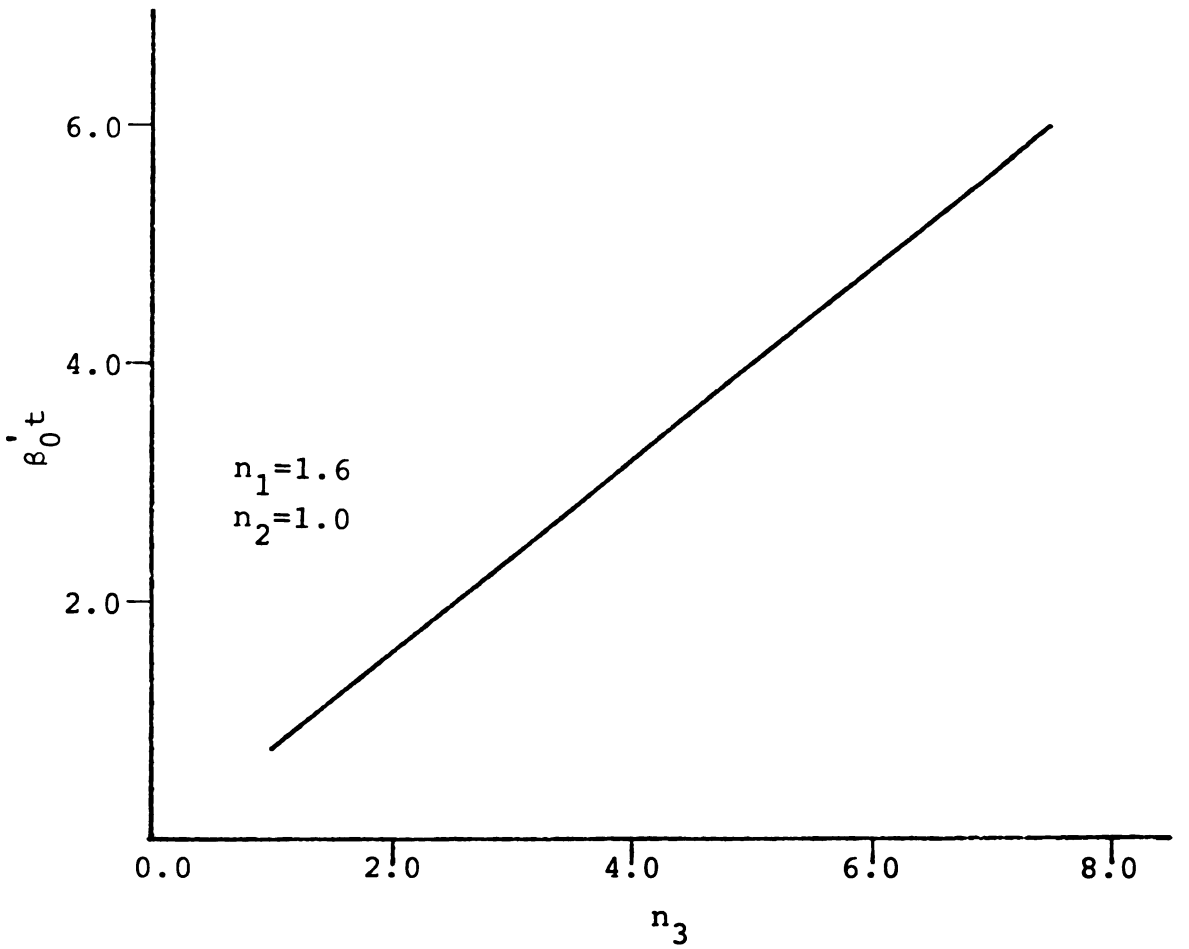

Figure 3.4 Normalized phase constant as a function of refractive index n_3 of the slice region for the axial propagation in the slice discontinuity region.

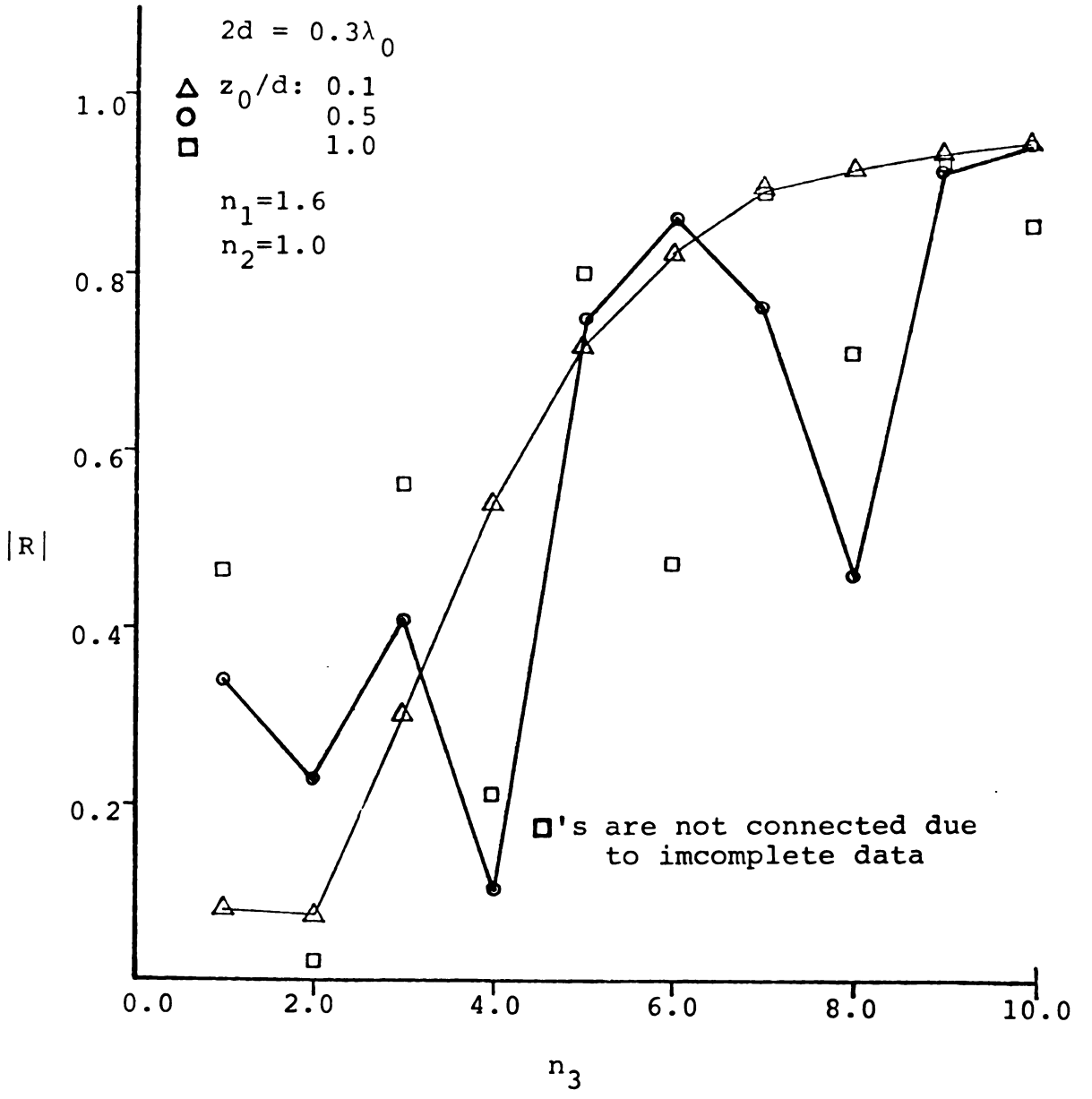

Figure 3.5 Magnitude of reflection coefficient as a function of its refractive index n_3 for three values of the normalized lengths of the slice-discontinuity region.

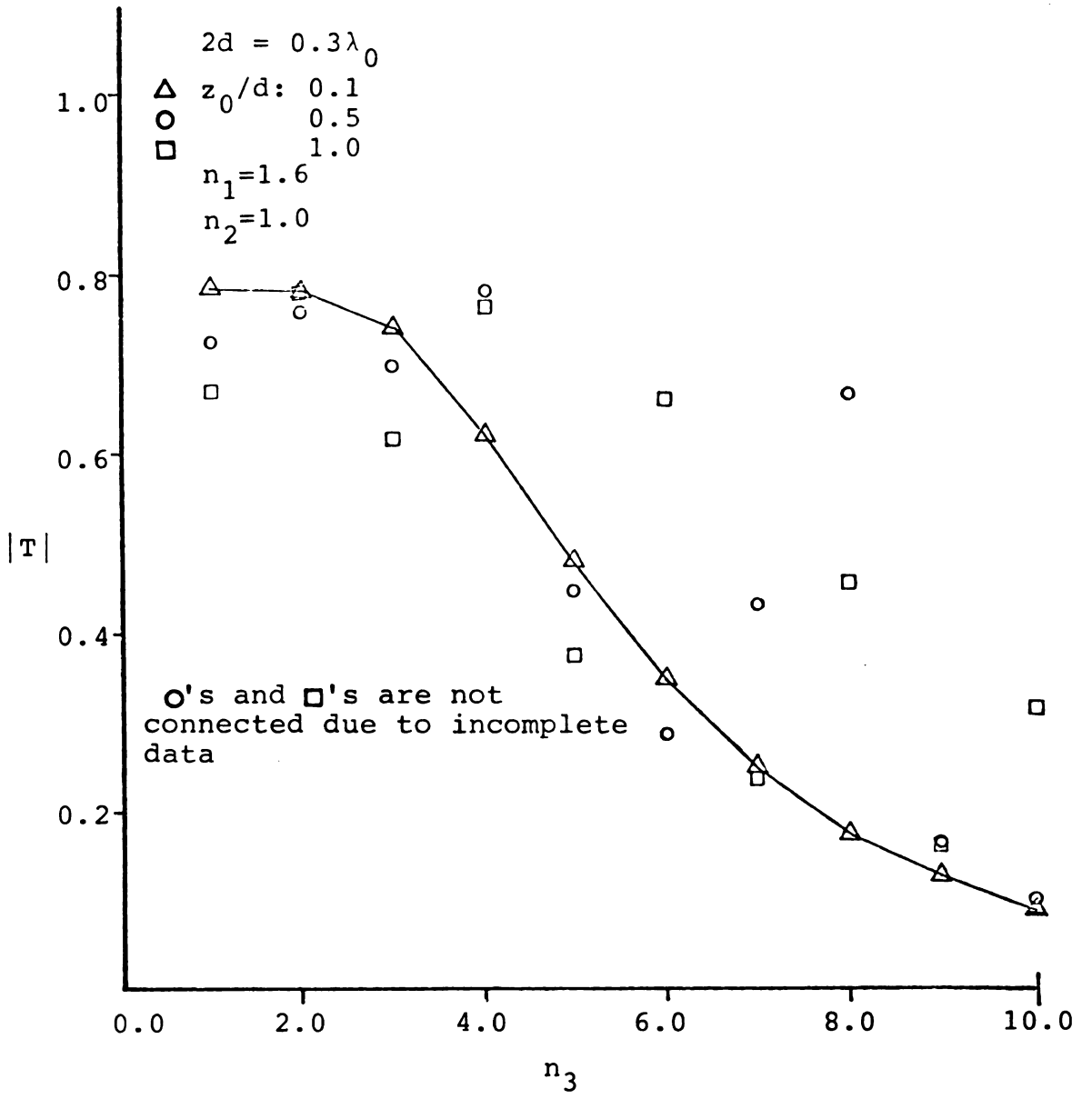

Figure 3.6 Magnitude of transmission coefficient as a function of its refractive index n_3 for three values of the normalized lengths of the slice-discontinuity region.

3.2.2 Approximate Solution for Radiating Discontinuity

When radiation coupling in the scattering process is considered, $\bar{E}(\bar{r})$ of (2.5.18) assumes that the discontinuity field maintains the eigenfield distribution and yet possesses axial propagation constant from the analytical radiationless solution. From the resulting matrix equation of (2.5.22) and (2.5.23)

$$\sum_{\ell=1}^{2} C_{p\ell} a_\ell = b_p \qquad p = 1,2$$

where the matrix elements, when specialized for a mono-mode slab waveguide, becomes (p=1,2)

$$c_{p1} = e_{y0}(x_p) e^{-j\beta_0' z_p} - \frac{jk_0}{z_0} \int_{LCS} \delta n^2(x') \bar{\bar{G}}(x_p, z_p | x', z') \times e_{y0}(x') e^{-j\beta_0' z'} \, dx'dz'$$

$$c_{p2} = e_{y0}(x_p) e^{+j\beta_0' z_p} - \frac{jk_0}{z_0} \int_{LCS} \delta n^2(x') \bar{\bar{G}}(x_p, z_p | x', z') \times e_{y0}(x') e^{+j\beta_0' z'} \, dx'dz'$$

$$b_p = E_0 e_{y0}(x_p) e^{-j\beta_0 z_p} \qquad (3.2.3)$$

Two matching points for the delta-function at $\bar{r}_p = (x_p, z_p) = (0, -z_0)$ and $(0, z_0)$ are selected for the calculation of two unknown coefficients a_1 and a_2. The results are shown in Figure 3.7 for the subsequently obtained values of $|R|$ and $|T|$; in the Figure, $z_0/d = 0.5$ is chosen in order to compare with results of analytical solution of the last section.

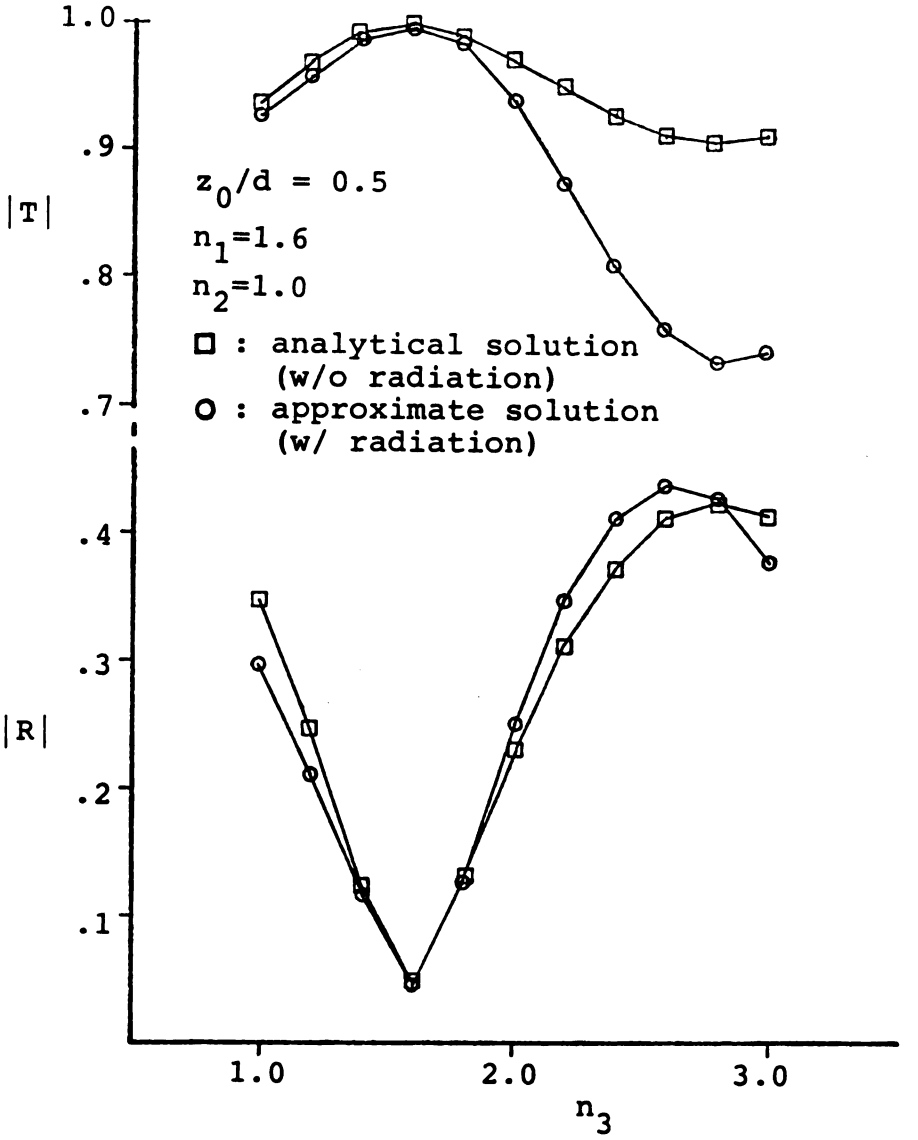

Figure 3.7 Comparison of reflection and transmission coefficients obtained for slice-discontinuity in a slab waveguide with $2d/\lambda_0$= 0.3.

Although the comparison shows no significant change in reflection coefficient between the two solutions, there is substantial increase of radiation when n_3 is greater than 2 (as can be seen from the sharp increase of transmission coefficient). Similar phenomenon exists in Figure 3.8 for discontinuity of smaller size ($z_0/d = 0.1$), there appear to have less amount of coupling to the radiation when n_3 increases from 2 to 3; this should be expected since discontinuity's size is now only 1.5% of the scattered wavelength ($2d = 0.3\lambda_0$).

3.3 Moment Method Numerical Solution

3.3.1 Discretization of scalar 2-d EFIE to MoM Matrix Equation

Refer to Figure 3.9, in which the region of discontinuity V_d is uniformly partitioned in both the x and z directions. The two-dimensional pulse-function expansion of unknown field $E_y(x,z)$ is defined as

$$E_y(x,z) = \sum_{n=1}^{N_p} E_n p_n(x,z) \qquad \text{with} \tag{3.3.1}$$

$$p_n(x,z) = \begin{cases} 1 \ \ldots \ \text{for } (x,z) \in (\Delta S)_n \\ 0 \ \ldots \ \text{for otherwise} \end{cases} \tag{3.3.2}$$

where N_p is the total number of partitioning with $N_p = N_x \times N_z$; N_x is the number of partitions of length $\Delta x = 2d/N_x$ along x; N_z is the number of partitions of length $\Delta z = 2z_0/N_z$

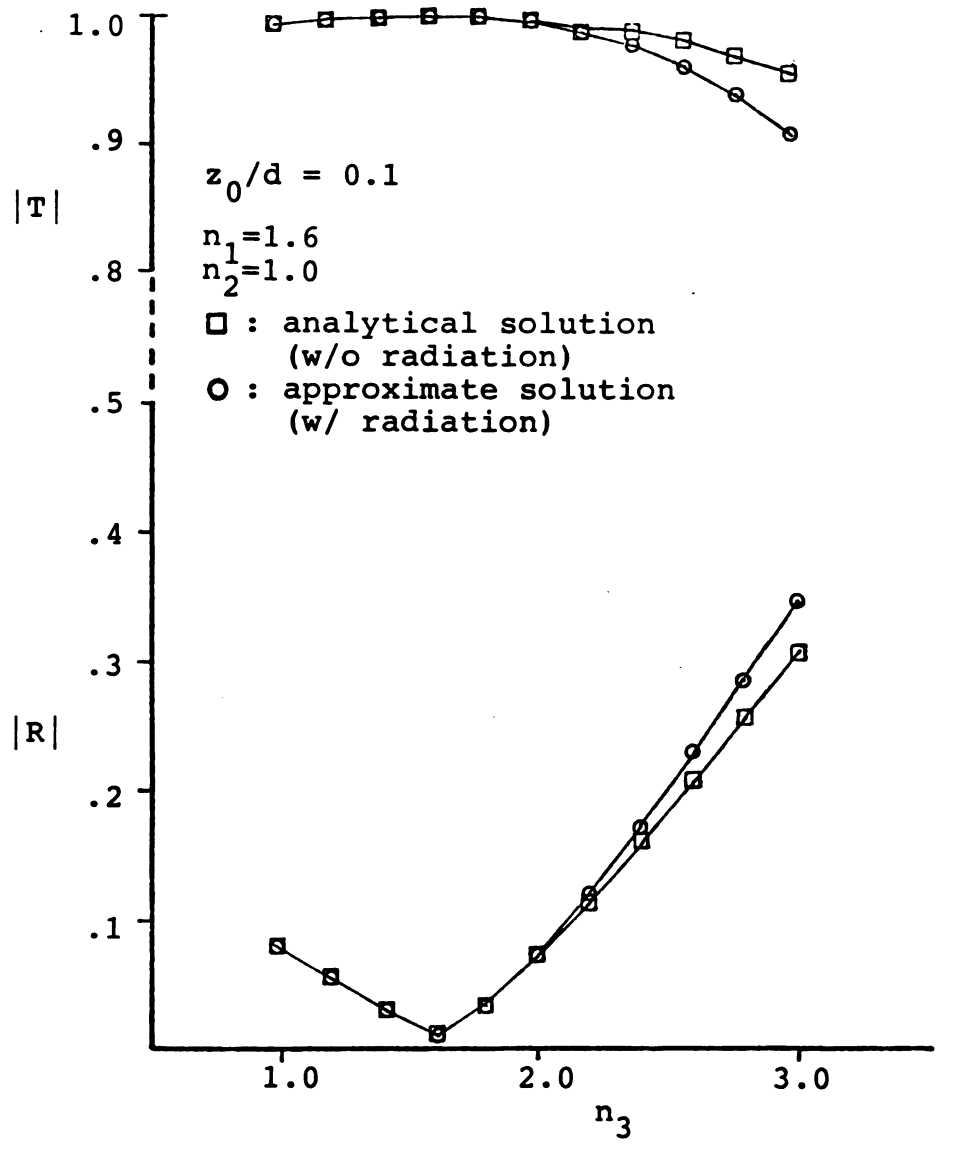

Figure 3.8 Comparison of reflection and transmission coefficients obtained for slice-discontinuity in a slab waveguide with $2d/\lambda_0$= 0.3.

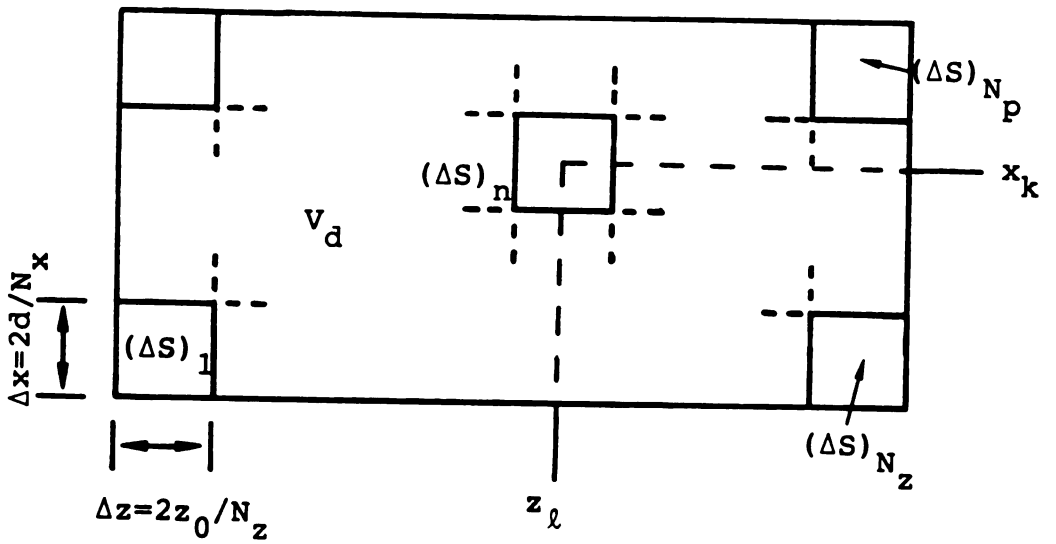

Figure 3.9 Partitions of slice-discontinuity region V_d for the application of Method of Moment solution.

along z. $(\Delta S)_n$ is the surface element centered at $\bar{\rho}=\bar{\rho}_n = \hat{x}x_k+\hat{z}z_\ell$ where $x_k = -d+(k-0.5)\Delta x$ and $z_\ell = -z_0+(\ell-0.5)\Delta z$; n is the running index covering all partitions, i.e., $n = k+(\ell-1)N_x$. From equation (2.5.25) the three-dimensional integral equation is then reduced to the following two-dimensional form for the slab waveguide

$$\sum_{n=1}^{N_p} E_n\left[P_n(x,z) - \frac{j\delta n^2 k_0}{z_0}\int_{(\Delta s)_n} G_{yy}(x,z|x',z')dx'dz'\right] = E_0 e_{y0}(x)e^{-j\beta_0 z} \tag{3.3.3}$$

Multiply (3.3.3) by the delta-funtion operator

$$\sum_{n=1}^{N_p}\int_{(\Delta s)_n}\delta(x-x_i,z-z_j)\{\quad\}\,dxdz\ , \tag{3.3.4}$$

this essentially forces IE (3.4.3) to be satisfied at discrete matching points (x_i,z_j) or at $\bar{\rho}_m=\hat{x}x_i+\hat{z}z_j$ where $m=i+(j-1)N_x$, $1\le i\le N_x$, and $1\le j\le N_z$; thus completing the discretization of the EFIE to yield N_p linear algebrac equations in E_n as

$$\sum_{n=1}^{N_p} E_n\left[P_n(\bar{\rho}_m) - \frac{j\delta n^2 k_0}{z_0}\int_{(\Delta s)_n} G_{yy}(x_i,z_j|x',z')dx'dz'\right] = E_0 e_{y0}(x_i)e^{-j\beta_0 z_j} \quad \text{... for } 1\le i\le N_x,\ 1\le j\le N_z\ . \tag{3.3.5}$$

With $p_n(\bar{\rho}_m)=\delta_{mn}$ from (3.3.2), above expression can be written in the more concise form

$$\sum_{n=1}^{N_p} A_{mn}E_n = B_m \quad \ldots \text{ for } m = 1,2, \ldots, N_p \tag{3.3.6}$$

or in matrix representation

$$\begin{bmatrix} \\ A_{mn} \\ \\ \end{bmatrix} \begin{bmatrix} \\ E_n \\ \\ \end{bmatrix} = \begin{bmatrix} \\ B_m \\ \\ \end{bmatrix} \tag{3.3.7}$$

where the elements A_{mn} of the N_x by N_z coefficient matrix are defined as

$$A_{mn} = \delta_{mn} - \frac{jk_0\delta n^2}{Z_0} \int_{(\Delta s)_n} G_{yy}(x_i,z_j|x',z')dx'dz' \tag{3.3.8}$$

and

$$B_m = E_0 e_{y0}(x_i) e^{-j\beta_0 z_j} \ . \tag{3.3.9}$$

The unknown expansion coefficients E_n can therefore be obtained as the non-trivial solutions from matrix equation (3.3.7).

To facilitate the numerical calculation, we can further decompose (3.3.8) into the sum of A^d_{mn}, the contribution from discrete modes and A^r_{mn}, that of continuous modes

$$A_{mn} = A^d_{mn} + A^r_{mn} \ . \tag{3.3.10}$$

By re-defining the integration limits to be the center of its respective cells

$$x_k^{\pm} = x_k \pm \Delta x/2$$
$$z_\ell^{\pm} = z_\ell \pm \Delta z/2 \ , \qquad (3.3.11)$$

A_{mn}^d can be evaluated over the longitudinal cross section area dx'dz' as follows

$$A_{mn}^d = \delta_{mn} - \frac{jk_0\delta n^2}{z_0}\int_{z_\ell^-}^{z_\ell^+}\int_{x_k^-}^{x_k^+} G_{yy}^d(x_i,z_j|x',z')dx'dz'$$

$$= \delta_{mn} + \frac{jk_0\delta n^2}{z_0}\int_{z_\ell^-}^{z_\ell^+}\int_{x_k^-}^{x_\ell^+} e_{y0}(x_i)e_{y0}(x')e^{-j\beta_0|z_j-z'|}dx'dz'$$

$$= \delta_{mn} + 2(n_3^2 - n_1^2)\left(\frac{k_0 d}{\beta_0 \bar{d}}\right)2\left\{\frac{\cos(\kappa dx_i)\cos(\kappa dx_k)\sin(\kappa d\Delta x/2)}{\left(\frac{\kappa d}{\gamma\bar{d}}\right)\cos^2(\kappa d) + \left[\kappa d + \frac{\sin(2\kappa d)}{2}\right]}\right\}$$

$$\times \begin{cases} je^{-j\beta_0 d|\tilde{z}_j - \tilde{z}_\ell|}\sin(\beta_0 d\Delta\tilde{z}/2) & \text{... for } \ell \neq j \\ (1 - e^{-j\beta_0 d\Delta\tilde{z}/2}) & \text{... for } \ell = j \end{cases}$$

(3.3.12)

where eigenfunction $e_{y0}(x)$ is expressed as (3.1.3) in the above derivation. It is noted that the final form of A_{mn}^d above is expressed in terms of normalized quantities, i.e., $\tilde{x}_i = x_i/d$, $\tilde{z}_j = z_j/d$, $\Delta\tilde{x} = \Delta x/d$ and $\Delta\tilde{z} = \Delta z/d$ as well as κd and γd,

for the convenience of numerical calculation. Following the same procedure, A^r_{mn} can be reduced to

$$A^r_{mn}$$

$$= \frac{jk_0\delta n^2}{4}\int_0^\infty Z_{TE}(\xi)\,d\xi \int_{z_\ell^-}^{z_\ell^+}\int_{x_k^-}^{x_k^+} e_y(x_i,\xi)e_y(x',\xi)e^{-j\beta(\xi)|z_j-z'|}\,dx'dz'$$

$$= \frac{2(n_3^2 - n_1^2)(k_0d)^2}{\pi}\int_0^\infty d\tilde{\xi}\tilde{\xi}^2 \frac{\cos(\tilde{\sigma}\tilde{x}_i)\cos(\tilde{\sigma}\tilde{x}_k)\sin(\tilde{\sigma}\Delta\tilde{x}/2)}{(\tilde{\xi}^2 + \tilde{\upsilon}^2\sin^2\tilde{\sigma})\tilde{\beta}^2\tilde{\sigma}}$$

$$\times \begin{cases} je^{-j\tilde{\beta}|\tilde{z}_j-\tilde{z}_\ell|}\sin(\tilde{\beta}\Delta\tilde{z}/2) & \text{... for } j \neq \ell \\ (1 - e^{-j\tilde{\beta}\Delta\tilde{z}/2}) & \text{... for } j = \ell \end{cases} \qquad (3.3.13)$$

with normalized variables $\tilde{\sigma}=\sigma d$, $\tilde{\xi}=\xi/d$ and $\tilde{\beta}=\beta d$. Also noted that the integrand in the above expression for A^r_{mn} has a singularity at $\tilde{\xi}=k_2d$, i.e., when $\tilde{\beta}=0$ since $\tilde{\xi}^2=(k_2d)^2 - \tilde{\beta}^2$ by definition. In order to evaluate this improper integral, let the integration be divided into three subintervals

$$\int_0^\infty \{\quad\} d\tilde{\xi} = \left[\int_0^{k_2d-\varepsilon} + \int_{k_2d-\varepsilon}^{k_2d+\varepsilon} + \int_{k_2d+\varepsilon}^\infty\right] R(\tilde{\xi})\,\frac{d\tilde{\xi}}{\tilde{\beta}^2} \begin{cases} j\sin(\tilde{\beta}\Delta\tilde{z}/2) & \text{... for } j \neq \ell \\ (1 - e^{-j\tilde{\beta}\Delta\tilde{z}/2}) & \text{... for } j = \ell \end{cases}$$

$$= I_1 + I_2 + I_3 \qquad (3.3.14)$$

where

$$R(\tilde{\xi}) = \frac{\tilde{\xi}^2 \cos(\tilde{\sigma}\tilde{x}_i)\cos(\tilde{\sigma}\tilde{x}_k)\sin(\tilde{\sigma}\tilde{\Delta}x/2)}{(\tilde{\xi}^2 + \tilde{\upsilon}^2 \sin\tilde{\sigma})\tilde{\sigma}}$$

$$\times \begin{cases} e^{-j\tilde{\beta}|\tilde{z}_j - \tilde{z}_\ell|} & \ldots \text{ for } j \neq \ell \\ 1 & \ldots \text{ for } j = \ell \end{cases}$$

(3.3.15)

In the limit as $\tilde{\beta} \to 0$, $R(\tilde{\xi})$ is regarded as a constant, taking its value at $\tilde{\xi} = k_2 d$. Furthermore,

$$\lim_{\tilde{\beta}\to 0} j \sin(\tilde{\beta}\Delta\tilde{z}/2) = j\tilde{\beta}\Delta\tilde{z}/2 \quad \text{and}$$

$$\lim_{\tilde{\beta}\to 0} (1 - e^{-j\tilde{\beta}\Delta\tilde{z}/2}) = j\tilde{\beta}\Delta\tilde{z}/2 \ ,$$

I_2 of (3.3.14) then becomes

$$\lim_{\tilde{\beta}\to 0} I_2 = \frac{j\Delta\tilde{z}R(k_2 d)}{2} \int_{k_2 d-\varepsilon}^{k_2 d+\varepsilon} \frac{d\tilde{\xi}}{\tilde{\beta}}$$

$$= \frac{j\Delta\tilde{z}R(k_2 d)}{2} \left[\int_{k_2 d-\varepsilon}^{k_2 d} \frac{d\tilde{\xi}}{\sqrt{(k_2 d)^2 - \tilde{\xi}^2}} \right.$$

$$\left. + \int_{k_2 d}^{k_2 d+\varepsilon} \frac{d\tilde{\xi}}{\sqrt{\tilde{\xi}^2 - (k_2 d)^2}} \right] .$$

(3.3.16)

Both integrations in (3.3.16) above can be evaluated by changing the variables: $\tilde{\xi} = k_2 d\sin t$ in the first and $\tilde{\xi} = k_2 d\cosh t$ in the second to yield

$$\lim_{0} I_2 = \frac{j\Delta\tilde{z}R(k_2d)}{2}\left[\frac{\pi}{2} - \sin^{-1}(1 - \frac{\varepsilon}{k_2d}) + j\cosh^{-1}(1 + \frac{\varepsilon}{k_2d})\right] . \tag{3.3.17}$$

Finally A^r_{mn} has the form

$$A^r_{mn} = \frac{2(n_3^2 - n_1^2)(k_0d)^2}{\pi}(I_1 + I_2 + I_3) , \tag{3.3.18}$$

with I_2 shown in (3.3.17), I_1 and I_3 can be written from (3.3.14) and (3.3.15) as

$$I_1 = \int_0^{k_2d-\varepsilon} \frac{d\tilde{\xi}}{\tilde{\beta}^2} R(\tilde{\xi}) \begin{cases} j\sin(\tilde{\beta}\Delta\tilde{z}/2) & \text{... for } j \neq \ell \\ (1 - e^{-j\tilde{\beta}\Delta\tilde{z}/2}) & \text{... for } j = \ell \end{cases} \tag{3.3.19}$$

$$I_3 = \int_{k_2d+\varepsilon}^{\infty} \frac{d\tilde{\xi}}{\tilde{\beta}^2} R(\tilde{\xi}) \begin{cases} j\sin(\tilde{\beta}\Delta\tilde{z}/2) & \text{... for } j \neq \ell \\ (1 - e^{-j\tilde{\beta}\Delta\tilde{z}/2}) & \text{... for } j = \ell \end{cases} \tag{3.3.20}$$

where the infinite upper limit of I_3 integral is replaced by a finite value in the numerical process as long as sufficient convergence of end result is obtained.

3.3.2 Numerical Results

MONO-MODE SLAB WAVEGUIDE

First to be studied is a slab waveguide with refractive indices $n_1 = 1.6$ for the core region, $n_2 = 1.0$ for the cladding and $n_3 = 3.0$ for the slice discontinuity. With other guide parameters also indicated, Figure 3.10 shows the distribution of $E_y(x,z)$, the field inside the dielectric slice discontinuity region, in the transverse cross section at various axial locations. It is evident that the almost uniform distribution of E_y near the entrance plane at $z/z_0 = -0.875$ as compared with those toward the exit plane which possess a cosine type distribution leads to a prediction that strong radiation is expected at the slab-discontinuity interface. This is verified from Table 3.1 that indeed a relative radiated power of 24% is obtained. Listed in Table 3.1 are values of reflection and transmission coefficients and its relative powers including the radiated powers for various value of parameters; Of all the cases calculated, shown here are primarily the cases of $n_3 = 1$ and 3, each with two axial discontinuity lengthes, 0.1 and 0.5. Results obtained from approximate solutions of Section 3.2 (both radiationless, $G^r_{yy}=0$, and radiating, $G^r_{yy}\neq 0$) are also included for comparison.

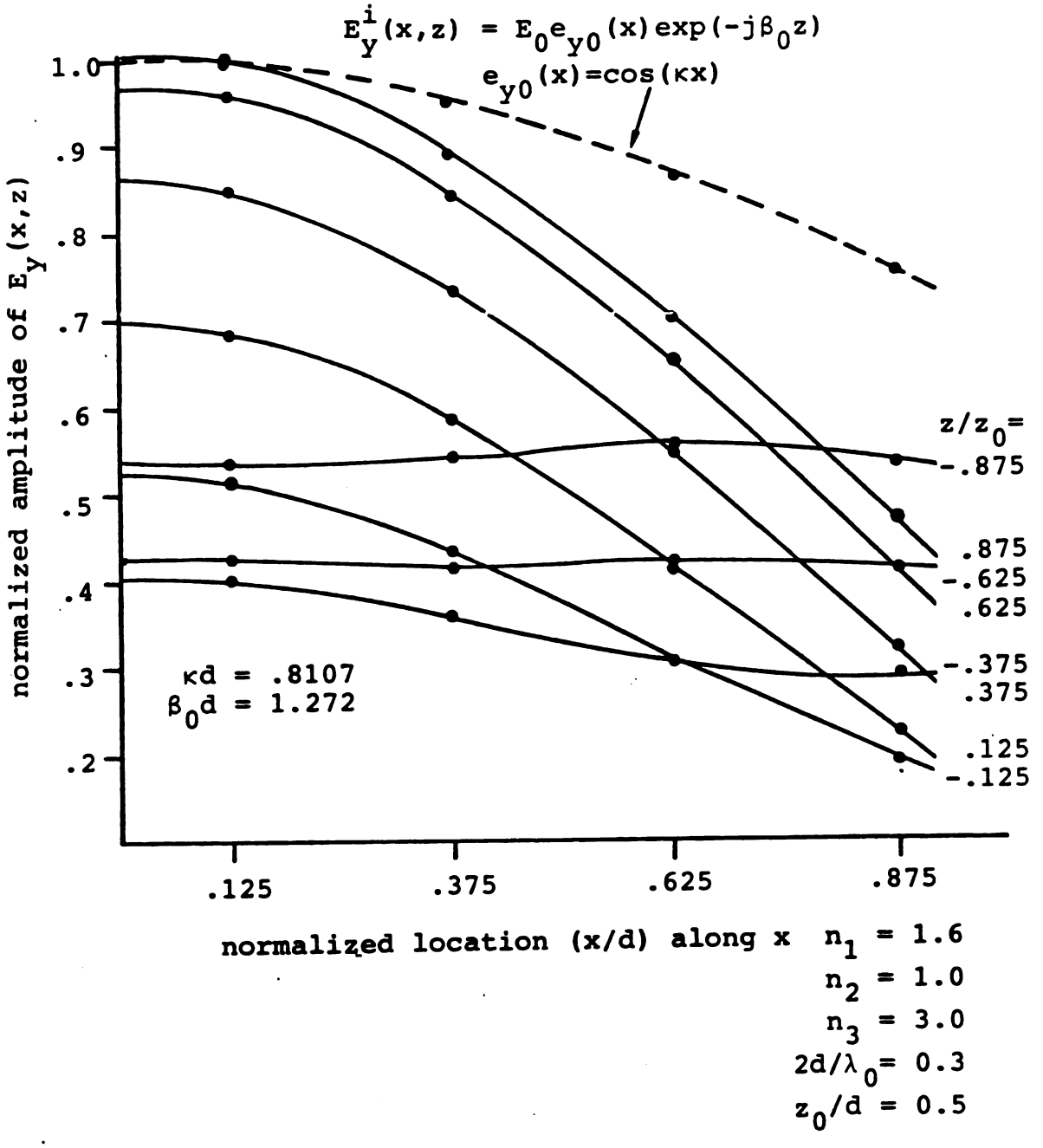

Figure 3.10 Distribution of field $E_y(x,z)$ excited in the slice-discontinuity region of slab waveguide by TE_0 incident mode wave.

Table 3.1 Reflection and transmission coefficients for TE_0 slab-waveguide mode incident upon dielectric-slice discontinuity of various configurations, as calculated by several methods; resulting reflected, transmitted, and radiated powers included. ($2d/\lambda_0=0.3$, $n_1=1.6, n_2=1.0$)

CONFIGURATION AND TYPE OF SOLUTIONS	R_0	T_0	R_0^2	T_0^2	$1-R_0^2-T_0^2$
$n_3=1.0$ $z_0/d=0.1$ analytical					
($G_r=0$)	.08050	.9968	.00648	.9936	-.000090
approximate					
($G_r\neq0$)	.0782	.9956	.0061	.9912	.0027
MoM ($G_r=0$)	.08072	.9967	.00651	.9934	.000073
MoM ($G_r\neq0$)	.07871	.9956	.00620	.9912	.002585
$n_3=3.0$ $z_0/d=0.1$ analytical					
($G_r=0$)	.3063	.9519	.0936	.9061	.000067
approximate					
($G_r\neq0$)	.3459	.9029	.1196	.8152	.0651
MoM ($G_r=0$)	.3071	.9518	.0943	.9059	-.000234
MoM ($G_r\neq0$)	.3288	.9203	.1081	.8470	.044938
$n_3=1.0$ $z_0/d=0.5$ analytical					
($G_r=0$)	.3445	.9388	.1187	.8813	-.000026
approximate					
($G_r\neq0$)	.2972	.9319	.0883	.8684	.0432
MoM ($G_r=0$)	.3465	.9385	.1201	.8808	-.000845
MoM ($G_r\neq0$)	.3047	.9247	.0928	.8551	.052088
$n_3=3.0$ $z_0/d=0.5$ analytical					
($G_r=0$)	.4137	.9104	.1711	.8288	.000024
approximate					
($G_r\neq0$)	.3698	.7459	.1367	.5564	.3069
MoM ($G_r=0$)	.4186	.9098	.1752	.8277	-.000296
MoM ($G_r\neq0$)	.4482	.7482	.2009	.5598	.239313

Note that the results of the radiationless analytical and MoM solutions agree perfectly (as they should), thus confirming the correctness of both; the small (positive and negative) radiated powers are due here totally to numerical truncation errors. Discrepancies between the accurate radiating and approximate radiationless results increase with the "strength" of the discontinuity; radiation increase for "stronger" discontinuities with progression downward in Table 3.1. These results indicate those paramaters which constitute a "strong" discontinuity as well as conditions for a "small" discontinuity where either the closed-form radiationless solution or the approximate solution with radiation might be adequate.

DUAL-MODE SLAB WAVEGUIDE

Here the MoM solutions is implemented to study the mode conversion process discussed in Section 2.4, several waveguide parameters are chosen to allow the excitation of two principal modes, the TE_0 and TE_2 modes. Assuming a TE_0 mode incidence, the results are shown in Figure 3.11 through 3.13. The plot of axial variations of $E_y(x,z)$ in Figure 3.11 for the low contrast case of ($\delta n = 0.15$) shows the increase of standing wave pattern as well as rapid phase change in longitudinal direction when the length of the discontinuity z_0/d is extended from a value of 0.1 to 0.5. As a comparison, the cases of higher contrast ($\delta n = 1.4$) is shown in Figure 3.12 with $z_0/d = 0.2$ and 0.4. While holding

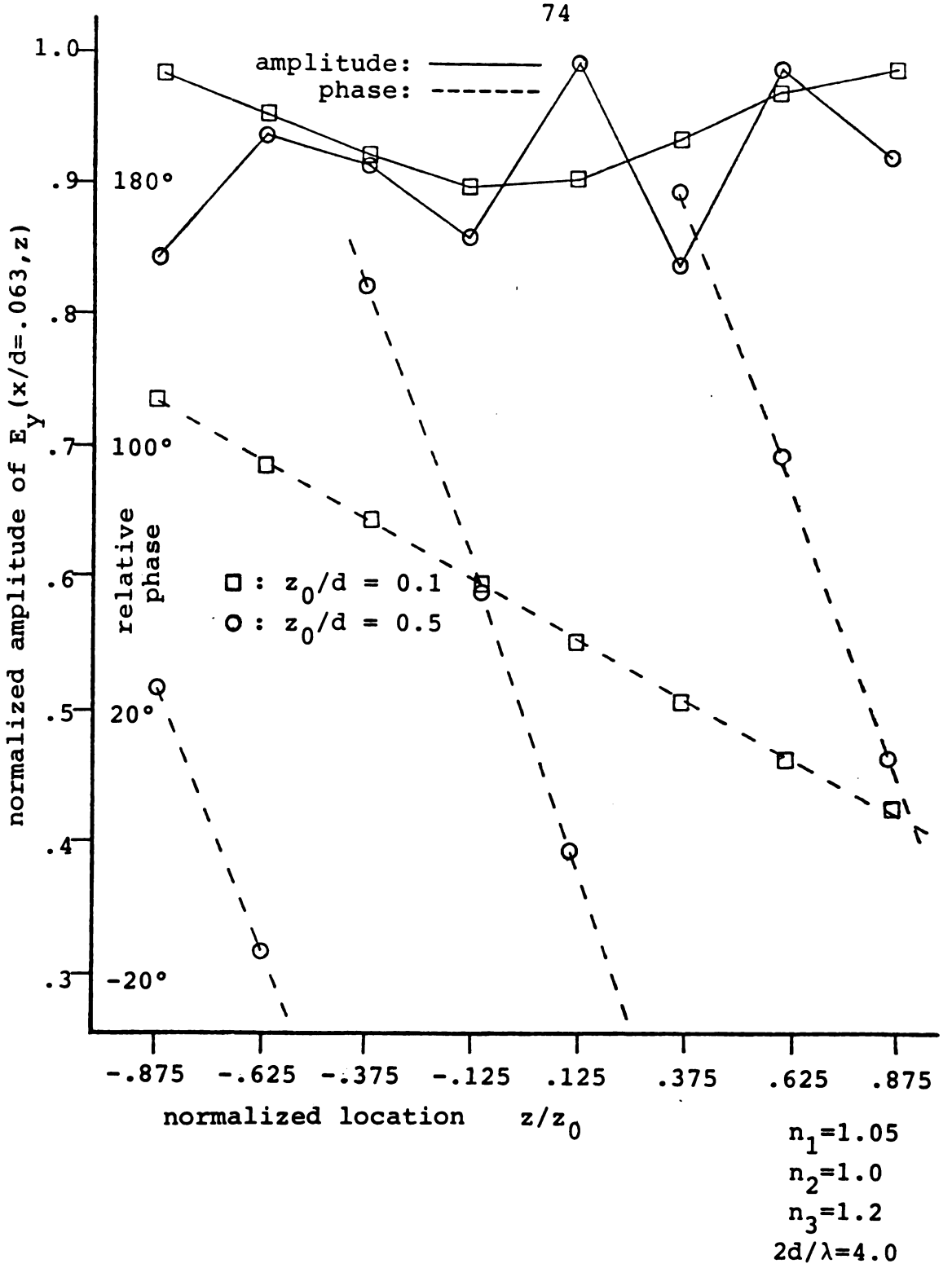

Figure 3.11 Relative amplitudes and phases of fields in the slice-discontinuity region as a function of normalized axial locations. The slab supports dual modes with a TE_0 mode incident.

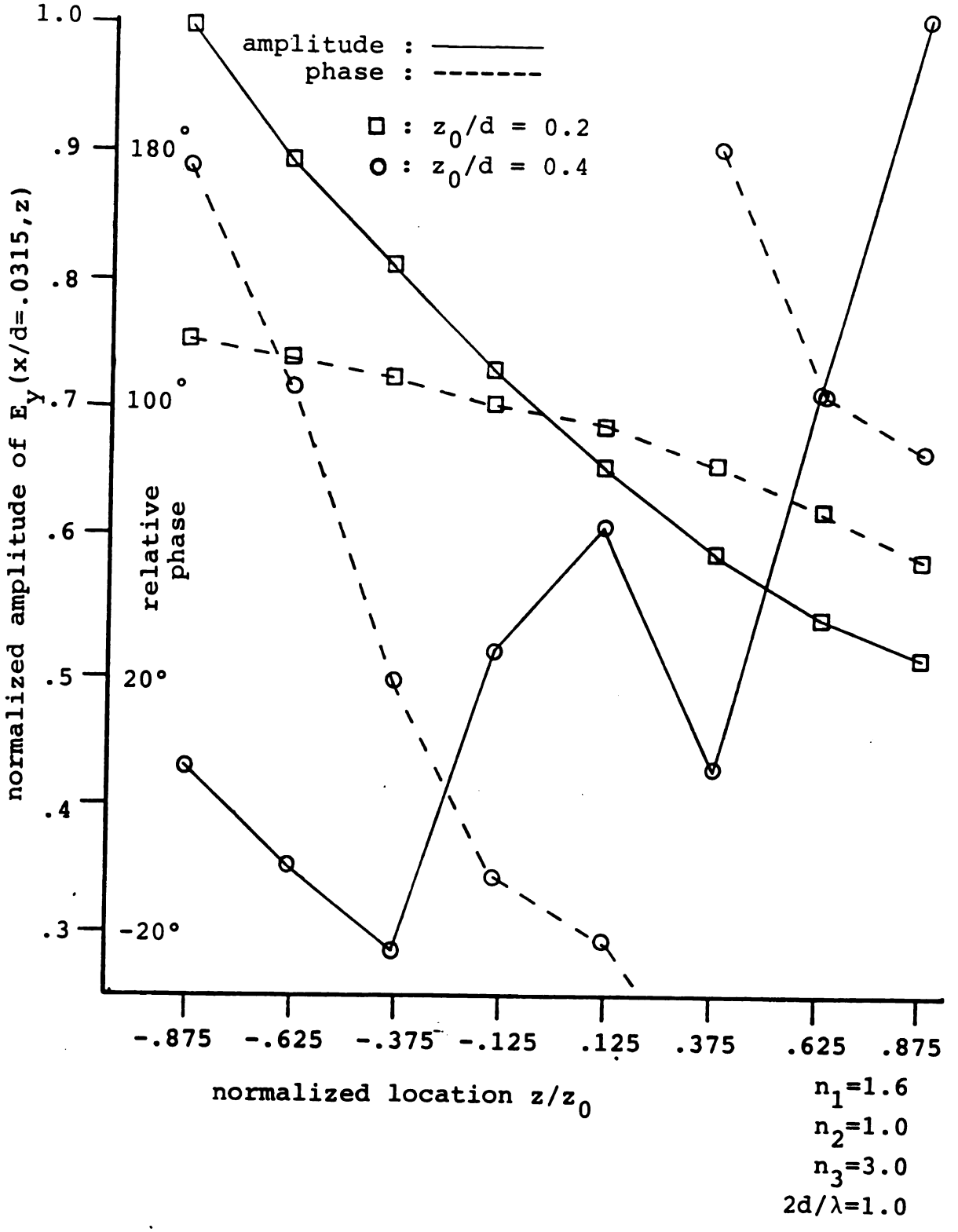

Figure 3.12 Relative amplitude and phases of fields in the slice-discontinuity region as a function of normalized axial locations. The slab supports dual modes with a TE_0 mode incident.

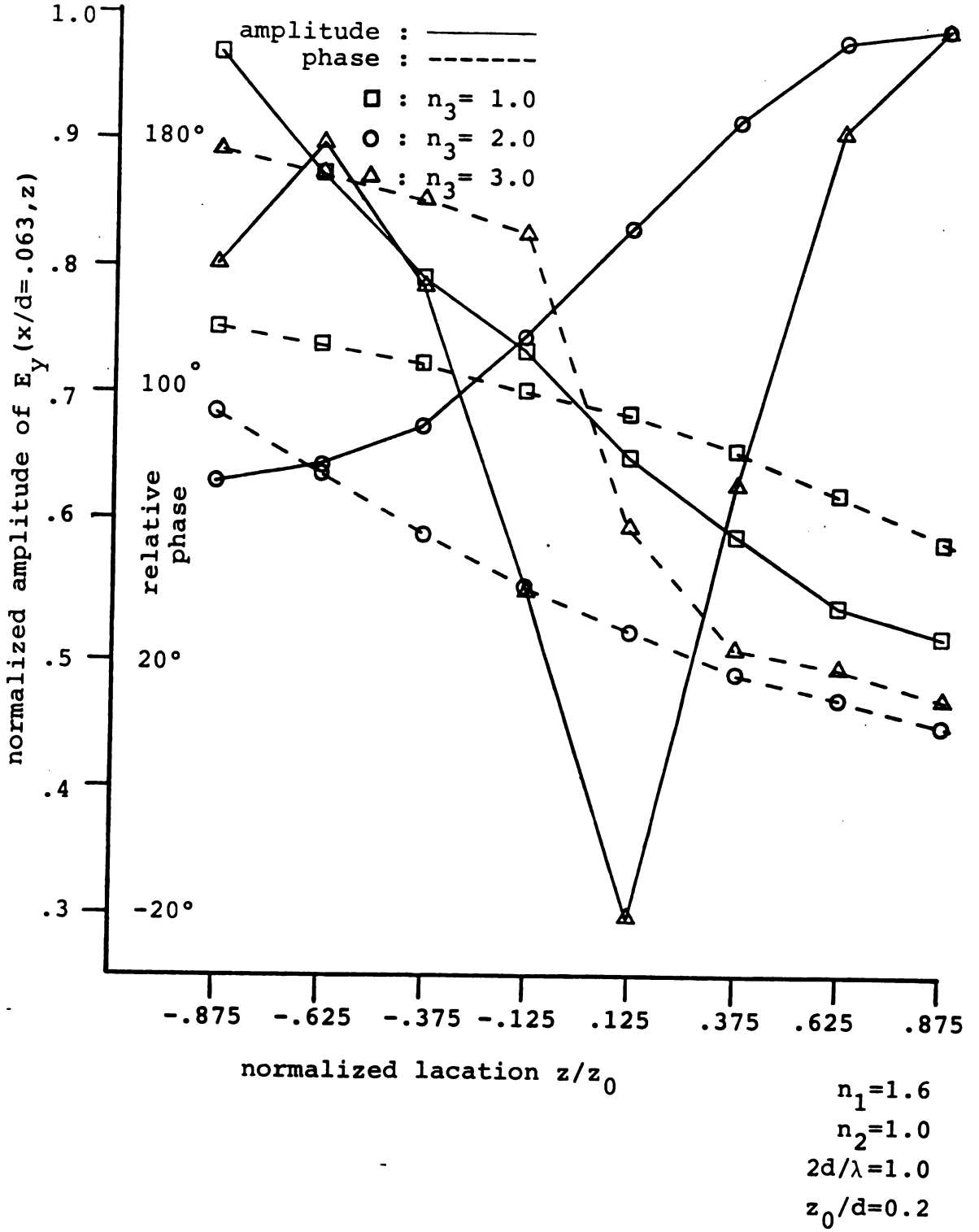

Figure 3.13 Relative amplitudes and phases in the slice-discontinuity region with various indices for the slice region, as a function of normalized axial lications. The slab supports dual-mode propagation.

z_0/d constant and varying n_3, Figure 3.13 shows the existence of a stronger axial standing wave for $n_3 = 3.0$ and is also evident from Table 3.2, there it shows a 32.4% of radiated power. A study of Table 3.2 reveals that when z_0/d is changed from 0.2 to 0.4, there is a increase of mode conversion from TE_0 to TE_2 mode, as evident from the almost equal percentage content of reflected and transmitted power in TE_2 mode; in fact, more power is converted to TE_2 mode and transmitted than TE_0 mode, at the same time, radiated power is decreased by nearly 79%. Different phenomenon is seen in changing n_3 from the value of 1.0 to 2.0, in that the reflected power of TE_2 mode is greatly reduced when compared to that of TE_0 mode as well as the transmitted power is dominated by incident TE_0 mode; accompanied with slight increase in radiated power.

As a final observation, despite the infinite upper limit involved in the continuous spectrum integral I_3 of (3.3.20), no difficulty was encountered in obtaining adequate convergence in all the above MoM results. Moreover, various partitioning for the discontinuity region ranging from 4 by 8 to 8 by 16 (leads to a 128 by 128 matrix elements) rectangular cells were used and less than 60 seconds of computing time on the MSU CDC Cyber 750 system was consumed for each case. (source listing and sample output attached as Appendix A and B).

Table 3.2 Mode conversion coefficients (reflection and transmission) for TE_0 slab-waveguide mode incident upon dielectric-slice discontinuity of various configurations; slab width is such that it supports the propagation of TE_0 and TE_2 modes.

CONFIGURATIONS	z_0/d	R_0/R_2	T_0/T_2	% power radiated
n_1= 1.6	.025	.297/.019	.953/.019	.2
n_2= 1.0	.075	.556/.068	.815/.074	1.65
n_3= 3.0	.2	.259/.251	.608/.42	32.4
d/λ_0= 0.5	.4	.42 /.39	.51 /.58	6.96
	n_3			
n_1= 1.6	1.0	.197/.123	.899/.145	11.76
n_2= 1.0	2.0	.136/.0226	.920/.092	12.6
d/λ_0= 0.5	3.0	.259/.251	.608/.42	32.4
z_0/d= 0.2				

3.4 Iterative Solution

The $\ell+1$'th iterative solution $\bar{E}_{\ell+1}(\bar{r})$ to EFIE (2.2.16) has the form

$$\bar{E}_{\ell+1}(\bar{r}) = \bar{E}^{i}(\bar{r}) + \frac{jk_0}{Z_0}\int_{V_d} \delta n^2(\bar{r}')\bar{\bar{G}}(\bar{r}|\bar{r}') \cdot \bar{E}_{\ell}(\bar{r})dV' \ . \tag{2.5.30}$$

when the longitudinal cross sectional discontinuity is again partitioned as indicated in Figure 3.9, the above IE can be discretized for the field at (x_m, z_n) as

$$\bar{E}_{\ell+1}(x_m,z_n = \bar{E}^{i}(x_m,z_n) + \frac{jk_0}{Z_0}\sum_{j=1}^{N_z}\sum_{i=1}^{N_x} \delta n^2(x_i,z_j)$$

$$\times \bar{\bar{G}}(x_m,z_n|x_i,z_j) \cdot \bar{E}_{\ell}(x_i,z_j)\Delta x\Delta z$$

$$\ldots \text{ for } (x_m,z_n) \in \text{LCS}. \tag{3.4.1}$$

By substituting Green's function (3.1.16) appropriate for the mono-mode slab waveguide, (3.1.3) and (3.1.6) for $e_{y0}(x)$, and $e_y(x,\xi)$ respectively, into (3.4.1), it yields

$$E_{\ell+1}(x_m,z_n) = E^{i}(x_m,z_n)$$

$$- \frac{jk_0}{Z_0} A^2 \cos\kappa x_m \sum_{j=1}^{N_z}\sum_{i=1}^{N_x} \delta n^2(x_i,z_j)E_{\ell}(x_i,z_j)$$

$$\times \cos\kappa x_i \, e^{-j\beta_0|z_n-z_j|}\Delta x\Delta z$$

$$- \frac{jk_0^2}{2\pi} \sum_{j=1}^{N_z} \sum_{i=1}^{N_x} \delta n^2(x_i, z_j) E_\ell(x_i, z_j)$$

$$\times \left\{ \left[\int_0^{k_2-\varepsilon} + \int_{k_2-\varepsilon}^{\infty} \right] \frac{\cos\sigma x_i \cos\sigma x_m}{\beta(\xi) c^2(\xi)} e^{-j\beta(\xi)|z_n - z_j|} \, d\xi \right.$$

$$+ R(\xi = k_2) \left[\frac{\pi}{2} - \sin^{-1}\left(1 - \frac{\varepsilon}{k_2}\right) + j \cosh^{-1}\left(1 + \frac{\varepsilon}{k_2}\right) \right.$$

$$\left. \left. - 2j|z_n - z_j|\varepsilon \right] \right\} \Delta x \Delta z$$

$$\ldots \text{ for } m = 1,2, \ldots, N_x$$

$$n = 1,2, \ldots, N_z$$

(3.4.2)

where

$$R(\xi = k_2) = \left. \frac{\cos\sigma x_i \, \cos\sigma x_m}{c^2(\xi)} \right|_{\xi = k_2} .$$

With incident field E^i, chosen as the initial 0'th order solution as discussed in Section 2.5, such that

$$E_{\ell=0}(x_i, z_j) = E_0 A \cos\kappa x_i \, e^{-j\beta_0 z_j} ,$$

(3.4.3)

$E_1(x_m, z_n)$ can then be obtained from (3.4.2) and (3.4.3). Subsequent iteration will yield $E_2(x_m, z_n)$ and $E_3(x_m, z_n)$ etc. until convergent results are obtained.

NUMERICAL RESULTS

Several cases which were included in Table 3.2 (n_1= 1.6, n_2=1.0, n_3=3.0) are calculated. Listed below are number of iterations required for the total unknown field $E_{\ell+1}$ to converge to within 1% of E_ℓ, using the incident field as the 0'th iteration field.

		no. of iterations
I. d/λ_0=0.15	z_0/d=0.2	5
	0.3	6
II. d/λ_0=0.5	z_0/d=0.025	5
	0.075	6
	0.1	7

Worth noting from above results are that cases II support dual mode propagation yet the number of iteration required are not significantly increased due to 'small' discontinuity. Since most of the time is consumed in the calculation of Green's functions for all the partitions (average 30 seconds on Cyber 750), the time required for iterative process is far less in comparison. However, for larger discontinuities, a good initial estimate for the 0'th iteration field in addition to sufficient partitions are necessary for the correct converged results (when compared with that obtained by MoM). (source listing and sample output attached as Appendix C and D).

CHAPTER IV

INTEGRAL-OPERATOR FORMULATION OF COUPLED DIELECTRIC WAVEGUIDE SYSTEM

In open-boundary waveguide circuits, dispersion characteristics of the guided-wave modes are required to determine bandwidth and signal distortion, while the field distributions of these modes must be quantified to predict their interaction with other devices and excitation through coupling to other waveguides. Particularly, in optical communication, it is desirable to bunch many optical fibers into one cable; because of their proximity, the individual waveguides can exchange power, so that some part of signal that is being transmitted in one guide can enter a neighboring guide and interfere with the signal that is being transmitted there. In other applications, such as the directional coupler, waveguide coupling offers the possibility to feed power from one guide into another in a controlled manner.

In this chapter, a coupled multi-waveguide system is studied. The description of a single isolated waveguide, based upon an electric field integral-equation formulation for its unknown core field is first presented based upon an induced equivalent polarization current [14] and an electric

Green's dyadic as its kernel. This is followed by the generalization of that formulation to a system of N coupled waveguides. Polarization sources which radiate into the unbounded region and maintain the total field in the coupled system are identified. Homogeneous EFIE's for natural surface-wave modes supported by the coupled system are obtained. When the coupling is weak, assuming that field distributions in each individual guide do not change significantly from those of the isolate guide, a perturbation formulation is developed to obtain an approximate solution for the system-mode propagation constants and coupling coefficients.

4.1 Equivalent Polarization Description of Heterogeneous Waveguide Core

The Maxwell's equations appropriate for the description of electromagnetic fields $\bar{E}(\bar{r})$ and $\bar{H}(\bar{r})$ maintained in the heterogeneous waveguiding system by $\bar{P}^e$, the impressed polarization source density are

$$\nabla \cdot (\varepsilon \bar{E}) = - \nabla \cdot \bar{P}^e$$

$$\nabla \times \bar{E} = j\omega\mu_0 \bar{H}$$

$$\nabla \times \bar{H} = j\omega \bar{P}^e + j\omega\varepsilon \bar{E}$$

$$\nabla \cdot \bar{H} = 0 \qquad (4.1.1)$$

where the nature of low-loss dielectric media (graded-index

core and surround) is represented through the complex permittivity $\varepsilon(\bar{r})=\varepsilon'(\bar{r})-j\,\varepsilon''(\bar{r})$ with $\varepsilon''(\bar{r})=\sigma(\bar{r})/\omega\varepsilon'$ where $\sigma(\bar{r})$ is the conductivity of the material. An equivalent polarization density, which is induced due to the permittivity contrast between the graded-index core and its background surround cladding, can be identified from equation (4.1.1). If terms involving the permittivity ε_c of the surround are added and substracted in Maxwell's equations, they can be placed in the form

$$\nabla \cdot \left[\varepsilon_c \bar{E} + (\varepsilon - \varepsilon_c)\bar{E}\right] = - \nabla \cdot \bar{P}^e$$

$$\nabla \times \bar{E} = - j\omega\mu_0 \bar{H}$$

$$\nabla \times \bar{H} = j\omega \bar{P}^e + j\omega(\varepsilon - \varepsilon_c)\bar{E} + j\omega\varepsilon_c \bar{E}$$

$$\nabla \cdot \bar{H} = 0 \ .$$

The equivalent polarization is consequently identified as

$$\bar{P}_{eq} = \delta\varepsilon(\bar{r})\bar{E} = \left[\varepsilon(\bar{r}) - \varepsilon_c\right]\bar{E} \ . \qquad (4.1.2)$$

Thus when the system (4.1.1) is rearranged to emphasize the total effective source densities, the Maxwell's equations become

$$\nabla \cdot (\varepsilon_c \bar{E}) = - \nabla \cdot (\bar{P}^e + \bar{P}_{eq})$$

$$\nabla \times \bar{E} = - j\omega\mu_0 \bar{H}$$

$$\nabla \times \bar{H} = j\omega(\bar{P}^e + \bar{P}_{eq}) + j\omega\varepsilon_c \bar{E}$$

$$\nabla \cdot \bar{H} = 0 \qquad (4.1.3)$$

Applying a curl operation to Faraday's law in equations (4.1.3) followed by the substitution of Ampere's Law, leads to the well known wave equation for the electric field E(r)

$$\nabla \times \nabla \times \bar{E} - k_c^2 \bar{E} = \omega^2 \mu_0 (\bar{P}^e + \bar{P}_{eq}) \quad . \tag{4.1.4}$$

where $k_c = \omega\sqrt{\mu_0 \varepsilon_c} = n_c k_0$, is the wavenumber of the surround cladding of refractive index n_c. Expression (4.1.4) indicates that total field $\bar{E}$ along the waveguiding system is maintained by primary source $\bar{P}^e$ augumented by equivalent, induced $\bar{P}_{eq}$ both radiating into a uniform, unbounded region with wavenumber k_c. It is through this interpretation of equation (4.1.4) that the original problem involving a bounded, graded-index dielectric waveguiding structure has been replaced by an equivalent polarization density $\bar{P}_{eq}$ radiating into an unbounded surround medium. Equivalent induced polarization $\bar{P}_{eq} = \varepsilon_0 \delta n^2(\bar{r}) \bar{E}$ is proportional to total field $\bar{E}$ in the waveguide core region V; it is non-zero only in that core region where index contrast $\delta n^2(\bar{r}) = n^2(\bar{r}) - n_c^2$ is non-vanishing, i.e., for points $\bar{r} \in V$ where $\delta n^2 \neq 0$.

4.2 Electric Field Integral Equation Description for Guided Waves Supported by Open-Boundary Dielectric Waveguide System

The electric type Hertzian potential $\bar{\Pi}$, which is maintained by the total effective polarization density $\bar{P}_{tot} = \bar{P}^e + \bar{P}_{eq}$ embedded in a uniform medium of permittivity

ε_c satisfies the vector Helmholtz equation

$$\nabla^2\bar{\Pi} + k_c^2\bar{\Pi} = -\frac{\bar{P}_{tot}}{\varepsilon_c} \quad . \tag{4.2.1}$$

It is therefore appropriate to express the EM fields in the unbound region of homogeneous surround as [52]

$$\bar{E} = \nabla(\nabla \cdot \bar{\Pi}) + k_c^2\Pi$$

$$\bar{H} = j\omega\varepsilon_c\nabla \times \bar{\Pi} \quad . \tag{4.2.2}$$

The solution for Hertzian potential in the above three-dimensional Helmholtz equation is

$$\bar{\Pi} = \int_V \frac{\bar{P}_{tot}(\bar{r}')}{\varepsilon_c} G(\bar{r}|\bar{r}')dV' \tag{4.2.3}$$

with the well-known scalar, 3-d Green's function for an unbounded medium

$$G(\bar{r}|\bar{r}') = \frac{e^{-jk_cR(\bar{r},\bar{r}')}}{4\pi R(\bar{r},\bar{r}')} \tag{4.2.4}$$

where $R=|\bar{r} - \bar{r}'|$ is the distance between a source point at $\bar{r}'$ and the field point at $\bar{r}$. Therefore (4.2.2) can be written in the form of linear Integral Operator as

$$\bar{E}(\bar{r}) = \mathcal{L}\left\{\bar{P}_{tot}(\bar{r})\right\}$$

$$= (\nabla\nabla\cdot + k_c^2)\int_V \frac{\bar{P}_{tot}(\bar{r}')}{\varepsilon_c} G(\bar{r}|\bar{r}')dV' \ . \tag{4.2.5}$$

The fact that primary, impressed polarization $\bar{P}^e$ maintains an incident field $\bar{E}^i(\bar{r})$ while secondary, induced polarization $\bar{P}_{eq}$ excites the scattered field $\bar{E}^s(\bar{r})$ due to the non-uniform waveguiding region motivates the following field decomposition [53]

$$\bar{E}(\bar{r}) = \bar{E}^i(\bar{r}) + \bar{E}^s(\bar{r})$$

$$= \mathcal{L}\left\{\bar{P}^e(\bar{r})\right\} + \mathcal{L}\left\{\bar{P}_{eq}(\bar{r})\right\} \tag{4.2.6}$$

which leads to the 3-d, linear integral-operator equation

$$\bar{E}(\bar{r}) - \mathcal{L}\left\{\bar{P}_{eq}(\bar{r})\right\} = \bar{E}^i(\bar{r}) \ . \tag{4.2.7}$$

Substitution of $\mathcal{L}$ from definition (4.2.5) and $\bar{P}_{eq} = \delta\varepsilon\bar{E}$ into operator equation (4.2.7) leads to

$$\bar{E}(\bar{r}) - (\nabla\nabla\cdot + k_c^2)\int_V \frac{\delta\varepsilon(\bar{r}')}{\varepsilon_c} E(\bar{r}')G(\bar{r}|\bar{r}')dV' = \bar{E}^i(\bar{r}) \ . \tag{4.2.8}$$

where refractive indices satisfy $\varepsilon = n^2\varepsilon_0$, $\varepsilon_c = n_c^2\varepsilon_0$ and

$\delta\varepsilon=\varepsilon_0(n^2-n_c^2) = \varepsilon_0\delta n^2$. In terms of spatially dependent wavenumber quantities defined as $k^2=n^2k_0^2$, $k_c^2=n_c^2k_0^2$ and $\delta k^2=k^2-k_c^2$, integral equation (4.2.8) becomes

$$\bar{E}(\bar{r}) - (k_c^2 + \nabla\nabla\cdot)\int_V \frac{\delta k^2(\bar{r}')}{k_c^2}\,\bar{E}(\bar{r}')\bar{\bar{G}}(\bar{r}|\bar{r}')dV' = \bar{E}^i(\bar{r})$$

$$\ldots \text{ for } \bar{r}\in V \tag{4.2.9}$$

where V is that waveguiding region where $\delta n^2\neq 0$ and $\delta k^2\neq 0$. Expression (4.2.9) is a 3-d, volume, electric-field integral equation (EFIE) for unknown field $\bar{E}(\bar{r})$ excited in that waveguiding region by the impressed field $\bar{E}^i$ due to $\bar{P}^e$.

EFIE (4.2.9) can be expressed in terms of electric dyadic Green's function by carrying the differential Operator $(k_c^2 + \nabla\nabla\cdot)$ through the integral operator over V; the resulting integral must be evaluated in an appropriate principal-value sense. This leads to the conventional relation between the electric type dyadic Green's function $\bar{\bar{G}}_e(\bar{r}|\bar{r}')$ and scalar Green's function $\bar{\bar{G}}(\bar{r}|\bar{r}')$ [54] as

$$\bar{\bar{G}}_e(\bar{r}|\bar{r}') = (k_c^2\,\bar{\bar{I}} + \nabla\nabla)G(\bar{r}|\bar{r}') \tag{4.2.10}$$

where $\bar{\bar{I}}$ is the unit dyadic $\hat{x}\hat{x} + \hat{y}\hat{y} + \hat{z}\hat{z}$, and $\bar{\bar{G}}_e(\bar{r}|\bar{r}')$ is the solution to

$$(\nabla\times\nabla\times - k_c^2)\bar{\bar{G}}_e(\bar{r}|\bar{r}') = \bar{\bar{I}}\,k_c^2\delta(\bar{r}-\bar{r}') \tag{4.2.11}$$

in the unbounded medium of wavenumber k_c. We may rewrite EFIE (4.2.9) compactly in terms of $\bar{\bar{G}}_e$, taking into the consideration that the volume integral be evaluated in a principal value sense, such that a correction term from the excluded principal volume is required [48] as

$$\bar{E}(\bar{r}) - PV \int_V \frac{\delta k^2(\bar{r}')}{k_c^2} \bar{\bar{G}}_e(\bar{r}|\bar{r}') \cdot \bar{E}(\bar{r}')dV' + \frac{\delta k^2}{k_c^2} \bar{\bar{L}} \cdot \bar{E}(\bar{r}) = \bar{E}^i(\bar{r}) \tag{4.2.12}$$

where

$$\bar{\bar{L}} = \lim_{S_\delta \to 0} \frac{1}{4\pi} \int_{S_\delta} \frac{\hat{n}'\hat{R}}{R^2} dS \tag{4.2.13}$$

represents a three-dimensional depolarizing dyadic; S_δ encloses principal volume V_δ with outward normal as indicated in Figure 4.1. The contribution of this correction term is discussed in detail in Section 2.3 of Chapter 2.

Equation (4.2.12) is then the basic 3-d volume electric-field integral equation (EFIE) which describes the open-boundary dielectric waveguide systems. This vector EFIE is an in homogeneous Fredholm integral equation of the second kind [51] for unknown field $\bar{E}(\bar{r})$ excited in the heterogeneous waveguide core region V (where $\delta n^2 \neq 0$) by impressed field $\bar{E}^i(\bar{r})$ due to excitatory polarization $\bar{P}^e$. All following developments are based upon this fundamental EFIE.

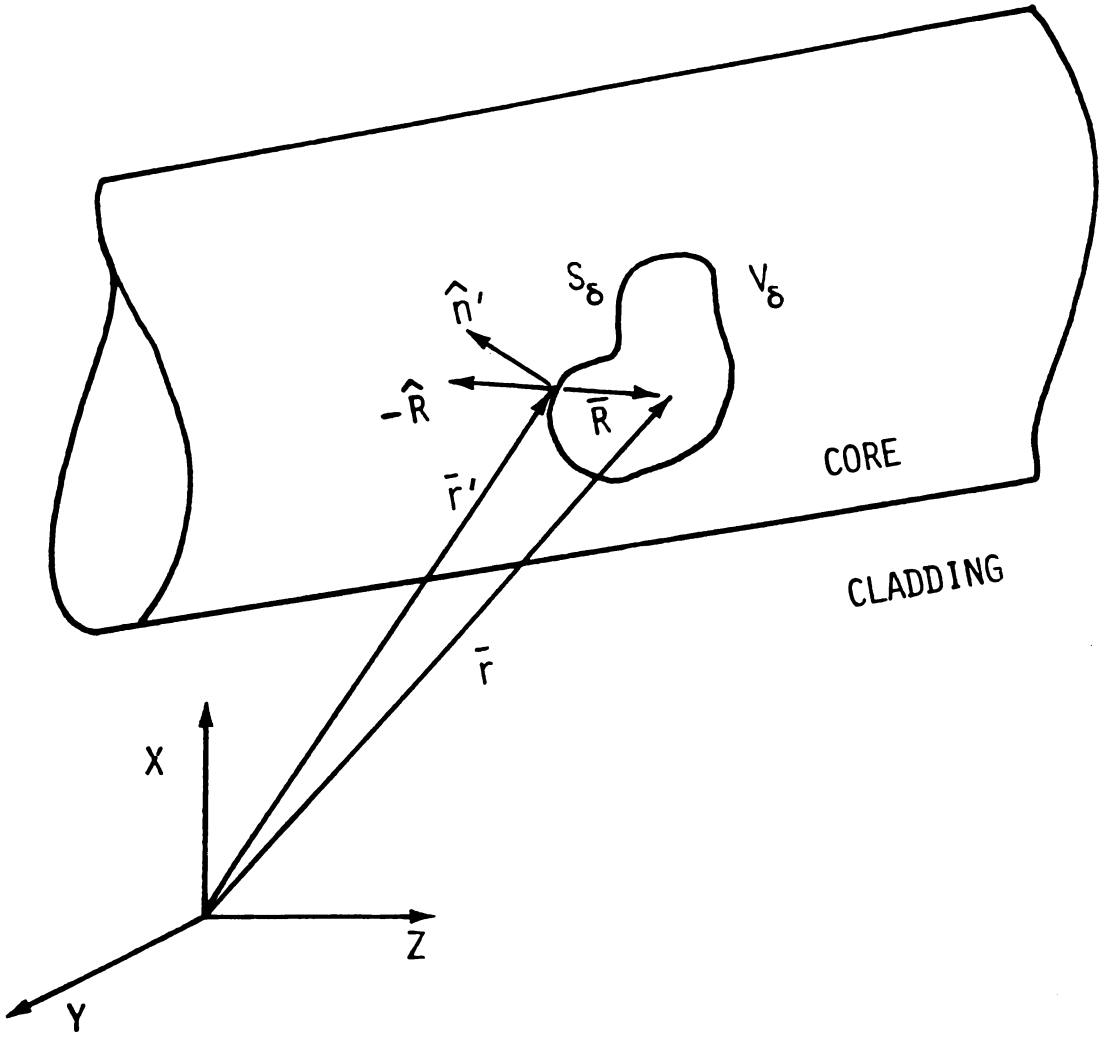

Figure 4.1 Three-dimensional configuration of principal volume which contributes to the depolarizing dyad of the 3-d EFIE for a open-boundary waveguide.

4.3 Homogeneous EFIE's for Natural Surface-Wave Modes along Coupled Waveguide System

A natural, surface-wave-mode field is that field which can exist on the open-boundary waveguide system in the absence of excitation, i.e., the non-trivial solution for $\bar{E}^i=0$. EFIE (4.2.12) then become the homogeneous equation

$$\bar{E}(\bar{r}) - PV \int_V \frac{\delta k^2(\bar{r}')}{k_c^2} \bar{\bar{G}}_e(\bar{r}|\bar{r}') \cdot \bar{E}(\bar{r}')dV' + \frac{\delta k^2(\bar{r})}{k_c^2} \bar{\bar{L}} \cdot \bar{E}(\bar{r}) = 0 \ . \tag{4.3.1}$$

In the case where the waveguide has a transversly graded dielectric profile with longitudinal-invariant dielectric properties, $\delta k(\bar{r})$ becomes $\delta k(\bar{\rho})$, where $\bar{\rho}=x\hat{x} + y\hat{y}$ is a two-dimensional position vector. Eigenfield solutions having an axially-travelling-wave nature with phase constant β

$$\bar{E}^{\pm}(\bar{r}) = \bar{e}(\bar{\rho})e^{\mp j\beta z} \ , \tag{4.3.2}$$

are supported by such a system, as demonstrated below.

The principal-value integral in EFIE (4.3.1) can be evaluated by exploiting $\bar{E}(\bar{r})$ and $\bar{\bar{G}}_e(\bar{r}|\bar{r}')$ based upon expressions (4.3.2) and (4.2.10), respectively, as

$$PV \int_V \frac{\delta k^2(\bar{\rho}')}{k_c^2} \bar{\bar{G}}_e(\bar{r}|\bar{r}') \cdot \bar{E}(\bar{r}')dV'$$

$$= PV \int_V \frac{\delta k^2(\bar{\rho}')}{k_c^2} \left[k_c^2 \bar{\bar{I}} + \nabla\nabla\right] \frac{e^{-jk_cR}}{4\pi R} \cdot \bar{e}(\bar{\rho}')e^{\mp j\beta z'} \, dV'$$

$$= PV \int_{CS} \frac{\delta k^2(\bar{\rho}')}{k_c^2} \left[k_c^2 \bar{\bar{I}} + \nabla\nabla\right] \int_{-\infty}^{\infty} e^{\mp j\beta z'} \frac{e^{-jk_cR}}{4\pi R} dz' \cdot \bar{e}(\bar{\rho}')dS' \, . \tag{4.3.3}$$

Making the change of variables u=(z-z') for the component z'-integral of result (4.3.3) above, leads to [55]

$$\int_{-\infty}^{\infty} e^{\mp j\beta z'} \frac{e^{-jk_cR}}{4\pi R} dz'$$

$$= \frac{1}{4\pi} e^{\mp j\beta z} \int_{-\infty}^{\infty} e^{\pm j\beta u} \frac{e^{-jk_c\sqrt{|\bar{\rho} - \bar{\rho}'|^2 + u^2}}}{\sqrt{|\bar{\rho} - \bar{\rho}'|^2 + u^2}} du$$

$$= \frac{e^{\mp j\beta z}}{2\pi} K_0(\gamma|\bar{\rho} - \bar{\rho}'|) \tag{4.3.4}$$

where K_0 is the modified Bessel Function of second kind and γ is an eigenvalue parameter defined as

$$\gamma = \sqrt{\beta^2 - k_c^2} \, . \tag{4.3.5}$$

The asymptotic exponential decay of K_0 for large real arguments leads to the expected surface-wave-mode field confinement. A condition for real γ is therefore identified

as $\beta > k_c$. This condition is consistent with the well known result [9,11]; it permits the phenomenon of total internal reflection at the core-cladding interface and, as a result, the existence of confined, guided surface-wave modes. Each term in EFIE (4.3.1) is therefore proportional to $\exp(\mp j\beta z)$, and expression (4.3.2) is therefore indeed an eigenmode solution.

Depolarizing dyad $\bar{\bar{L}}$ is defined as [48]

$$\bar{\bar{L}} = \frac{1}{4\pi} \int_{S_\delta} \frac{\hat{n}'\hat{R}}{R^2} \, dS'$$

$$= \frac{1}{4\pi} \oint_{C_\delta} d\ell' \hat{n}' \int_{-\infty}^{\infty} \frac{\hat{R}}{R^2} \, dz' \qquad (4.3.6)$$

where C_δ is the principal contour as shown in Figure 4.2. The integration over z' in (4.3.6) can be carried out by changing of variable from z' to u=(z-z') such that

$$\int_{-\infty}^{\infty} \frac{\hat{R}}{R^2} \, dz' = \int_{-\infty}^{\infty} \frac{(\bar{\rho} - \bar{\rho}') + \hat{z}u}{\left[(\bar{\rho} - \bar{\rho}')^2 + u^2\right]^{3/2}} \, du$$

$$= \frac{2(\bar{\rho} - \bar{\rho}')}{|\bar{\rho} - \bar{\rho}'|^2} .$$

Let $\bar{r}=\bar{\rho}-\bar{\rho}'$, then the depolarizing, or Green's-correction, dyad becomes

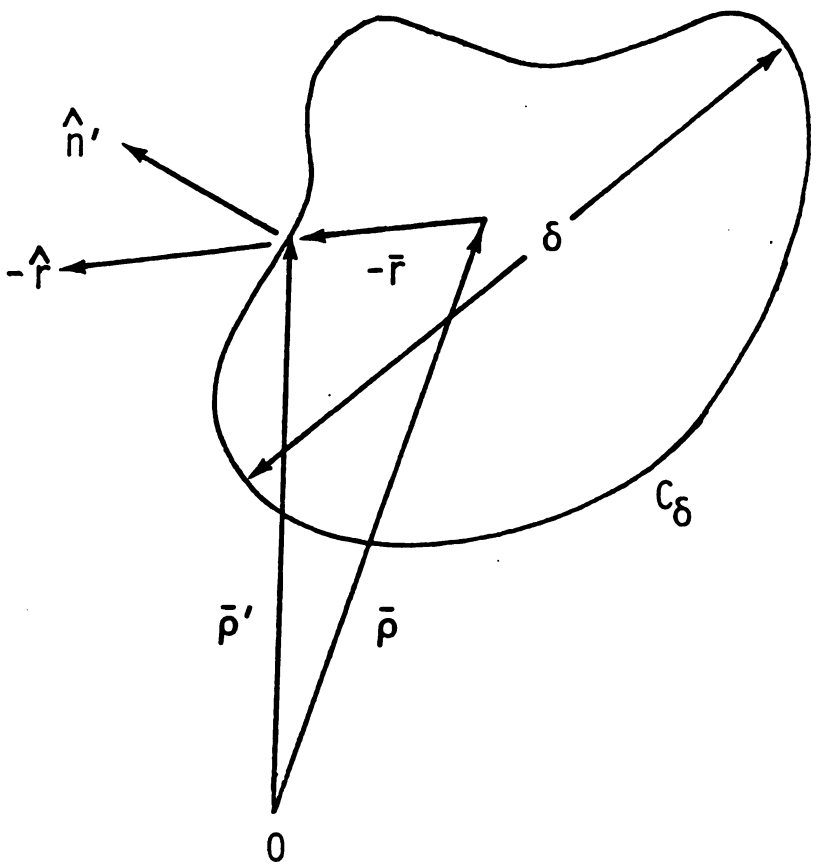

Figure 4.2 Two-dimensional configuration of principal volume shown as enclosed by principal contour C_δ.

$$\bar{\bar{L}} = \frac{1}{2\pi} \oint_{C_\delta} \frac{\hat{n}'\hat{r}}{r} \, d\ell' = \bar{\bar{\ell}} \tag{4.3.7}$$

for the two-dimensional, open-boundary wave guide geometry.

With results (4.3.2), (4.3.3), (4.3.4) and (4.3.7), the three-dimensional volume EFIE (4.3.1) then reduces to the desired vector two-dimensional form

$$\left[\bar{\bar{I}} + \frac{\delta k^2(\bar{\rho})}{k_c^2} \bar{\bar{\ell}}\right] \cdot \bar{e}(\bar{\rho}) - PV \int_{CS} \frac{\delta k^2(\bar{\rho}')}{k_c^2} \bar{\bar{g}}_{e\beta}^{(\pm)}(\bar{\rho}|\bar{\rho}') \cdot \bar{e}(\bar{\rho}') dS' = 0 \, .$$

$$\ldots \text{ for all } \bar{\rho} \in CS, \tag{4.3.8}$$

$\bar{\bar{g}}_{e\beta}^{(\pm)}(\bar{\rho}|\bar{\rho}')$ represents the corresponding β-dependent two-dimensional Green's dyadic function and is defined as

$$\bar{\bar{g}}_{e\beta}^{(\pm)}(\bar{\rho}|\bar{\rho}') = \left[k_c^2 \bar{\bar{I}} + (\nabla_t \mp j\beta\hat{z})(\nabla_t \mp j\beta\hat{z})\right] K_0(\gamma|\bar{\rho} - \bar{\rho}'|) \tag{4.3.9}$$

where $\bar{\bar{I}}$ is the unit dyad and the ∇ operator has been decomposed into the transverse operator ∇_t and its longitudinal component.

In a multi-waveguiding system as indicated in Figure 4.3, EFIE (4.3.7) can be generalized to describe surface-wave modes supported by the coupled system of N waveguides. Since the system-mode field propagates with common phase

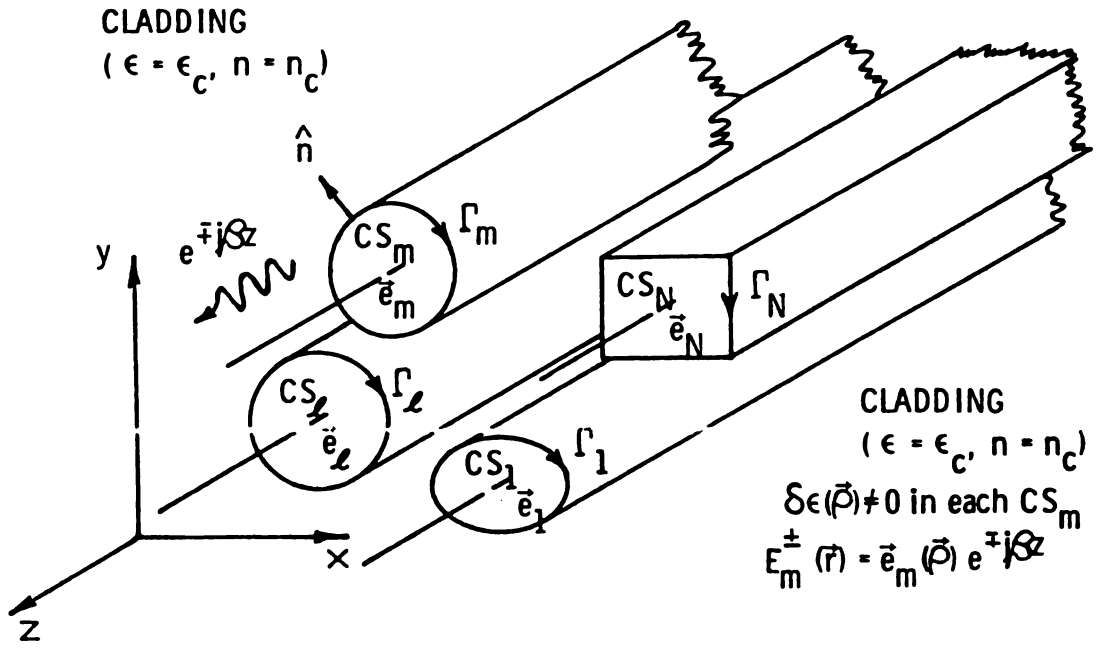

Figure 4.3 Configuration of N-coupled, open-boundary dielectric waveguides.

constant β and scattered field $\bar{e}^s$ is maintained by polarization density $\bar{P}_{eq}$ which exists wherever $\delta k^2(\bar{\rho}) \neq 0$, then it is only necessary to extend the integration over each guide of cross section CS_n, n=1, 2, ..., N, to obtain

$$\left[\bar{\bar{I}} + \frac{\delta k^2(\bar{\rho})}{k_c^2}\,\bar{\bar{\ell}}\right] \cdot \bar{e}(\bar{\rho}) - \sum_{n=1}^{N} PV \int_{CS_n} \frac{\delta k^2(\bar{\rho}')}{k_c^2}\,\bar{\bar{g}}_{e\beta}^{(\pm)}(\bar{\rho}|\bar{\rho}') \cdot \bar{e}(\bar{\rho}')dS'$$

$$= 0 \qquad \text{... for all } \bar{\rho} \in CS_m$$

$$m = 1,2, \ldots, N. \qquad (4.3.10)$$

Equations (4.3.10) are a system of N simultaneous EFIE's for eigenmode fields $\bar{e}_m$ in each waveguide core. Non-trivial solutions are obtained only for discrete phase-constant eigenmodes $\beta = \beta_m$ corresponding to the m'th surface-wave mode. The coupled system of 2-d EFIE's (4.3.10) can be expressed alternatively as

$$\left[\bar{\bar{I}} + \frac{\delta n^2(\bar{\rho})}{n_c^2}\,\bar{\bar{\ell}}\right] \cdot \bar{e}(\bar{\rho}) - \sum_{n=1}^{N} PV \int_{CS_n} \frac{\delta n^2(\bar{\rho}')}{n_c^2}\,\bar{\bar{g}}_{e\beta}(\bar{\rho}|\bar{\rho}') \cdot \bar{e}(\bar{\rho}')dS'$$

$$= 0 \qquad \text{... for } \bar{\rho} \in CS_m,\ m=1,2, \ldots, N, \qquad (4.3.11)$$

where wavenumber k is replaced by refractive index n from the relation $k = nk_0$, '$\pm$' for $\bar{\bar{g}}_{e\beta}$ is dropped but implied.

A similar result, yet provides better formats for

physical interpretation and the convenience in actual computation (without the source point singularity of $\bar{\bar{G}}_e$) can be obtained by first carrying out the divergence operator in (4.2.9) followed by the use of the symmetric property of the scalar Green's function $\nabla\nabla G=-\nabla\nabla' G$[59]. Subsequent application of the same divergent identity leads to

$$\bar{E}(\bar{r}) + \sum_{n=1}^{N} \nabla \int_V \Big\{ \nabla' \cdot \Big[\frac{\delta k^2(\bar{r}')}{k_c^2} \bar{E}(\bar{r}') G(\bar{r}|\bar{r}') \Big] - \Big[\nabla' \cdot \frac{\delta k^2(\bar{r}')}{k_c^2} \bar{E}(\bar{r}') \Big] G(\bar{r}|\bar{r}') \Big\} dV' - \sum_{n=1}^{N} \int_V \delta k^2(\bar{r}') \bar{E}(\bar{r}') G(\bar{r}|\bar{r}') dV' = \bar{E}^i(\bar{r}) \quad \ldots \text{ for } \bar{r} \in V_m,\ m=1,2,\ \ldots,\ N. \tag{4.3.12}$$

It is observed that the second term in the above expression is the scattered field due to the scalar potential maintained by the surface charges and volume charges in the core regions. Since $\nabla' \cdot [\frac{\delta k^2(\bar{r}')}{k_c^2} \bar{E}(\bar{r}')] = \nabla' \cdot [(\frac{k^2(\bar{r}')}{k_c^2} - 1) \bar{E}(\bar{r}')] = -\nabla' \cdot \bar{E}(\bar{r}')$ due to $\nabla' \cdot (\varepsilon \bar{E}) = 0$ in a source free region, together with $\nabla' \cdot \bar{E} = -\nabla' \varepsilon \cdot \bar{E} / \varepsilon_c$, and the invoking of eigenfield (4.3.2), (4.3.12) above then yields [57]

$$\bar{e}(\bar{\rho}) + \sum_{n=1}^{N} \frac{1}{2\pi} \int_{\Gamma_{Cn}} \frac{\delta k^2(\bar{\rho}')}{k_c^2} \hat{n}' \cdot \bar{e}(\bar{\rho}') (\nabla_t \mp j\beta\hat{z}) K_0(\gamma|\bar{\rho} - \bar{\rho}'|) d\ell'$$

$$- \sum_{n=1}^{N} \frac{1}{2\pi} \int_{CS_n} \frac{\bar{e}(\bar{\rho}') \cdot \nabla' k^2(\bar{\rho}')}{k^2(\bar{\rho}')} (\nabla_t \mp j\beta\hat{z}) K_0(\gamma|\bar{\rho} - \bar{\rho}'|) dS'$$

$$- \sum_{n=1}^{N} \frac{1}{2\pi} \int_{CS_n} \delta k^2(\bar{\rho}') \bar{e}(\bar{\rho}') K_0(\gamma|\bar{\rho} - \bar{\rho}'|) dS' = 0$$

$$\ldots \text{ for } \bar{\rho} \in CS_m, \quad m=1,2, \ldots, N. \tag{4.3.13}$$

The effects of equivalent-induced charge and current are readily seen in (4.3.13); the contribution from the surface charge due to the jump discontinuity in index contrast between each core and its surround is evident from the contour integral along Γ_{Cn} of the n'th guide; while the volume polarization charge which is proportional to the gradient of the continuous index profile (interior to each core) is given by the second integral and the last integral in (4.3.13) represents the scattered field maintained by equivalent-induced polarization current.

4.4 Integral-Operator-Based Coupled-Mode Perturbation Approximation

Guided-wave field $\bar{E}=\bar{e}(\bar{\rho})\exp(-j\beta z)$ supported by a system of N dielectric waveguides (Figure 4.3) described by refractive-index contrast $\delta n^2(\bar{\rho})$ satisfies the coupled EFIE's

$$\left[\bar{\bar{I}} + \frac{\delta n_m^2(\bar{\rho})}{n_c^2} \bar{\bar{\ell}}\right] \cdot \bar{e}(\bar{\rho}) - \sum_{n=1}^{N} PV \int_{CS_n} \frac{\delta n_n^2(\bar{\rho}')}{n_c^2} \bar{\bar{g}}_{e\beta}(\bar{\rho}|\bar{\rho}') \cdot \bar{e}(\rho') dS'$$

$$= 0$$

$$\ldots \text{ for all } \bar{\rho} \in CS_m,$$

$$m=1,2, \ldots, N.$$

(4.4.1)

The eigenfield $\bar{e}_n(\bar{\rho})$ for the n'th guide when isolated satisfies EFIE

$$\left[\bar{\bar{I}} + \frac{\delta n_n^2(\bar{\rho})}{n_c^2}\,\bar{\bar{\ell}}\right] \cdot \bar{e}_n(\bar{\rho}) - PV \int_{CS_n} \frac{\delta n_n^2(\bar{\rho}')}{n_c^2}\,\bar{\bar{g}}_{en}(\bar{\rho}\,|\,\bar{\rho}') \cdot \bar{e}_n(\bar{\rho}')\,dS' = 0$$

$$\ldots \text{ for all } \bar{\rho} \in CS_n$$

(4.4.2)

where $\beta=\beta_n$, the eigenvalue associate with isolated eigenfield $\bar{e}_n(\bar{\rho})$, is implied in letting $\bar{\bar{g}}_{e\beta} = \bar{\bar{g}}_{en}$.

To obtain a system of scalar equations, operate term by term on eq. (4.4.1) with the integral operator

$$\int_{CS_m} dS\, \frac{\delta n_m^2}{n_c^2}\, \bar{e}_m(\bar{\rho}) \cdot \{\quad\} \qquad \ldots \text{ for } m=1,2, \ldots, N.$$

(4.4.3)

where $\bar{e}_m$ is the isolated m'th guide eigenfield, to obtain

$$\int_{CS_m} \frac{\delta n_m^2(\bar{\rho})}{n_c^2}\, \bar{e}_m(\bar{\rho}) \cdot \left[\bar{\bar{I}} + \frac{\delta n_m^2(\bar{\rho})}{n_c^2}\,\bar{\bar{\ell}}\right] \cdot \bar{e}(\bar{\rho})\,dS$$

$$- \sum_{n=1}^{N} \int_{CS_n} dS'\, \frac{\delta n_n^2(\bar{\rho}')}{n_c^2}\, \bar{e}(\bar{\rho}') \cdot PV \int_{CS_m} \frac{\delta n_m^2(\bar{\rho})}{n_c^2}\, \bar{\bar{g}}_{e\beta}(\bar{\rho}'\,|\,\bar{\rho}) \cdot \bar{\bar{e}}_m(\bar{\rho})\,dS$$

$$= 0$$

... for m=1,2, ..., N.

(4.4.4)

Use was made of the well-known reciprocal property of the electric Green's dyad [58] to obtain (4.4.4); that property allows

$$\bar{e}_m(\bar{\rho}) \cdot \bar{\bar{g}}_{e\beta}(\bar{\rho}|\bar{\rho}') \cdot \bar{e}(\bar{\rho}') = \bar{e}(\bar{\rho}') \cdot \bar{\bar{g}}_{e\beta}(\bar{\rho}'|\bar{\rho}) \cdot \bar{e}_m(\bar{\rho}) \tag{4.4.5}$$

when it appears within the integrand of EFIE (4.4.2) subsequent to application of operator (4.4.3).

In a system with coupled-mode propagation, the system mode phase constant β is embedded in Green's dyadic $\bar{\bar{g}}_{e\beta}$. To extract β in this approximate coupled-mode theory, the 2-d Green's dyadic is expanded, retaining only the leading terms of a Taylor's expansion for $\bar{\bar{g}}_{e\beta}$ about its value at $\beta=\beta_m$ for the m'th isolated guide; this approximation will be adequate given the condition that weak coupling prevails. Therefore,

$$\bar{\bar{g}}_{e\beta} \cong \bar{\bar{g}}_{em} + \delta\bar{\bar{g}}_{em}\Delta\beta_m + \ldots \tag{4.4.6}$$

where $\bar{\bar{g}}_{em}$ is the value of $\bar{\bar{g}}_{e\beta}$ at $\beta=\beta_m$, and

$$\delta\bar{\bar{g}}_{em} = \left.\frac{\partial\bar{\bar{g}}_{e\beta}}{\partial\beta}\right|_{\beta=\beta_m},$$

$$\Delta\beta_m = \beta - \beta_m .$$

Inserting (4.4.6) into the second term of (4.4.4) leads to the following expansions

$$- \sum_{n=1}^{N} \int_{CS_n} dS' \, \frac{\delta n_n^2(\bar{\rho}')}{n_c^2} \, \bar{e}(\bar{\rho}') \cdot PV \int_{CS_m} \frac{\delta n_m^2(\bar{\rho})}{n_c^2} \left[\bar{\bar{g}}_{em} + \delta \bar{\bar{g}}_{em} \Delta\beta_m \right] \cdot \bar{e}_m(\bar{\rho}) \, dS$$

$$= - \sum_{n=1}^{N} \int_{CS_n} dS' \, \frac{\delta n_n^2(\bar{\rho}')}{n_c^2} \, \bar{e}(\bar{\rho}') \cdot PV \int_{CS_m} \frac{\delta n_m^2(\bar{\rho})}{n_c^2} \, \bar{\bar{g}}_{em}(\bar{\rho}' \mid \bar{\rho}) \cdot e_m(\bar{\rho}) \, dS$$

$$- \sum_{n=1}^{N} \Delta\beta_m \int_{CS_n} dS' \, \frac{\delta n_n^2(\bar{\rho}')}{n_c^2} \, \bar{e}(\bar{\rho}') \cdot PV \int_{CS_m} \frac{\delta n_m^2(\bar{\rho})}{n_c^2} \, \delta \bar{\bar{g}}_{em} \cdot \bar{e}_m(\bar{\rho}) \, dS \, .$$

(4.4.7)

Applying the defining EFIE for eigenmode field $\bar{e}_m(\bar{\rho}')$ from eq. (4.4.2)

$$\left[\bar{\bar{I}} + \frac{\delta n_m^2(\bar{\rho}')}{n_c^2} \, \bar{\bar{\ell}} \right] \cdot \bar{e}_m(\bar{\rho}') = PV \int_{CS_m} \frac{\delta n_m^2(\bar{\rho})}{n_c^2} \, \bar{\bar{g}}_{em}(\bar{\rho}' \mid \bar{\rho}) \cdot \bar{e}_m(\bar{\rho}) \, dS$$

in the first term of the R.H.S. of expression (4.4.7) provides

$$- \sum_{n=1}^{N} \int_{CS_n} dS' \, \frac{\delta n_n^2(\bar{\rho}')}{n_c^2} \, \bar{e}(\bar{\rho}') \cdot PV \int_{CS_m} \frac{\delta n_m^2(\bar{\rho})}{n_c^2} \, \bar{\bar{g}}_{em}(\bar{\rho}' \mid \bar{\rho}) \cdot \bar{e}_m(\bar{\rho}) \, dS$$

$$= - \sum_{n=1}^{N} \int_{CS_n} dS' \, \frac{\delta n_n^2(\bar{\rho}')}{n_c^2} \, \bar{e}(\bar{\rho}') \cdot \left[\bar{\bar{I}} + \frac{\delta n_m^2(\bar{\rho}')}{n_c^2} \, \bar{\bar{\ell}} \right] \cdot \bar{e}_m(\bar{\rho}') \ .$$

(4.4.8)

Since $\delta n_m^2(\bar{\rho}')=0$ for $\bar{\rho}' \in CS_n$, then the system (4.4.4) leads, subsequent to use of results (4.4.7),(4.4.8), and the use of $\bar{\bar{I}} \cdot \bar{e}_m(\bar{\rho}')=\bar{e}_m(\bar{\rho}')$, to

$$\sum_{n \neq m}^{N} \int_{CS_n} \frac{\delta n_n^2(\bar{\rho})}{n_c^2} \, \bar{e}(\bar{\rho}) \cdot \bar{e}_m(\bar{\rho}) \, dS$$

$$+ \sum_{n=1}^{N} \Delta\beta_m \int_{CS_n} dS' \, \frac{\delta n_n^2(\bar{\rho}')}{n_c^2} \, \bar{e}(\bar{\rho}) \cdot PV \int_{CS_m} \frac{\delta n_m^2(\bar{\rho})}{n_c^2} \, \delta\bar{\bar{g}}_{em}(\bar{\rho}' \,|\, \bar{\rho}) \cdot \bar{e}_m(\bar{\rho}) \, dS$$

$$=0$$

... for m=1,2, ..., N.

(4.4.9)

Equation (4.4.9) represents a system of N simultaneous equations, one associated with each of the N weakly coupled dielectric waveguides; it involves N unknown fields, i.e., the $\bar{e}(\bar{\rho})$'s, one for each guide. Further approximation can be made based upon the assumption that the field of each guide in the coupled system will not differ significantly from its isolated eigenmode field distribution as long as

the coupling is weak; i.e., the assumption can be made that

$$\bar{e}(\bar{\rho}) \cong a_n \bar{e}_n(\bar{\rho}) \qquad \text{... for all } \bar{\rho} \in CS_n. \tag{4.4.10}$$

where a_n is an unknown amplitude coefficient that depends upon the coupling. Moreover, the second term in (4.4.9) can only have significant contribution when n=m since $\delta\bar{\bar{g}}_{em}(\bar{\rho}'|\bar{\rho})$ is small when $\bar{\rho}' \in CS_n$ while $\bar{\rho} \in CS_m$ when $n \neq m$. With this weak-coupling approximation, terms $n \neq m$ in the second sum of expression (4.4.9) are dropped leading to

$$\sum_{n\neq m} a_n \int_{CS_n} \frac{\delta n_n^2(\bar{\rho})}{n_c^2} \bar{e}_n(\bar{\rho}) \cdot \bar{e}_m(\bar{\rho})\, dS$$

$$+ \Delta\beta_m a_m \int_{CS_m} \frac{\delta n_m^2(\bar{\rho}')}{n_c^2} \bar{e}_m(\bar{\rho}') \cdot PV \int_{CS_m} \frac{\delta n_m^2(\bar{\rho})}{n_c^2} \delta\bar{g}_{em}(\bar{\rho}'|\bar{\rho}) \cdot \bar{e}_m(\bar{\rho})\, dS$$

$$= 0 \qquad \text{... for m=1,2, ..., N.} \tag{4.4.11}$$

where subscript 'n' and 'm' are used for index contrast δn^2 to indicate the summation index. Expression (4.4.11) can be written in the form of matrix equation as

$$\sum_{n=1}^{N} C_{mn}(\beta) a_n = 0 \qquad \text{... for m=1,2, ..., N.} \tag{4.4.12}$$

where matrix element C_{mn} is defined as

$$C_{mn} = \begin{cases} (\beta - \beta_m)\tilde{C}_{mm} & \ldots \text{ for } n=m \\ \int_{CS_n} \frac{\delta n_n^2(\bar{\rho})}{n_c^2} \bar{e}_n(\bar{\rho}) \cdot \bar{e}_m(\bar{\rho}) dS & \ldots \text{ for } n \neq m \end{cases} \tag{4.4.13}$$

and C_{mm}, a normalization constant depending upon eigenfield $\bar{e}_m$ and $\partial \bar{\bar{g}}_{em}/\partial\beta$ evaluated at isolated eigenvalue $\beta = \beta_m$ is defined as

$$\tilde{C}_{mm} = \int_{CS_n} dS \frac{\delta n_m^2(\bar{\rho})}{n_c^2} \bar{e}_m(\bar{\rho}) \cdot PV \int_{CS_m} \frac{\delta n_m^2(\bar{\rho}')}{n_c^2} \delta \bar{\bar{g}}_{em}(\bar{\rho}|\bar{\rho}') \cdot \bar{e}_m(\bar{\rho}') dS' . \tag{4.4.14}$$

The system mode eigenvalues are those β's which lead to a non-trivial solution to system (4.4.12) when $\det\left[C_{mn}(\beta)\right] = 0$. Relative modal amplitudes a_n are subsequently obtained from the resulting homogeneous matrix equation of order (N-1) obtained from system (4.4.12) after setting $a_n=1$ and discarding one of the equations.

SPECIALIZATION TO COUPLED TWO GUIDE SYSTEM

When a coupled system consist of only two waveguides, eq. (4.4.12) is reduced to

$$\begin{bmatrix} (\beta-\beta_1)\tilde{C}_{11} & C_{12} \\ C_{21} & (\beta-\beta_2)\tilde{C}_{22} \end{bmatrix} \begin{bmatrix} a_1 \\ a_2 \end{bmatrix} = \begin{bmatrix} 0 \\ 0 \end{bmatrix} \tag{4.4.15}$$

where the vanishing determinant for the coefficient matrix leads to non-trivial solutions when

$$\beta^2 - (\beta_1 + \beta_2)\beta + \beta_1\beta_2 - \frac{C_{12}C_{21}}{\tilde{C}_{11}\tilde{C}_{22}} = 0 \ .$$

By solving the above quadratic equation for system mode phase constants β, we obtain

$$\beta = \bar{\beta} \pm \delta\beta \tag{4.4.16}$$

where

$$\bar{\beta} = \frac{\beta_1 + \beta_2}{2} \quad \text{and}$$

$$\delta\beta = (\Delta^2 + \delta^2)^{\frac{1}{2}} \quad \text{with}$$

$$\Delta = \frac{\beta_1 - \beta_2}{2} \ , \ \delta^2 = \frac{C_{12}C_{21}}{\tilde{C}_{11}\tilde{C}_{22}} \ .$$

The amplitude ratio of the coupled surface modes on each guide can be found from eq. (4.4.15) as

$$\frac{a_2}{a_1} = - \frac{(\beta - \beta_1)\tilde{C}_{11}}{C_{12}}$$

(4.4.17)

Since $\tilde{C}_{mm}$s' are the self-coupling terms, it is convenient to choose the normalization of $\bar{e}_m(\bar{\rho})$ in expression (4.4.14) such that

$$\tilde{C}_{11} = \tilde{C}_{22} = -1 \ ;$$

(4.4.18)

subsequently, for degenerate or nearly degenerate coupling $\beta_1 \cong \beta_2 \cong \beta_0$, and from (4.4.16),

$$\delta\beta = \sqrt{C_{12}C_{21}} \ .$$

(4.4.19)

The ratio of coupled modal amplitudes then becomes

$$a_2^{\pm} = \pm \sqrt{\frac{C_{21}}{C_{12}}}\, a_1^{\pm}$$

(4.4.20)

where superscripts '+' and '-' denote the coupled-mode amplitudes associated with system modes having phase constants $\beta = \beta_0 + \delta\beta$ and $\beta = \beta_0 - \delta\beta$. The corresponding longitudinal wave functions $A_n(z)$, assuming the coupled-surface-wave modes are well above cut off, can be written as a linear combination of these fields as

$$A_1(Z) = a_1^+ e^{-j(\beta+\delta\beta)z} + a_1^- e^{-j(\beta-\delta\beta)z}$$

$$A_2(Z) = a_2^+ e^{-j(\beta+\delta\beta)z} + a_2^- e^{-j(\beta-\delta\beta)z} \quad . \tag{4.4.21}$$

The initial values of $A_n(z)$ at z=0 can be chosen arbitrarily. Taking for simplicity $|A_1(0)|^2=0$ and $|A_2(0)|^2=1$, i.e., the initial power of the surface-wave mode in guide 2 being unity, susbsequent substitution of these initial conditions into (4.4.21), and the use of relation (4.4.20) yields

$$a_1^+ = - a_1^- = \frac{1}{2}\sqrt{\frac{C_{12}}{C_{21}}} \tag{4.4.22}$$

$$A_1(Z) = - j\sqrt{\frac{C_{12}}{C_{21}}}\sin(\delta\beta z)e^{-j\beta z}$$

$$A_2(Z) = \cos(\delta\beta z)e^{-j\beta z} \quad . \tag{4.4.23}$$

Expressions for $A_1(z)$ and $A_2(z)$ in (4.4.23) are the solutions to the standard coupled mode equation with constant coupling coefficients for a general (single mode) coupled system [56]. It is noted from the expression for $A_1(z)$ above that total transfer of power from guide 2 to guide 1 will occur at

$$|z| = \ell = \frac{\pi}{2\delta\beta} \ .$$

This is the well known definition for 'coupling length'; furthermore, eq. (4.4.23) also indicates that power is periodically exchanged between the two coupled parallel guides.

It is therefore concluded that the above results agree with those from the more familiar, approximate differential-operator coupled mode theory. This serves to confirm the validity of the integral-operator analysis when applied to a coupled waveguiding system. The later theory has a conceptually-exact foundation prior to the coupled-mode approximation, and leads to explicit expressions for the coupling coefficients.

CHAPTER V

APPLICATION OF INTEGRAL-OPERATOR ANALYSIS TO COUPLED SLAB WAVEGUIDE SYSTEM

5.1 Introduction

Applications using integral-operator based coupled mode theory are sought for a uniformly-clad slab waveguide system [15]. Physically, when modal fields become coupled, a phase constant shift from the β's of the isolated guides to that of system modes occurs. In the degenerate coupling of the m'th mode along two identical guides with isolated phase constants β_m, the system modes have phase constants $\beta_m = \beta_{0m} \pm \Delta\beta$.

To begin, the general coupled system of EFIE is specialized to a slab waveguide system. A characteristic equation for unknown system-mode phase constant β of a two-guide system is obtained using Fourier-exponential transform method; parameters include slab refractive indices, dimensions and spacings. Either exact or approximate solutions can then be obtained for phase-constant shift $\Delta\beta$. Perturbation solutions, which approximate the coupled fields in the integral equations by the eigenfields of each individual isolated guide as described in the last chapter, are specialized for one-dimensional coupled TE modes. The

resulting coupling coefficients are obtained to implement an approximate solution of the N coupled, simultaneous EFIE's, resulting in a matrix equation for coupled-mode amplitudes. Phase-constant shifts due to the degenerate TE mode coupling of a weakly coupled two-guide system are finally obtained.

Subsequently, numerical results are obtained, using both solution approaches, for several cases of degenerate and non-degenerate coupling in a two guide system. There, the effect of coupling is demonstrated through the variation of index contrasts in the system as well as the widths and spacings of individual waveguides.

5.2 Specialization of EFIE for Coupled Slab-Waveguide System

The slab-waveguide system considered here has infinite dimensions in both the y and z directions. It is assumed that all waveguide parameters are both longitudinally and y invariant. It follows that in (4.3.13) using $\nabla_t = \hat{x}\,\partial/\partial x$, $\bar{e}(\bar{\rho}) = \bar{e}(x)$ and assuming the transversely-graded index profile $n(\bar{\rho}) = n(x)$, the integral of the y-dependent modified Bessel function K_0 can be carried out to obtain a one-dimensional Green's function $g(x|x')$ as

$$\frac{1}{2\pi}\int_{-\infty}^{\infty} K_0\left[\gamma|\bar{\rho}-\bar{\rho}'|\right]dy' = \frac{e^{-\gamma|x-x'|}}{2\gamma} = g(x|x') \quad . \tag{5.2.1}$$

Also, the contour integral enclosing the transverse cross section is reduced to contributions from surface charges at

both the upper and lower boundaries of each guide as shown in Figure 5.1. These specializations of (4.3.13) subsequently lead to the one-dimensional coupled EFIE's:

$$\bar{e}(x) + \sum_{n=1}^{N} \left\{ \frac{\delta k_n^2(x'=x_{2n}^-)}{k_c^2} \left[e_x(x_{2n}) (\hat{x} \frac{d}{dx} - j\beta\hat{z}) g(x|x_{2n}) \right] \right.$$

$$- \frac{\delta k_n^2(x'=x_{1n}^+)}{k_c^2} \left[e_x(x_{1n}) (\hat{x} \frac{d}{dx} - j\beta\hat{z}) g(x|x_{1n}) \right]$$

$$- \int_{x_{1n}}^{x_{2n}} e_x(x') \frac{dk_n^2(x')/dx'}{k_n^2(x')} (\hat{x} \frac{d}{dx} - j\beta\hat{z}) g(x|x') dx'$$

$$\left. - \int_{x_{1n}}^{x_{2n}} \delta k_n^2(x') \bar{e}(x') g(x|x') dx' \right\} = 0$$

$$\text{... for } x_{2m} \leq x \leq x_{1m}$$

$$m=1,2, \ldots, N, \qquad (5.2.2)$$

where the δk_n^2 are evaluated at the boundaries $x'=x_{1n}^+$ and $x'=x_{2n}^-$ as the result of one-dimensional contour integration; superscript '+' and '-' denote the interior side of the slab/cladding boundaries. Decomposition of (5.2.2) into its component equations leads to:

<u>x-component</u>:

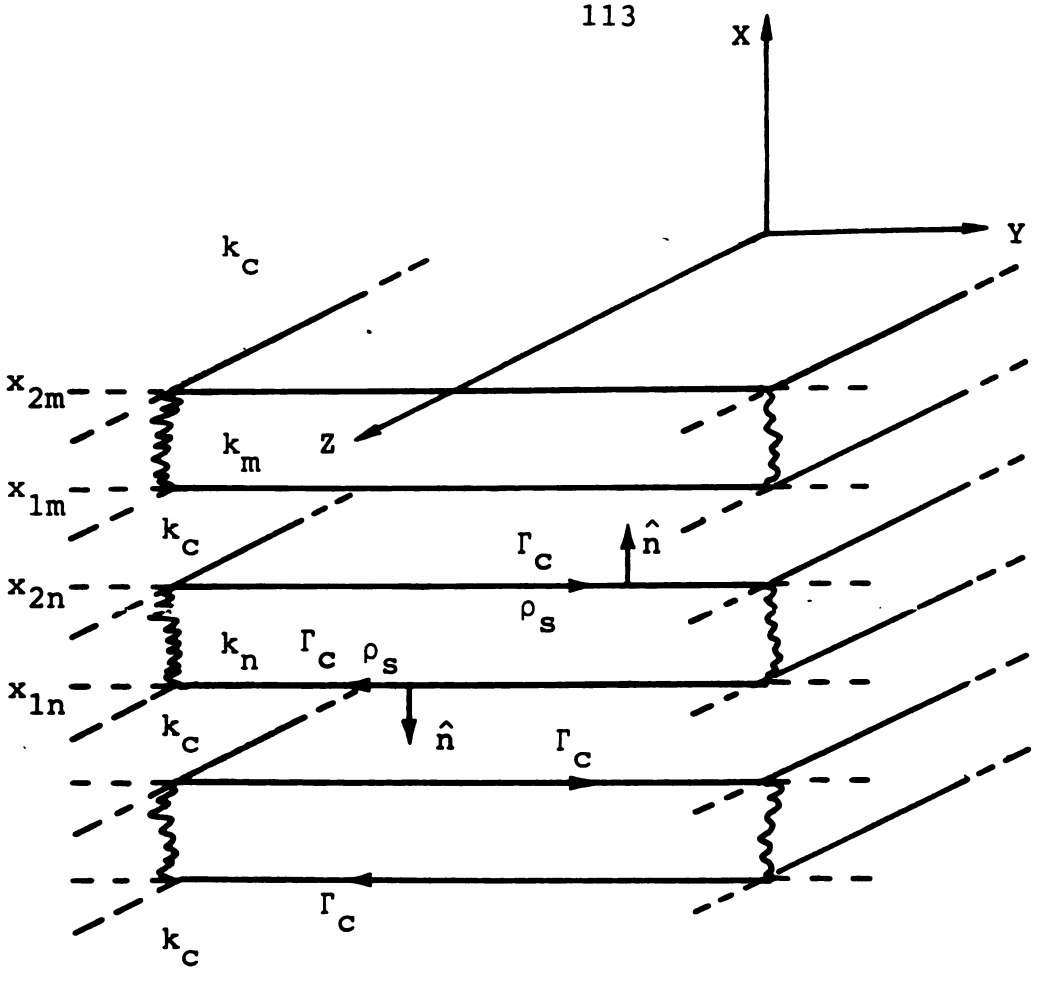

Figure 5.1 Contributions of surface charges which arise from the index discontinuity between each slab and its surround cladding.

$$\bar{e}_x(x) + \sum_{n=1}^{N} \left\{ \frac{\delta k_n^2(x'=x_{2n}^-)}{k_c^2} e_x(x_{2n}) \left[-\gamma \mathrm{sgn}(x-x_{2n})\right] g(x|x_{2n}) \right.$$

$$- \frac{\delta k_n^2(x'=x_{1n}^+)}{k_c^2} e_x(x_{1n}) \left[-\gamma \mathrm{sgn}(x-x_{1n})\right] g(x|x_{1n})$$

$$- \int_{x_{1n}}^{x_{2n}} \frac{dk_n^2(x')/dx'}{k_n^2(x')} e_x(x') \left[-\gamma \mathrm{sgn}(x-x')\right] g(x|x')\,dx'$$

$$\left. - \int_{x_{1n}}^{x_{2n}} \delta k_n^2(x') e_x(x') g(x|x')\,dx' \right\} = 0 \,, \qquad (5.2.3)$$

<u>y component</u>:

$$e_y(x) - \sum_{n=1}^{N} \int_{x_{1n}}^{x_{2n}} \delta k_n^2(x') e_y(x') g(x|x')\,dx' = 0 \,, \qquad (5.2.4)$$

<u>z component</u>:

$$e_z(x) + \sum_{n=1}^{N} \left\{ -j\beta \frac{\delta k_n^2(x'=x_{2n}^-)}{k_c^2} e_x(x_{2n}) g(x|x_{2n}) \right.$$

$$+ j\beta \frac{\delta k_n^2(x'=x_{1n}^+)}{k_c^2} e_x(x_{1n}) g(x|x_{1n})$$

$$\left. + j\beta \int_{x_{1n}}^{x_{2n}} \frac{dk_n^2(x')/dx'}{k_n^2(x')} e_x(x') g(x|x')\,dx' \right.$$

$$- \int_{x_{1n}}^{x_{2n}} \delta k_n^2(x') e_z(x') g(x|x') dx' \Bigg\} = 0 \ . \qquad (5.2.5)$$

The sgn function in eq. (5.2.3) has a value of 1 with positive argument and -1 for negative argument.

A study of the above component equations reveals that as a result of the one-dimensional slab system discussed here, i.e., for natural coupled TE modes, $e_x(x) = e_z(x) = 0$, and the only remaining y component equations are independent in $e_y(x)$. In the case of coupled TM eigenmodes, $e_y(x)=0$, therefore $\bar{e}(x) = \hat{x}e_x(x) + \hat{z}e_z(x)$ while $e_z(x)$ is coupled to $e_x(x)$ in (5.2.5). Also noted that TM-mode coupling is stronger due to the fact that there exist surface charges from the normal component of the field, i.e., e(x). This observation [57] parallels the discussion of scattering in the one-dimensional slab waveguide in Section 3.1.2. The following discussions on various solution techniques will concentrate on coupled TE mode systems; this is mainly due to the simplicity of the component equation involved as described above and the dominant nature of TE modes in dielectric waveguides. These solutions will enable us to understand the coupling phenomena in other more complex systems.

5.3 Fourier-Expontial Transform Solution for Step-Index Slabs

5.3.1 Coupled TE Modes

Application of the coupled EFIE system (5.2.2) is demonstrated by studying the coupled non-degenerate TE surface-wave modes supported by the step-index slab-waveguide system as shown in Figure 5.2. In this system, the planar, slab waveguides have thickness (t_1, t_2), constant refractive indices (n_1, n_2), wavenumbers (k_1, k_2) and separation s. EFIE (5.2.4) appropriate for the TE modes, having only y-component of electric field can be written for guide fields $e_{y1}(x)$ and $e_{y2}(x)$ of slab 1 and 2 as

$$e_{y1}(x) - \frac{k_1^2-k_c^2}{2\gamma}\int_{-t_1}^{0} e_{y1}(x')e^{-\gamma|x-x'|}dx' - \frac{k_2^2-k_c^2}{2\gamma}\int_{s-t_2}^{s} e_{y2}(x')e^{-\gamma|x-x'|}dx' = 0 \quad \text{... for } -t_1 \le x \le 0 \tag{5.3.1}$$

$$e_{y2}(x) - \frac{k_2^2-k_c^2}{2\gamma}\int_{s-t_2}^{s} e_{y2}(x')e^{-\gamma|x-x'|}dx' - \frac{k_1^2-k_c^2}{2\gamma}\int_{-t_1}^{0} e_{y1}(x')e^{-\gamma|x-x'|}dx' = 0 \quad \text{... for } s-t_2 \le x \le s \tag{5.3.2}$$

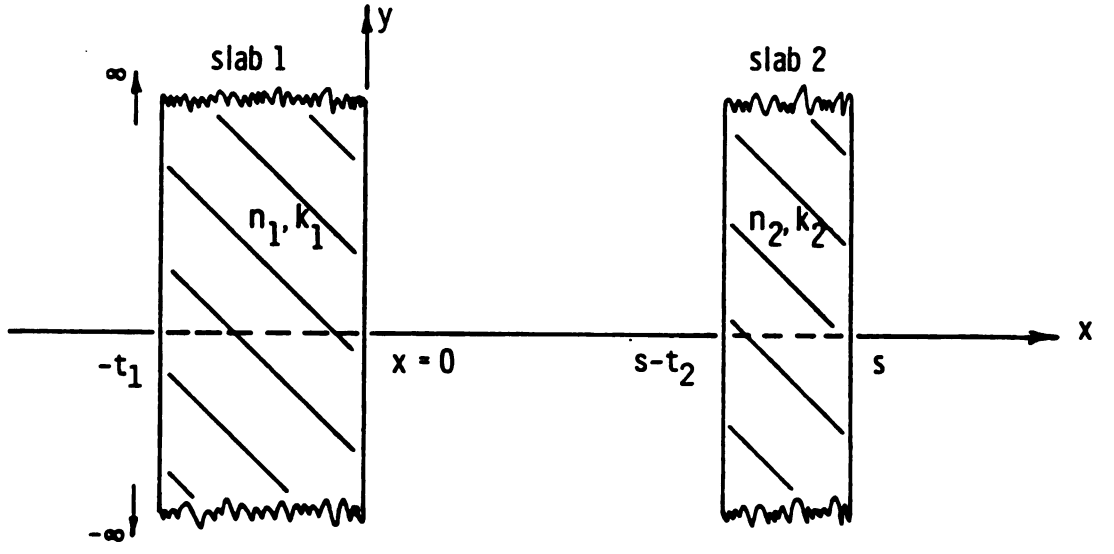

Figure 5.2 Configuration appropriate for study of non-degenerate TE surface-wave mode coupling between two slab waveguides.

where k_c is the wavenumber of the surrounding cladding with refractive index n_c.

Physically, it is noted that the third terms of both the above expressions represent the coupling from the neighboring guide. As the separation between waveguides increases, the effect of these coupling terms becomes neglibible because of the rapid decay of $\exp(-\gamma|x-x'|)$ (with x' as source point in one slab and x as field point in the other) since γ is positive real for the coupled surface-wave modes. This coupled system then reduces to two independent EFIE's for individual isolated slab waveguides.

For the purpose of simplicity, let $k_1 = k_2$, i.e., both slabs have the same refractive index; such a configuration has common applications in practice such as symmetric directional coupler. With $k_1^2-k_c^2=k_2^2-k_c^2= \Delta k^2$, apply the following inverse Fourier-exponential transform to represent unknown fields in both (5.3.1) and (5.3.2)

$$e_i(x) = \frac{1}{2\pi}\int_{-\infty}^{\infty} E_i(\eta)e^{j\eta x}d\eta \qquad i=1,2 \text{ for slab 1 and 2.} \tag{5.3.3}$$

After integration over x', we have

<u>slab 1</u>:

$$\frac{2\gamma}{\Delta k^2}\int_{-\infty}^{\infty} E_1(\eta)e^{j\eta x}d\eta - \int_{-\infty}^{\infty} E_1(\eta)d\eta\left[\frac{e^{j\eta x}-e^{-(j\eta+\gamma)t_1-\gamma x}}{j\eta+\gamma}\right]$$

$$-\int_{-\infty}^{\infty} E_1(\eta)d\eta\left[\frac{e^{\gamma x}-e^{j\eta x}}{j\eta-\gamma}\right]$$

$$- \int_{-\infty}^{\infty} E_2(\eta)\, d\eta \left[\frac{e^{(j\eta-\gamma)s} - e^{(j\eta-\gamma)(s-t_2)}}{j\eta-\gamma} \right] e^{\gamma x} = 0 \tag{5.3.4}$$

slab 2:

$$\frac{2\gamma}{\Delta k^2} \int_{-\infty}^{\infty} E_2(\eta) e^{j\eta x} d\eta - \int_{-\infty}^{\infty} E_2(\eta)\, d\eta \left[\frac{e^{j\eta x} - e^{(j\eta+\gamma)(s-t_2)-\gamma x}}{j\eta+\gamma} \right]$$

$$- \int_{-\infty}^{\infty} E_2(\eta)\, d\eta \left[\frac{e^{(j\eta-\gamma)s+\gamma x} - e^{j\eta x}}{j\eta-\gamma} \right]$$

$$- \int_{-\infty}^{\infty} E_1(\eta)\, d\eta \left[\frac{1-e^{-(j\eta+\gamma)t_1}}{j\eta+\gamma} \right] e^{-\gamma x} = 0 \,. \tag{5.3.5}$$

By collecting $e^{j\eta x}$ terms of either (5.3.4) or (5.3.5) above and exploiting the linear independence of $e^{j\eta x}$, $e^{\gamma x}$, and $e^{-\gamma x}$, it is concluded that

$$\int_{-\infty}^{\infty} E_1(\eta) \left[\frac{2\gamma}{\Delta k^2} - \frac{1}{j\eta+\gamma} + \frac{1}{j\eta-\gamma} \right] e^{j\eta x} d\eta = 0 \,.$$

This is essentially an inverse transform, and its vanishing requires the bracketed quantity to vanish since $E_1(\eta) \neq 0$. This then leads to the discrete allowable eigenvalues for this nondegenerate coupled system

$$\eta = \pm \kappa = \pm \sqrt{k_1^2 - \beta^2} \tag{5.3.6}$$

such that the transformed solution for $E_i(\eta)$ associated with

$e_i(x)$ in (5.3.3) becomes

$$E_1(\eta) = A\delta(\eta-\kappa) + B\delta(\eta+\kappa) \tag{5.3.7}$$

for slab 1 and

$$E_2(\eta) = C\delta(\eta-\kappa) + D\delta(\eta+\kappa) \tag{5.3.8}$$

for slab 2, where A, B, C and D are unknown amplitude coefficients. The remaining terms from eq. (5.3.4) provide

$$\int_{-\infty}^{\infty} E_1(\eta)\,d\eta \left[\frac{e^{-(j\eta+\gamma)t_1-\gamma x}}{j\eta+\gamma} - \frac{e^{\gamma x}}{j\eta+\gamma} \right] -$$

$$\int_{-\infty}^{\infty} E_2(\eta)\,d\eta \left[\frac{e^{(j\eta-\gamma)s} - e^{(j\eta-\gamma)(s-t_2)}}{j\eta-\gamma} \right] e^{\gamma x} = 0 \tag{5.3.9}$$

while from eq. (5.3.5)

$$\int_{-\infty}^{\infty} E_2(\eta)\,d\eta \left[\frac{e^{(j\eta+\gamma)(s-t_2)-\gamma x}}{j\eta+\gamma} - \frac{e^{(j\eta-\gamma)s+\gamma x}}{j\eta-\gamma} \right] -$$

$$\int_{-\infty}^{\infty} E_1(\eta)\,d\eta \left[\frac{1-e^{-(j\eta+\gamma)t_1}}{j\eta+\gamma} \right] e^{-\gamma x} = 0 \ . \tag{5.3.10}$$

If the transform solutions (5.3.7) and (5.3.8) are utilized in eqs. (5.3.9) and (5.3.10) above, and linear independence of the $e^{\pm\gamma x}$ is exploited we then have a homogeneous system of four simultaneous equations as

$$A\,\frac{e^{-(j\kappa+\gamma)t_1}}{j\kappa+\gamma} - B\,\frac{e^{(j\kappa-\gamma)t_1}}{j\kappa-\gamma} = 0 \tag{5.3.11}$$

$$\frac{A}{\gamma-j\kappa} + \frac{B}{\gamma+j\kappa} + C\,\frac{e^{(j\kappa-\gamma)s}-e^{(j\kappa-\gamma)(s-t_2)}}{\gamma-j\kappa}$$

$$+ D\,\frac{e^{-(\gamma+j\kappa)s}-e^{-(\gamma+j\kappa)(s-t_2)}}{\gamma+j\kappa} = 0 \tag{5.3.12}$$

$$C\,\frac{e^{(j\kappa-\gamma)s}}{\gamma-j\kappa} + D\,\frac{e^{-(\gamma+j\kappa)s}}{\gamma+j\kappa} = 0 \tag{5.3.13}$$

$$A\,\frac{e^{-(\gamma+j\kappa)t_1}-1}{\gamma+j\kappa} + B\,\frac{e^{(j\kappa-\gamma)t_1}-1}{\gamma-j\kappa} + C\,\frac{e^{(\gamma+j\kappa)(s-t_2)}}{\gamma+j\kappa}$$

$$+ D\,\frac{e^{(\gamma-j\kappa)(s-t_2)}}{\gamma-j\kappa} = 0\ . \tag{5.3.14}$$

To obtain a non-trivial solution for coefficients A, B, C and D from (5.3.11) through (5.3.14), it is necessary that their determinant be made to vanish. As a result, it yields the characteristic equation for eigenvalue γ of the coupled system as

$$e^{-2\gamma(s-t_2)} = \frac{(\gamma+j\kappa)^2 e^{j\kappa t_2} - (\gamma-j\kappa)^2 e^{-j\kappa t_2}}{(e^{j\kappa t_1} - e^{-j\kappa t_1})(e^{j\kappa t_2} - e^{-j\kappa t_2})}$$

$$\times \frac{(\gamma+j\kappa)^2 e^{j\kappa t_1} - (\gamma-j\kappa)^2 e^{-j\kappa t_1}}{(\gamma-j\kappa)^2 (\gamma+j\kappa)^2} \quad . \tag{5.3.15}$$

The same result can be confirmed by conventional differential-operator and boundary condition technique; also, in the limiting case where the separation between slabs is such that coupling no longer exists, i.e., $s \to \infty$, (5.3.15) reduces to the well known [42] characteristic equation of an isolated slab,

$$\tan\kappa t = \frac{2\gamma\kappa}{\kappa^2 - \gamma^2} \quad . \tag{5.3.16}$$

Moreover, when $t_1 = t_2 = t$, a practical special case where both slabs are identical (having same isolated eigenmodes), characteristic eq. (5.3.15) can be shown to reduce for these degenerate coupled TE modes, to

$$\pm (\gamma^2+\kappa^2) \sin\kappa t e^{-\gamma(s-t)} = 2\gamma\kappa\cos\kappa t + (\gamma^2-\kappa^2) \sin\kappa t \quad . \tag{5.3.17}$$

The "$\pm$" signs should be properly chosen to correspond to symmetric and asymmetric modal fields which exist on either slab for this degenerate coupling.

$\Delta\beta$ FOR WEAK DEGENERATE COUPLING

In the case of weak coupling, an approximate solution, utilizing the above characteristic equation, can be obtained for $\Delta\beta$, i.e., the shift of system mode phase constant $\beta = \beta_0 + \Delta\beta$ from the corresponding phase constant β_0 of the isolated guide. The approximation is that $\Delta\beta$ is small enough such that $(\Delta\beta)^2 \cong 0$; this also enables us to express the transverse wavenumbers κ and γ in terms of $(\beta_0, \Delta\beta)$ in (5.3.17) as $\kappa = \kappa_0 + \Delta\kappa$, and $\gamma = \gamma_0 + \Delta\gamma$. The latter follow from definitions $\kappa^2 = k_1^2 - \beta^2$, $\gamma^2 = \beta^2 - k_c^2$, where k_1, k_c are wavenumbers for the slab and cladding regions, respectively. Therefore,

$$\kappa^2 = (\kappa_0 + \Delta\kappa)^2 = k_1^2 - (\beta_0 + \Delta\beta)^2$$
$$= \kappa_0^2 - 2\beta_0\Delta\beta - \Delta\beta^2$$

which leads to

$$\Delta\kappa \cong - \beta_0\Delta\beta/\kappa_0 \cdot \qquad (5.3.18)$$

Similarly from $\gamma^2 = (\gamma_0 + \Delta\gamma)^2$, we obtain

$$\Delta\gamma \cong \beta_0\Delta\beta/\gamma_0 \cdot \qquad (5.3.19)$$

Substitution of above approximations to κ and γ in terms of κ_0, γ_0, $\Delta\kappa$ and $\Delta\gamma$ into eq. (5.3.17), as well as expanding both the Sine and Cosine function into their corresponsing power series, yields

$$\Delta\beta \cong \frac{\pm \sin\kappa_0 t(\gamma_0^2 + \kappa_0^2) e^{-\gamma_0(s-t)}}{F(s, \beta_0)} \qquad (5.3.20)$$

where

$$F(s,\beta_0) = \beta_0 \cos\kappa_0 t \left[\frac{2(\kappa_0^2-\gamma_0^2)}{\gamma_0\kappa_0} + \frac{(\kappa_0^2-\gamma_0^2)t}{\kappa_0}\right]$$

$$+ \beta_0 \sin\kappa_0 t(4+2\gamma_0 t) \pm \beta_0(\gamma_0^2+\kappa_0^2)e^{-\gamma_0(s-t)}$$

$$\times \left[\frac{t\cos\kappa_0 t}{\kappa_0} + \frac{(s-t)\sin\kappa_0 t}{\gamma_0}\right] \tag{5.3.21}$$

5.3.2 Coupled TM Modes

Further demonstration of the Fourier transfrom method is shown below for the case of degenerate TM mode coupling between a pair of identical slab waveguides such that $\Delta k^2 = k_1^2-k_c^2 = k_2^2-k_c^2$ and $t=t_1=t_2$. Since both symmetric and asymmetric modes exist in a degenerate coupled system, therefore

$$e_{2x}(x) = \pm e_{1x}(-x+s-t) \ . \tag{5.3.22}$$

From the independent x-component equation of (5.2.3)

$$e_{1x}(x) + \frac{\Delta k^2}{2k_2^2}\left[e_{1x}(-t)e^{-\gamma(x+t)} + e_{1x}(0)e^{\gamma x}\right]$$

$$- \frac{\Delta k^2}{2\gamma}\int_{-t}^{0} e_{1x}(x')e^{-\gamma|x-x'|}dx'$$

$$+ \frac{\Delta k^2}{2k_2^2}\left[e_{2x}(s)e^{\gamma(x-s)} - e_{2x}(s-t)e^{\gamma(x-s+t)}\right]$$

$$- \frac{\Delta k^2}{2\gamma}\int_{s-t}^{s} e_{2x}(x')e^{\gamma(x-x')}dx' = 0$$

$$-t \le x \le 0. \tag{5.3.23}$$

Subsequent to application of the inverse Fourier-exponential transform for $e_{1x}(x)$ and $e_{2x}(x)$ as described in eq. (5.3.3) followed by procedures similar to the TE-mode case above, we obtain the allowable discrete eigenvalues for the transform variable:

$$\eta = \pm \kappa = \pm \sqrt{k_1^2 - \beta^2} \tag{5.3.24}$$

and the characteristic equation

$$e^{j\kappa t}\left[1 + \frac{k_2^2}{\gamma(\gamma - j\kappa)}\right]\left\{1 + \frac{k_2^2}{\gamma(\gamma - j\kappa)} \pm \left[1 + \frac{k_2^2}{\gamma(\gamma + j\kappa)}\right]\right.$$

$$\left.\left[e^{-j\kappa t - \gamma s} - e^{\gamma(t-s)}\right]\right\} =$$

$$e^{-j\kappa t}\left[1 + \frac{k_2^2}{\gamma(\gamma - j\kappa)}\right]\left\{1 + \frac{k_2^2}{\gamma(\gamma - j\kappa)} \pm \left[\frac{k_2^2}{\gamma(\gamma + j\kappa)}\right]\right.$$

$$\left.\times\left[e^{j\kappa t - \gamma s} - e^{\gamma(t-s)}\right]\right\} \tag{5.3.25}$$

Once more, when separation between slabs increases such that $s \to \infty$, we recover the familiar characteristic equation of the isolated TM mode slab waveguide as [42]

$$\tan\kappa t/2 = \begin{cases} \dfrac{k_1^2}{k_1^2}\left(\dfrac{\gamma}{\kappa}\right) & \ldots \text{ symmetric mode} \\ \dfrac{-k_2^2}{k_1^2}\left(\dfrac{\kappa}{\gamma}\right) & \ldots \text{ asymmetric mode.} \end{cases} \tag{5.3.26}$$

It is therefore evident from above results that Fourier-exponential transform method yields exact solution to the coupled EFIE's which describe a system of parallel slab waveguides. These correct solutions offer evidence to confirm the validity of the integral-operator formulation and provide confidence for its application to more complex problems.

5.4 Perturbation Approximation

5.4.1 Specialization for Coupled TE Modes

An appropriate perturbation solution was obtained in Section 4.4 to the simultaneous EFIE's describing a system of N coupled dielectric waveguides having propagating modes with exp ($\mp j\beta z$) axial dependence. The result was a homogeneous matrix equation for the coupled modal amplitudes involving coupling coefficients C_{mn}. Recall system (5.2.4), the EFIE's for the coupled TE modes supported by a slab system,

$$e_y(x) - \sum_{n=1}^{N} \int_{x_{1n}}^{x_{2n}} \delta k^2(x') e_y(x') g(x|x') dx' = 0$$

$$\text{... for } x_{1m} \leq x \leq x_{2m}, \quad m=1,2, \ldots, N. \tag{5.4.1}$$

The corresponding matrix equation for the one-dimensional system can be written as

$$\sum_{n=1}^{N} C_{mn} a_n = 0 \qquad \text{... for } m=1,2, \ldots, N. \tag{5.4.2}$$

with

$$C_{mn} = (\beta-\beta_m)\tilde{C}_{mm} \qquad \text{... for } m=n$$

$$\tilde{C}_{mm} = \int_{x_{1m}}^{x_{2m}} \delta k_m^2(x) e_{my}(x)\,dx \int_{x_{1m}}^{x_{2m}} \delta k_m^2(x') e_{my}(x') \left.\frac{\partial g}{\partial \beta}\right|_{\beta=\beta_m} \tag{5.4.3}$$

$$C_{mn} = \int_{x_{1n}}^{x_{2n}} \delta k_n^2(x) e_{my}(x) e_{ny}(x)\,dx \qquad \text{... for } n\neq m \tag{5.4.4}$$

where $e_{my}(x)$ is the eigenfield of the m'th isolated guide and is related to the coupled field $e_y(x)$ through the assumption

$$e_y(x) \cong a_n e_{my}(x) \qquad \text{... for } x_{1m} \le x \le x_{2m},\ m=1, 2, \ldots, N. \tag{5.4.5}$$

The eigenfields, supported by each individual isolated guide, have the functional forms as discribed in Section 3.1:

$$e_{my}(x) = \begin{cases} A_m \cos\kappa_m x & \text{... for } x_{1m} \le x \le x_{2m} \\ A_m \cos\kappa_m (t_m/2) e^{-\gamma_m (x-t_m/2)} & \text{... for } x \ge x_{2m},\ x \le x_{1m} \end{cases} \tag{5.4.6}$$

where individual transverse wavenumbers κ_m and γ_m are defined by $\kappa_m^2=k_m^2-\beta^2$ and $\gamma_m^2=\beta_m^2-k_c^2$. Figure 5.3 shows the configuration of two slabs, the m'th and n'th of a coupled system of N slab waveguides, separated by a distance of s_{mn} with widths of $2d_m$ and $2d_n$ respectively. By exploiting fields (5.4.6) in definition (5.4.4) we obtain

$$C_{mn} = \Delta k_n^2 A_m A_n \int_{-d_n}^{d_n} \cos\kappa_n \cos\kappa_m d_m \; e^{-\gamma_m(|x-s_{mn}|-d_m)}\, dx$$

$$= \frac{2A_m A_n \cos\kappa_m d_m (\gamma_m \cos\kappa_n d_n \sinh\gamma_m d_n + \kappa_n \sin\kappa_n d_n \cosh\gamma_m d_n)}{1 + (\beta_m^2-\beta_n^2)/\Delta k_n^2} \times$$

$$e^{-\gamma_m(s_{mn}-d_m)}$$

(5.4.7)

where $\Delta k_n^2=k_n^2-k_c^2$; similarly, for the diagonal matrix elements, i.e., m=n

$$\tilde{C}_{mm} = \frac{\Delta k_m^2 \beta_m d_m A_m^2}{\gamma_m^2} \left[1 + 2\,\frac{\sin 2\kappa_m d_m}{2\kappa_m d_m} - \cos 2\kappa_m d_m\right].$$

(5.4.8)

In deriving (5.4.8), we utilized the following differential operation

$$\frac{\partial}{\partial\gamma} e^{-\gamma|x-x'|} = -|x-x'| \frac{1}{\gamma\,\mathrm{sgn}(x-x')} \frac{\partial}{\partial x'} e^{-\gamma|x-x'|}$$

$$= -(x-x') \frac{1}{\gamma} \frac{\partial}{\partial x'} e^{-\gamma|x-x'|}.$$

(5.4.9)

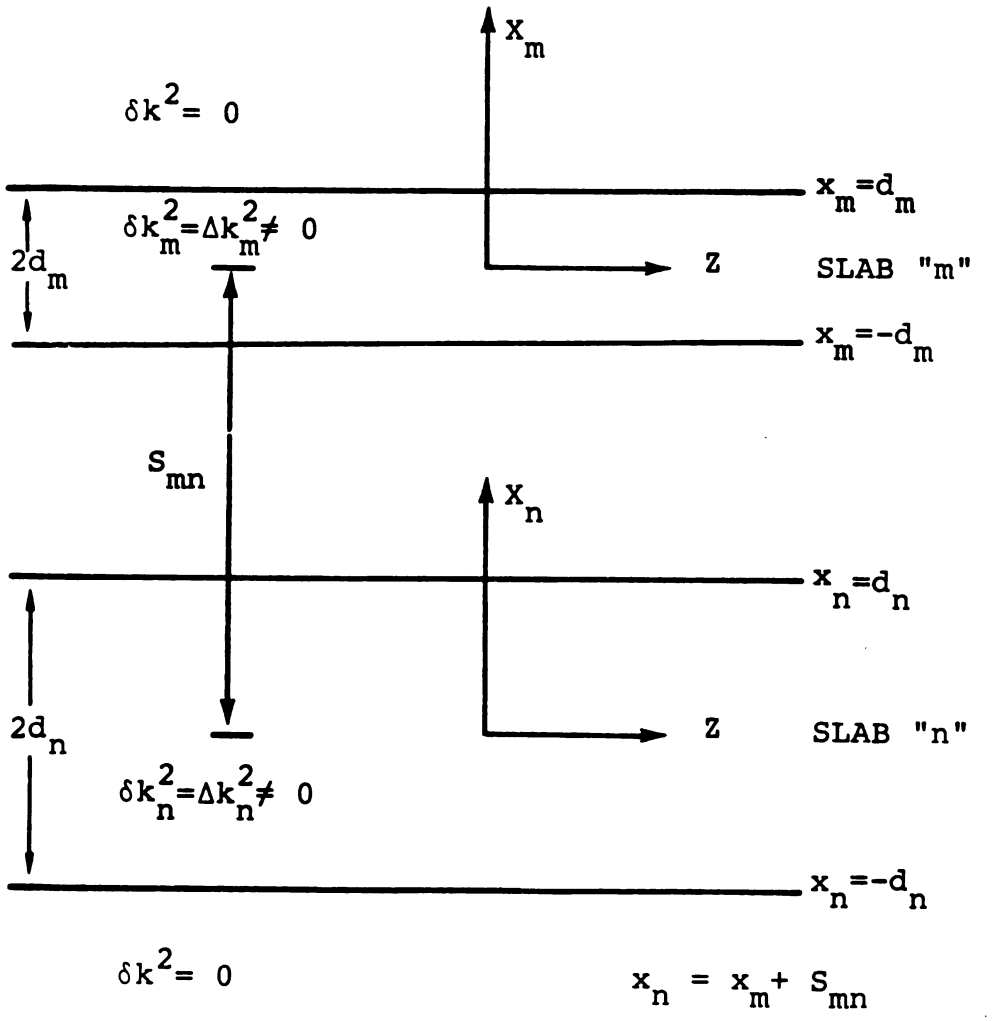

Figure 5.3 Configuration appropriate for study of non-degenerate TE surface-wave mode coupling between the m'th and the n'th guides in a N-coupled slab waveguide system.

5.4.2 Degenerately Coupled TE Modes between Two Slab Waveguides

For a pair of identical slab waveguide, the matrix equation reduces to a 2×2 system (Section 4.4), such that $a_2 = \pm a_1$, for even and odd surface-wave-mode coupling; furthermore $e_{1y}(x) = e_{2y}(x) = e_y(x)$, and $\beta_1 = \beta_2 = \beta_0$. From eq. (4.4.15)

$$\begin{bmatrix} C_{11} & C_{12} \\ C_{21} & C_{22} \end{bmatrix} \begin{bmatrix} a_1 \\ a_2 \end{bmatrix} = 0 \tag{5.4.10}$$

Since $C_{12}=C_{21}$, and $C_{11}=C_{22}$, the requirement of $\det [C_{mn}] = 0$ for non-trivial solution of (5.4.10) leads to

$$(\beta - \beta_0) = \Delta\beta = \pm \frac{C_{12}}{\tilde{C}_{11}} \tag{5.4.11}$$

This is the shift of propagation constant from that of the isolated slab in the presence of loose coupling to the decaying field of the other slab waveguide. Substituting (5.4.7) and (5.4.8) into (5.4.10) yields

$$\Delta\beta = \pm \frac{2\cos\kappa_0 d(\gamma_0\cos\kappa_0 d\sinh\gamma_0 d + \kappa_0\sin\kappa_0 d\cosh\gamma_0 d)\, e^{-\gamma_0(s-d)}}{\frac{\Delta k^2 \beta_0 d}{\gamma_0^2}\left[1 + 2\,\frac{2\sin 2\kappa_0 d}{2\kappa_0 d} - \cos 2\kappa_0 d\right]} \tag{5.4.12}$$

where 2d is the width of each slab waveguide. Relative amplitude for the coupled-mode fields, $a_2/a_1 = \pm 1$, can then be deduced from (5.4.10) corresponding to the system-mode propagation constant $\beta = \beta_0 \pm \Delta\beta$ for the symmetric and asymmetric system modes.

5.5 Numerical Results

DEGENERATE TE MODE SOLUTIONS

Refer to Figure 5.4, which indicates two identical, parallel slabs having normalized wavenumber $k_2t=32$, and the ratio of refractive index between slab and surrounding cladding (index contrast) as $n_1/n_2 = 1.01$. These are the parameters used in Marcuse's paper [31]. There are three allowable propagating TE modes with $\beta_0 t=32.06$, 32.248 and 32.32. The normalized phase shifts ($\Delta\beta t$), as calculated from result of weak coupling approximation to the exact eigenvalue equation (5.3.20), are shown in Figure 5.5 as a function of normalized separation s/t between guides. The results agree very well with those solutions to the exact eigenvalue equation.

Perturbation solutions, using both the delta-function (in effect, a point matching technigue) and the eigenfunction field of (4.5.2) of the isolated slab (which weights the solution across the width of the slab) testing operators yield ($\Delta\beta t$) as a function of s/t are shown in Figure 5.6. It is as expected that more accurate results are obtained in the simple point matching method from the solution

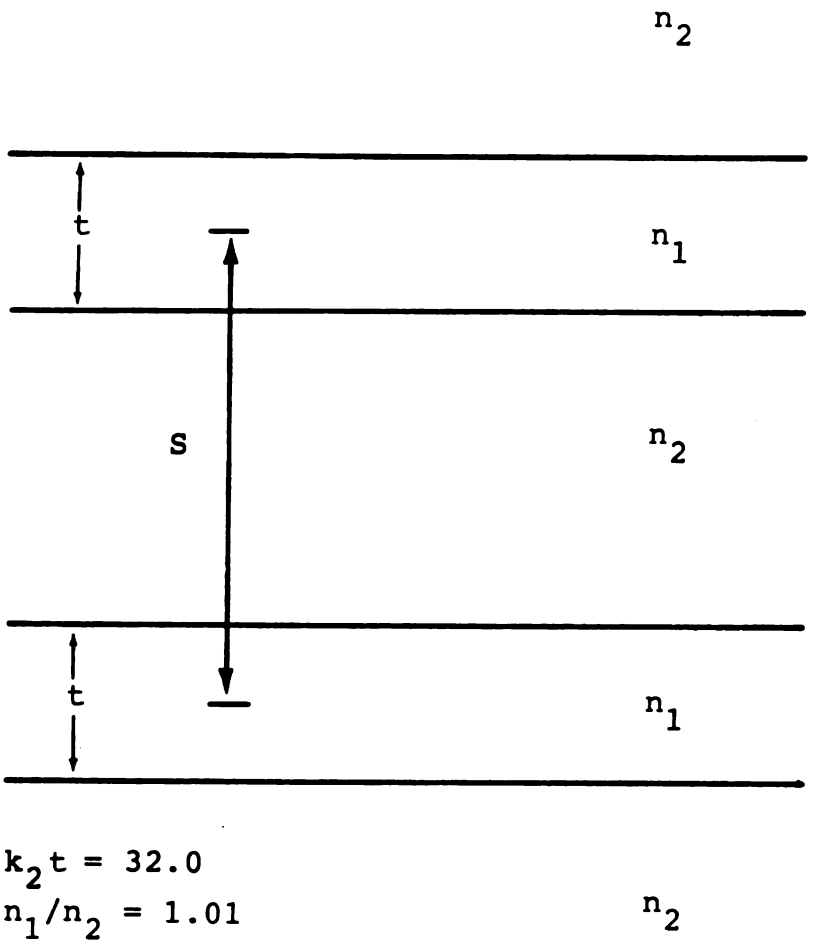

Figure 5.4 Configuration appropriate for study of degenerate TE surface-wave mode coupling between two identical slabs.

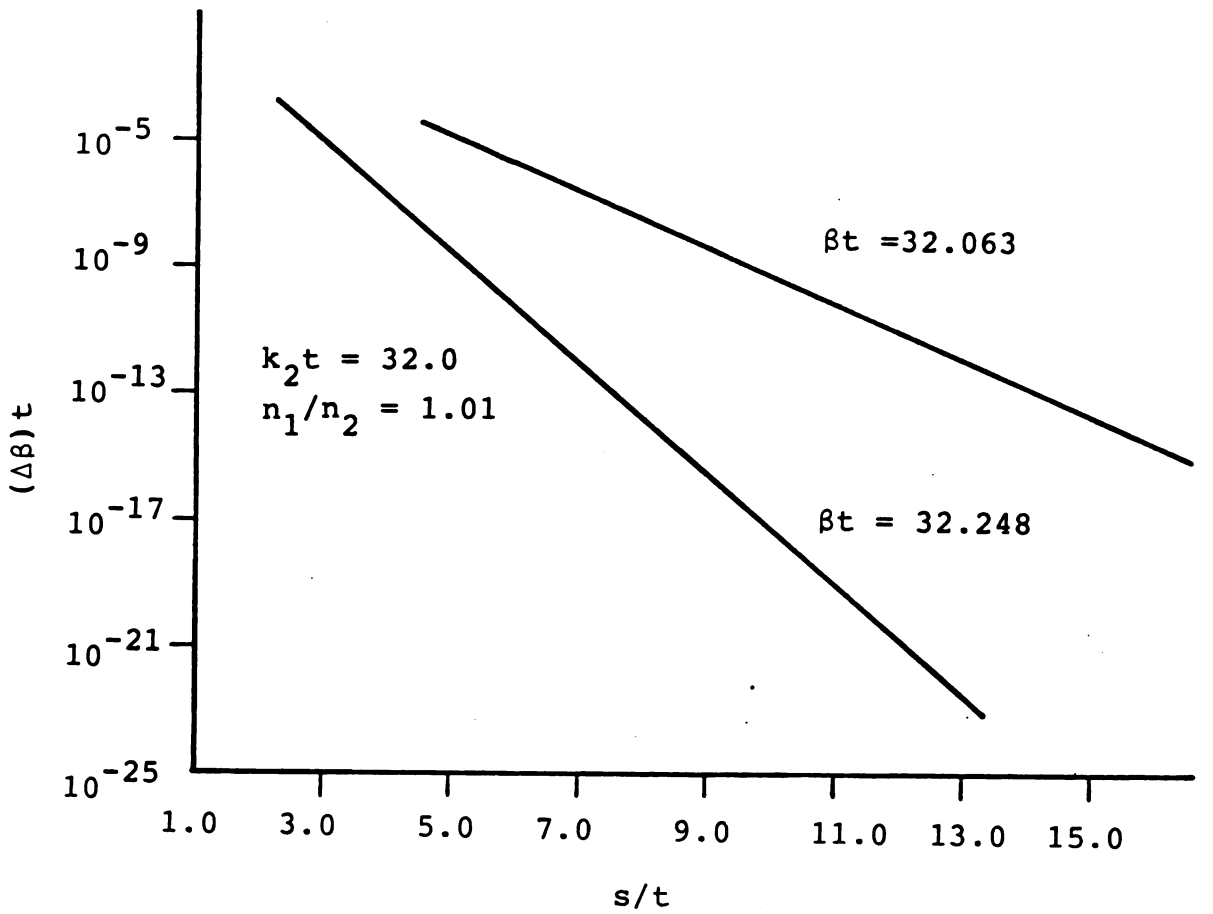

Figure 5.5 Normalized phase constant shift for two propagating modes of a degenerately coupled two-slab system. (n_1=1.6, n_2=1.0)

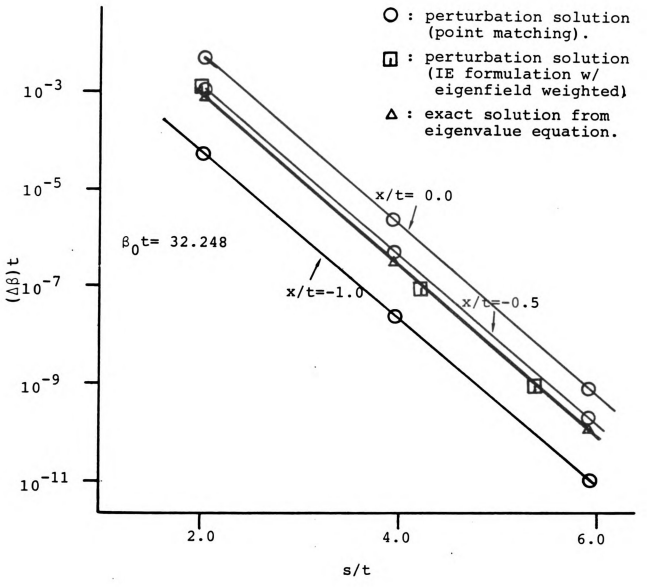

Figure 5.6 Comparison of resulting values for normalized phase constant shifts from various solutions in a degenerately coupled two-slab system. (n_1=1.6, n_2=1.0)

corresponding to a matching point at x/t=-0.5; this result confirms the intuitive expectation that a matching point at the guide center is most appropriate.

Perturbation solutions leading to $\Delta\beta$ as derived in expression (5.4.12) are shown in Figures 5.7 through 5.10 for another slab configurations. There, perturbation results are compared with numerical solutions obtained from the exact eigenvalue equation by Wilson and Reinhart [32]. In Figure 5.7, the small core/ surround index contrast (n_g/n_c=1.05) results in a slowly decaying field outside of each slab; consequently a stronger coupling is evident as comparison are made with those corresponding results of Figure 5.8 (n_g/n_c=1.6) and 5.9 (n_g/n_c=1.2). It is also observed from Figures 5.8 and 5.9 that the perturbation solutions converge to the exact solutions much faster in the later case due to weaker coupling arising from larger value of it's decay coefficient γ. The width of guide 2 is increased by a factor of 5 in Figures 5.10 from that of Figure 5.7 to study degenerate coupling between differing guides. The refractive index of guide 2 is reduced to n_g/n_c=1.02 as its width is increased to maintain an isolated phase constant $\beta_{02}=\beta_{01}$ equal to that of guide 1. Degenerate coupling between dissimilar guides is consequently implemented. Although the decay constants of the isolated surfce-wave modes are identical for such degenerate coupling, the coupling coefficients are modified due to the differing field distributions of the coupled modes.

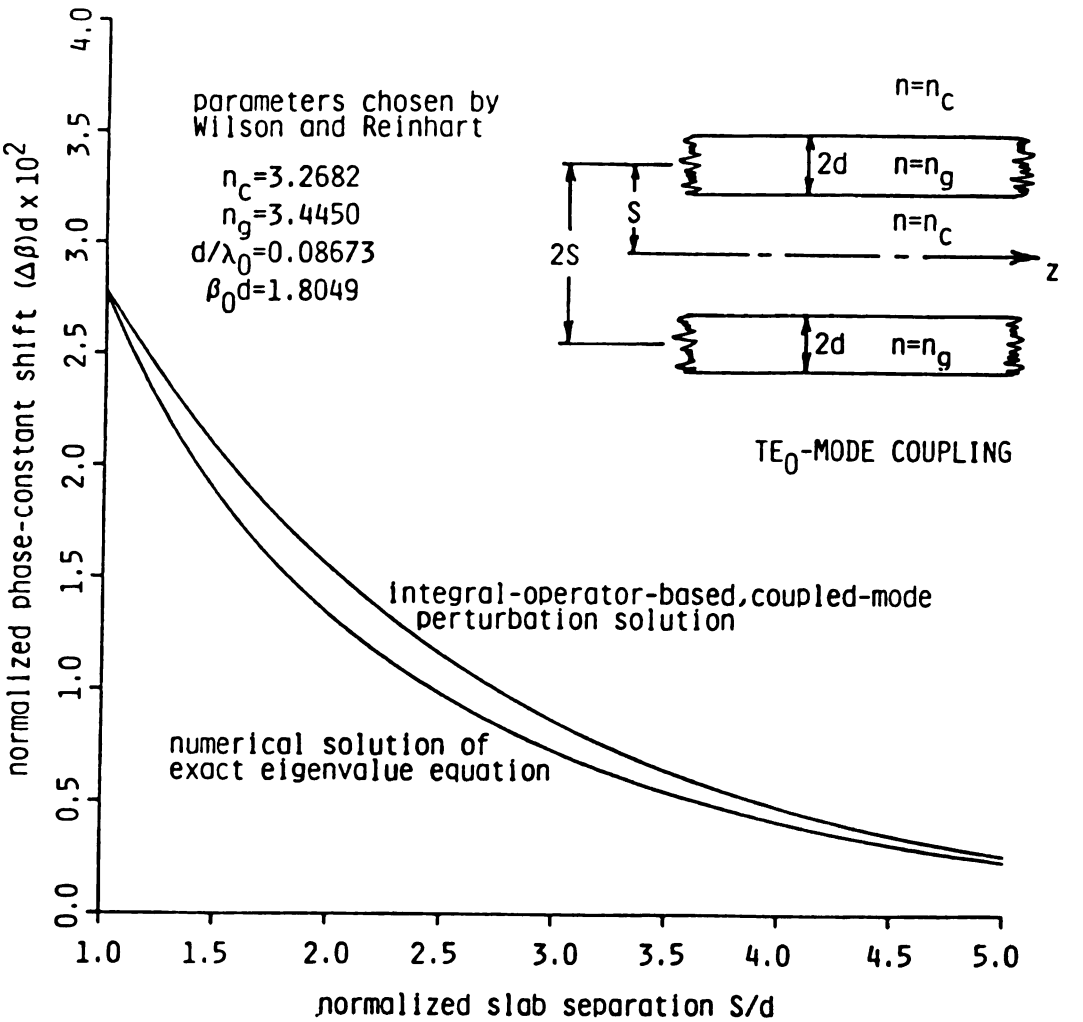

Figure 5.7 Comparison of results from integral-operator based, coupled-mode perturbation solution with numerical solutions to the exact eigenvalue equation for phase constant shift $(\Delta\beta)d$ due to degenerate-mode coupling between identical slab waveguides with variable spacing s/d.

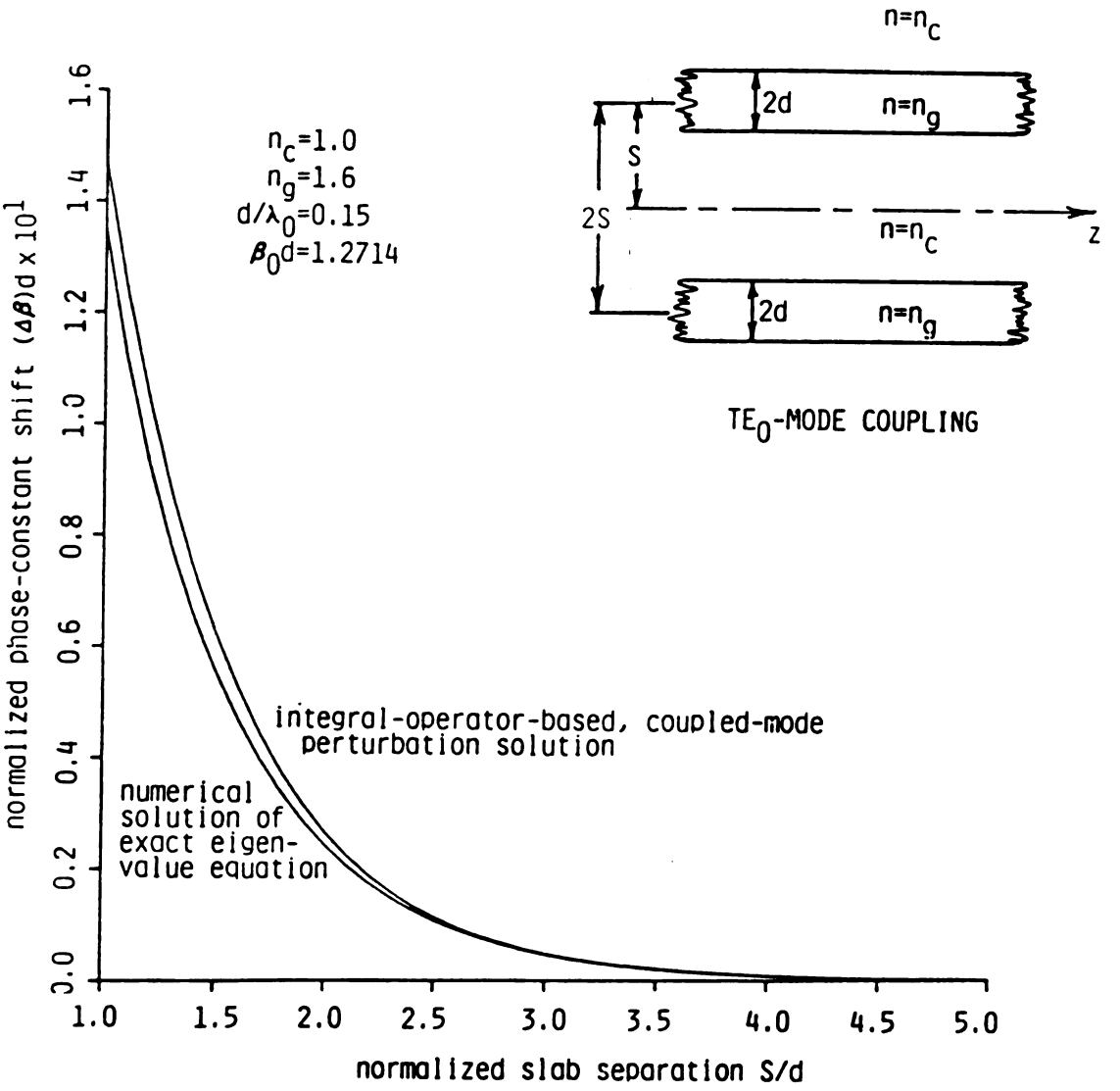

Figure 5.8 Comparison of results from integral-operator-based, coupled-mode perturbation solution with numerical solutions to the exact eigenvalue equation for phase-constant shift ($\Delta\beta$)d due to degenerate-mode coupling between identical slab waveguides with variable spacing s/d.

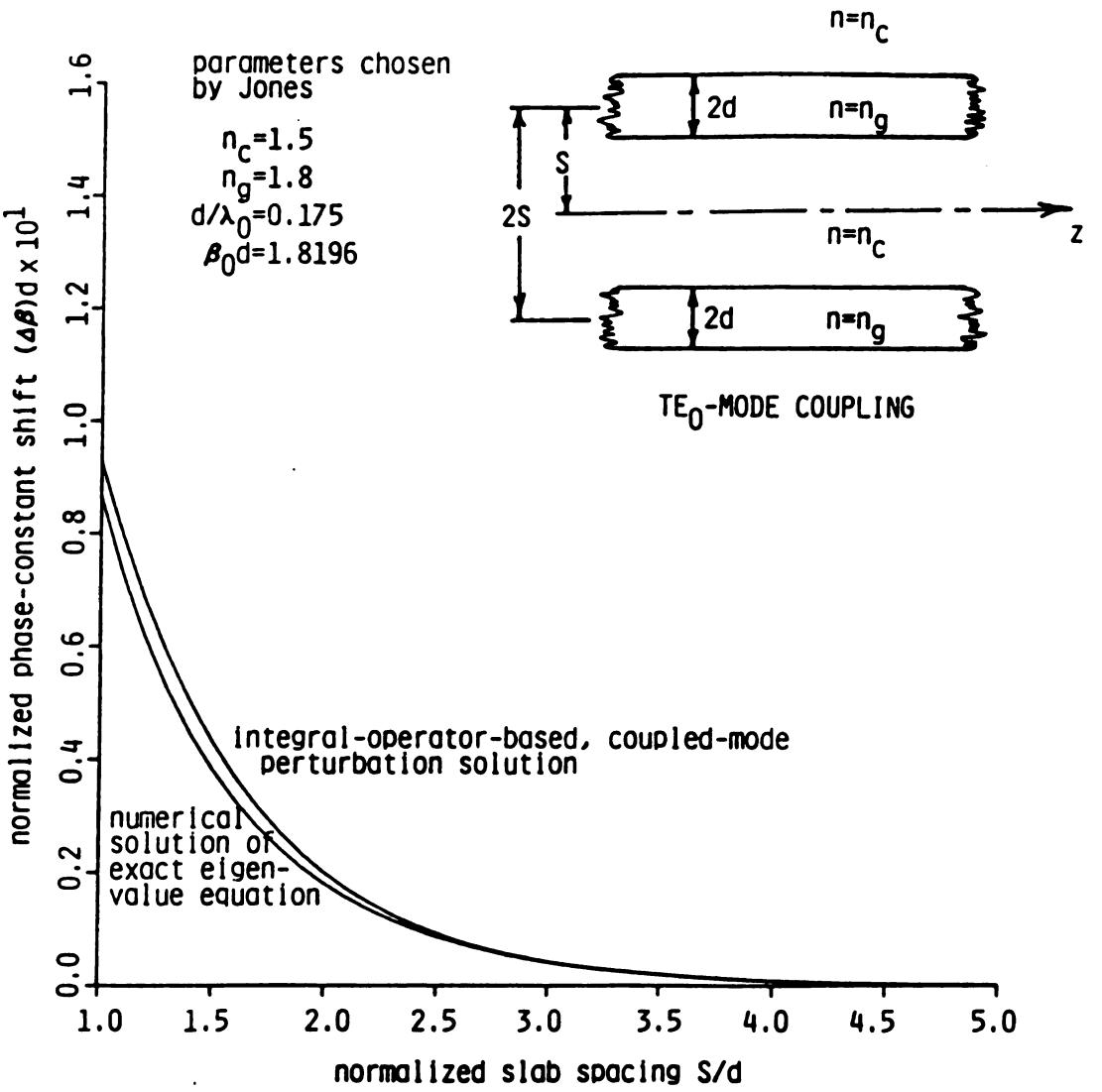

Figure 5.9 Comparison of results from integral-operator-based, coupled-mode perturbation solution with numerical solutions to the exact eigenvalue equation for phase-constant shift $(\Delta\beta)d$ due to degenerate-mode coupling between identical slab waveguides with variable spacing s/d.

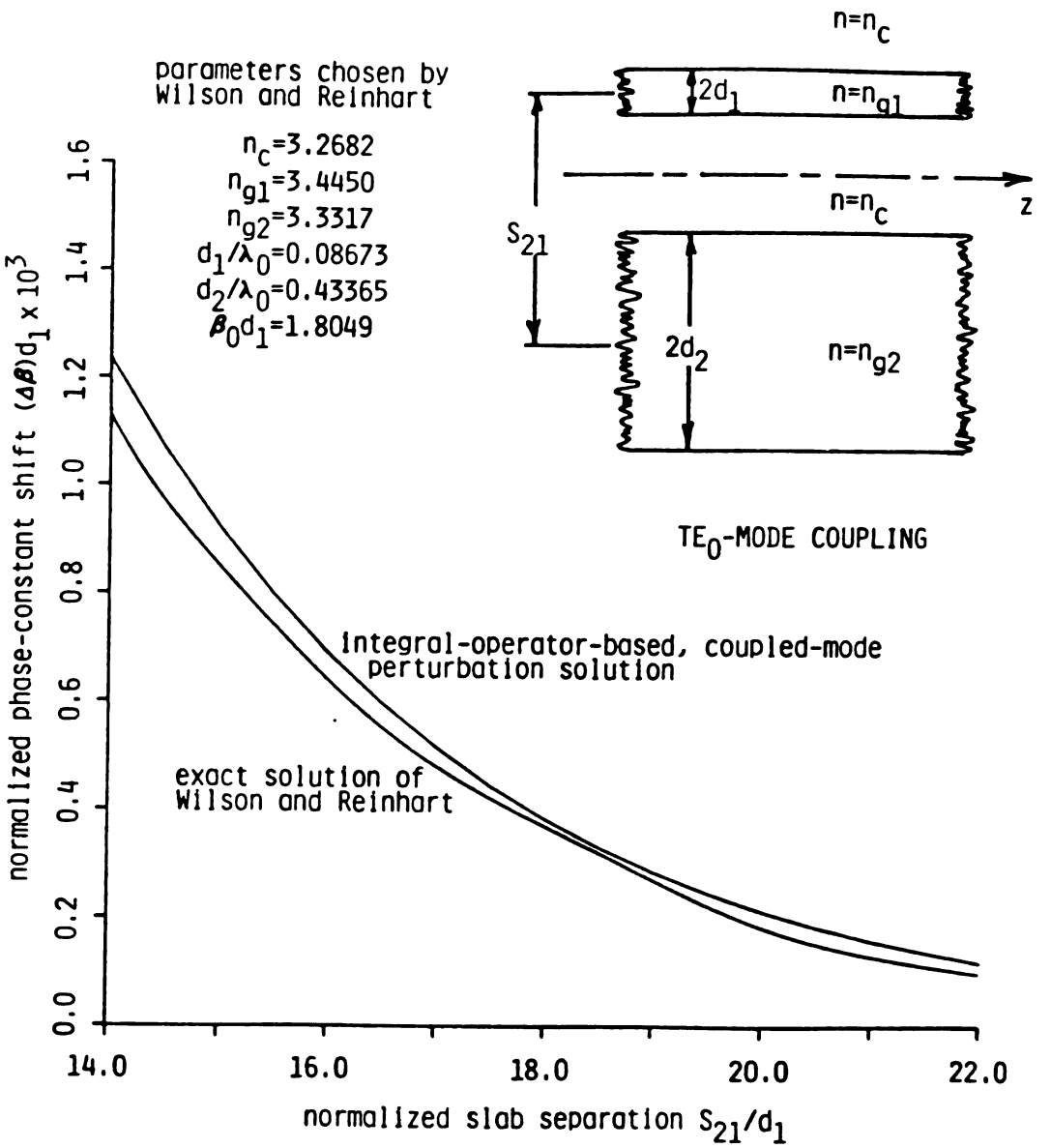

Figure 5.10 Comparison of results from integral-operator-based, coupled-mode perturbation solution with the exact solution of Wilson and Reinhart for phase-constant shifts $(\Delta\beta)d_1$ due to degenerate mode coupling between different slab waveguides with variable spacing s_{21}/d_1.

Excellent agreement with numerical solutions to the exact eigenvalue equation are again obtained.

NON-DEGENERATE TE MODE SOLUTIONS

Figure 5.11 through 5.15 demonstrate the coupling between two non-degenerately coupled slab waveguides. Shown in these figures are results for both system modes, i.e., $\beta = \bar{\beta} \pm \delta\beta$. Once more, good agreement is obtained for phase constant shift when compare the perturbation solution with those from the exact eigenvalue equation (Figure 5.11). Figure 5.13 shows the normalized coupled-modal amplitudes as a function of normalized slab spacings, using the ratio of the slab widthes as parameter. It is observed that when both guides are in proximity of each other, strong coupling results in almost equal modal amplitudes as expected intuitively. Also, when $d_2/d_1 = 1.0$, i.e., the coupling becomes degenerate, symmetric and asymmetric modes (having equal amplitudes) are obtained on both guides (Figure 5.15) as discussed in the last section.

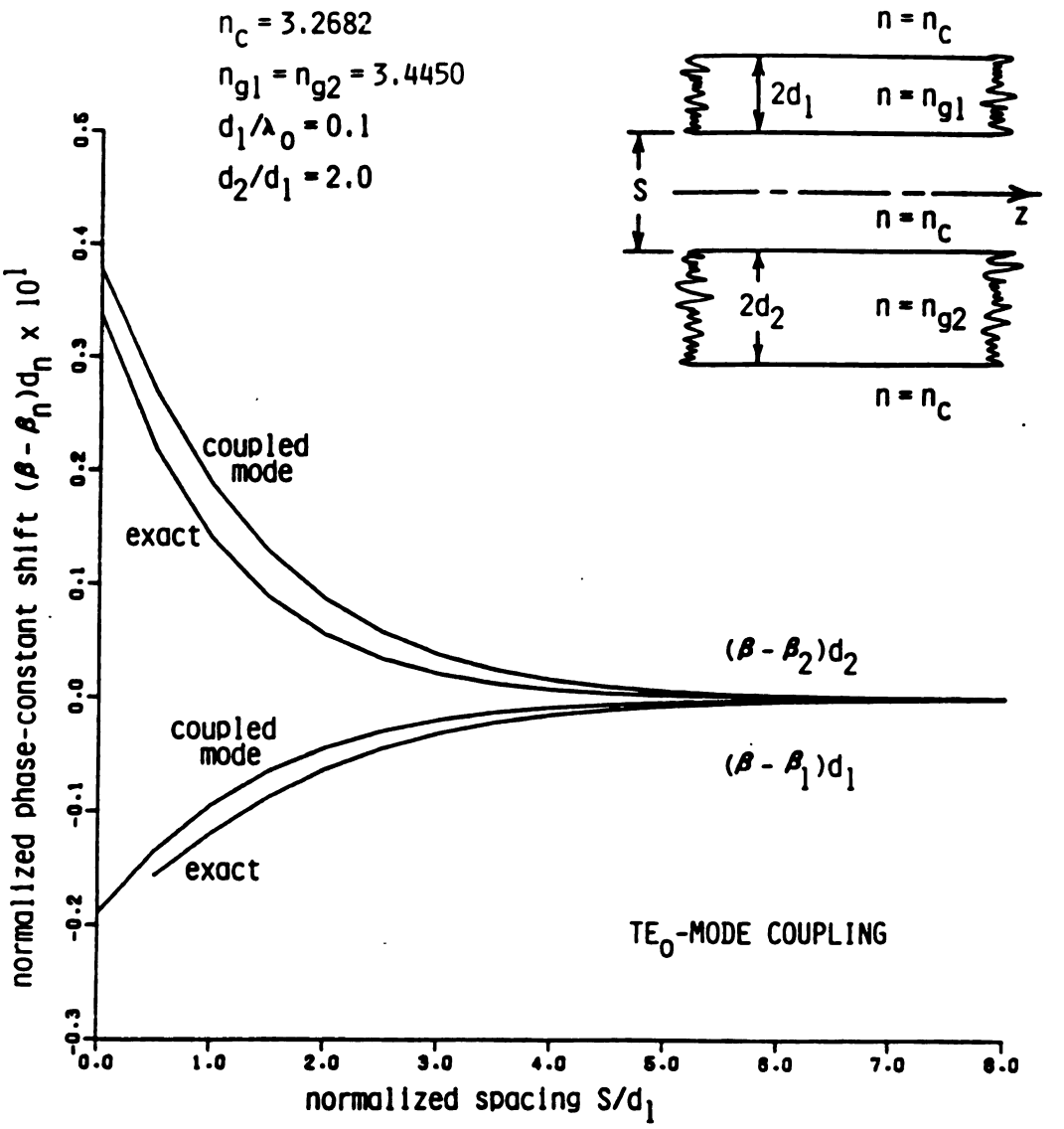

Figure 5.11 Results of integral-operator-based, coupled-mode perturbation solution for non-degenerate TE_0-mode coupling between differing slab waveguides; phase-constant shifts for variable spacing s/d_1.

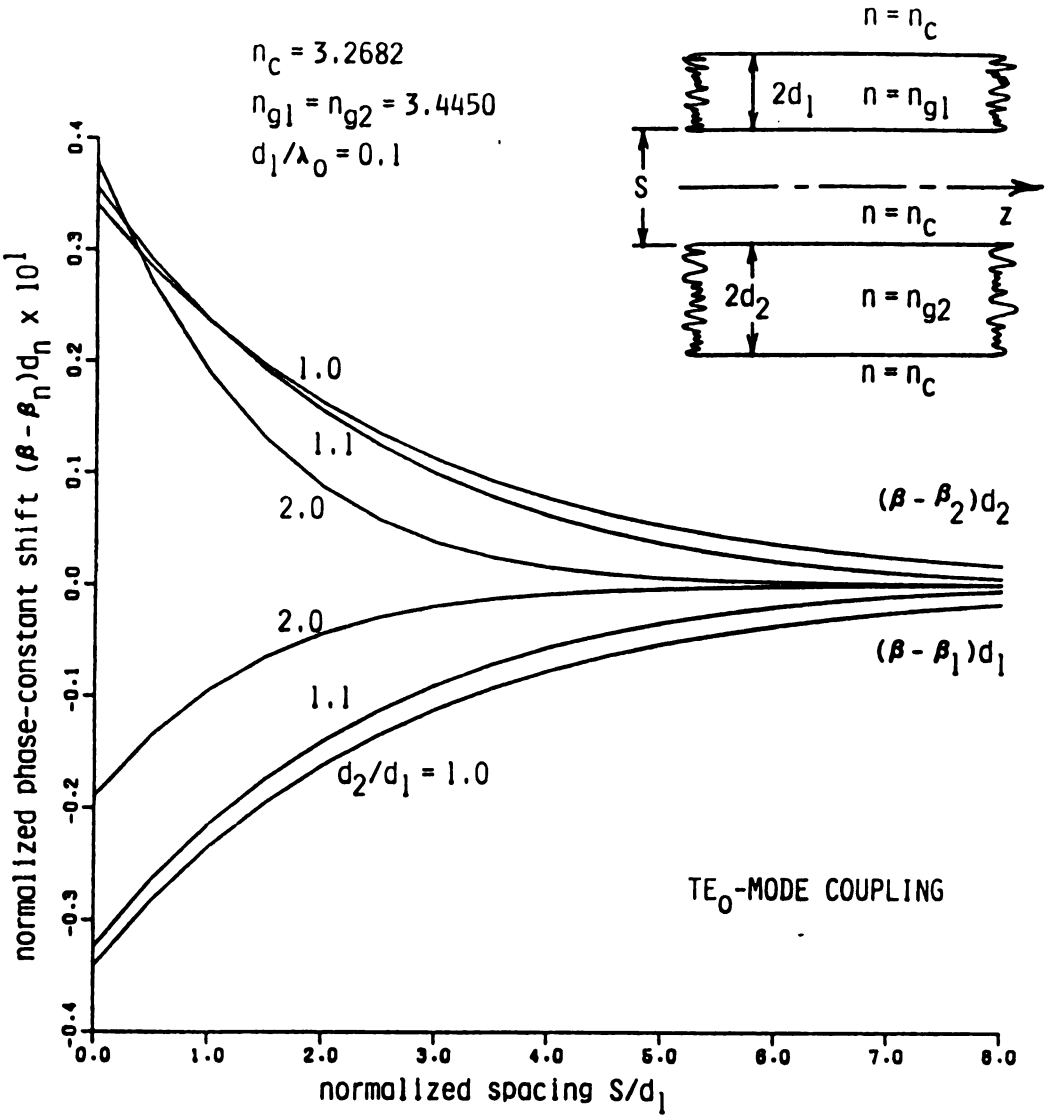

Figure 5.12 Results of integral-operator-based, coupled-mode perturbation solution for non-degenerate TE_0-mode coupling between differing slab waveguides; phase-constant shifts for variable spacing s/d_1.

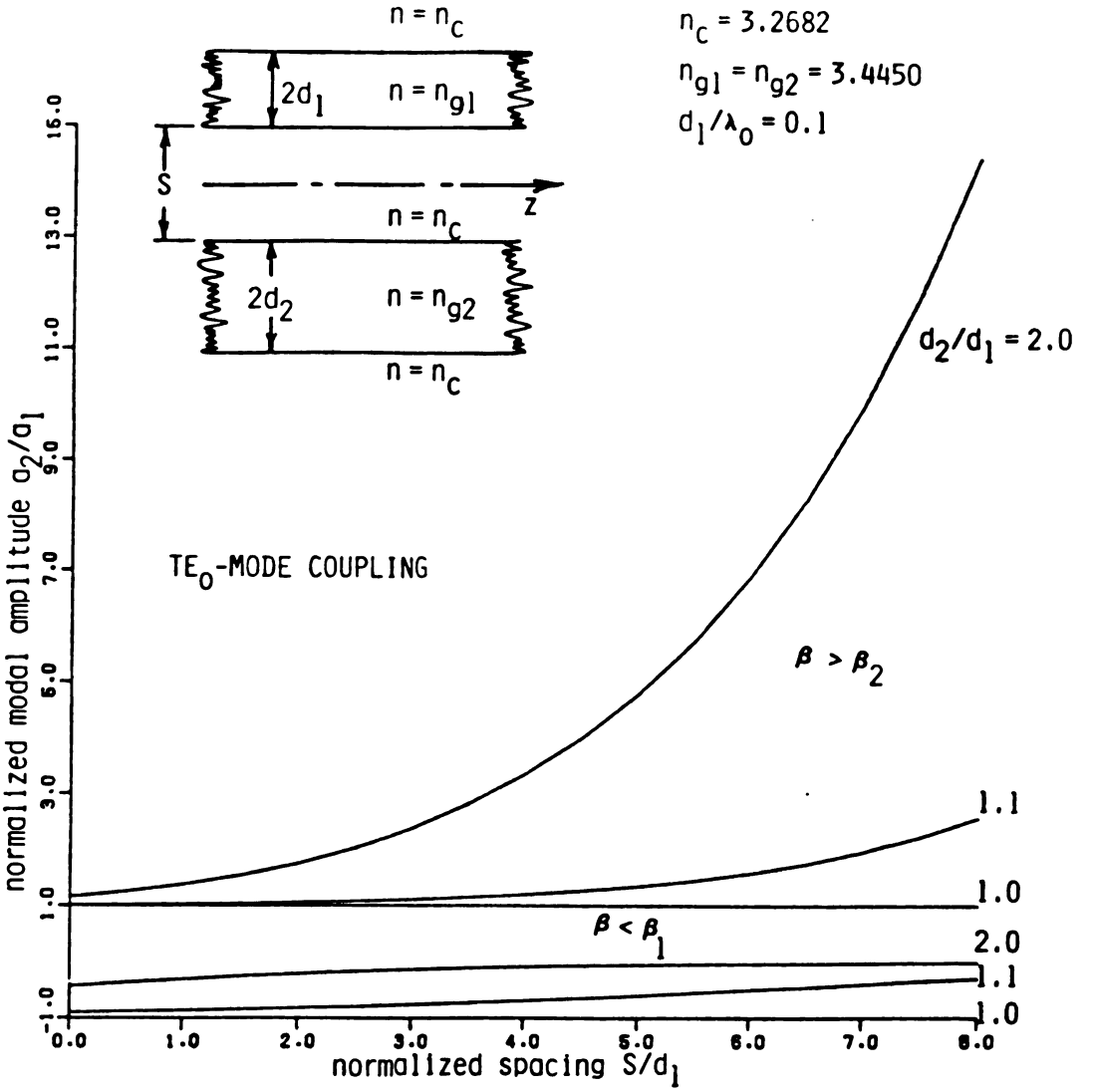

Figure 5.13 Results of integral-operator-based, coupled-mode perturbation solution for non-degenerate TE_0-mode coupling between differing slab waveguides; amplitude ratios for variable spacing s/d_1.

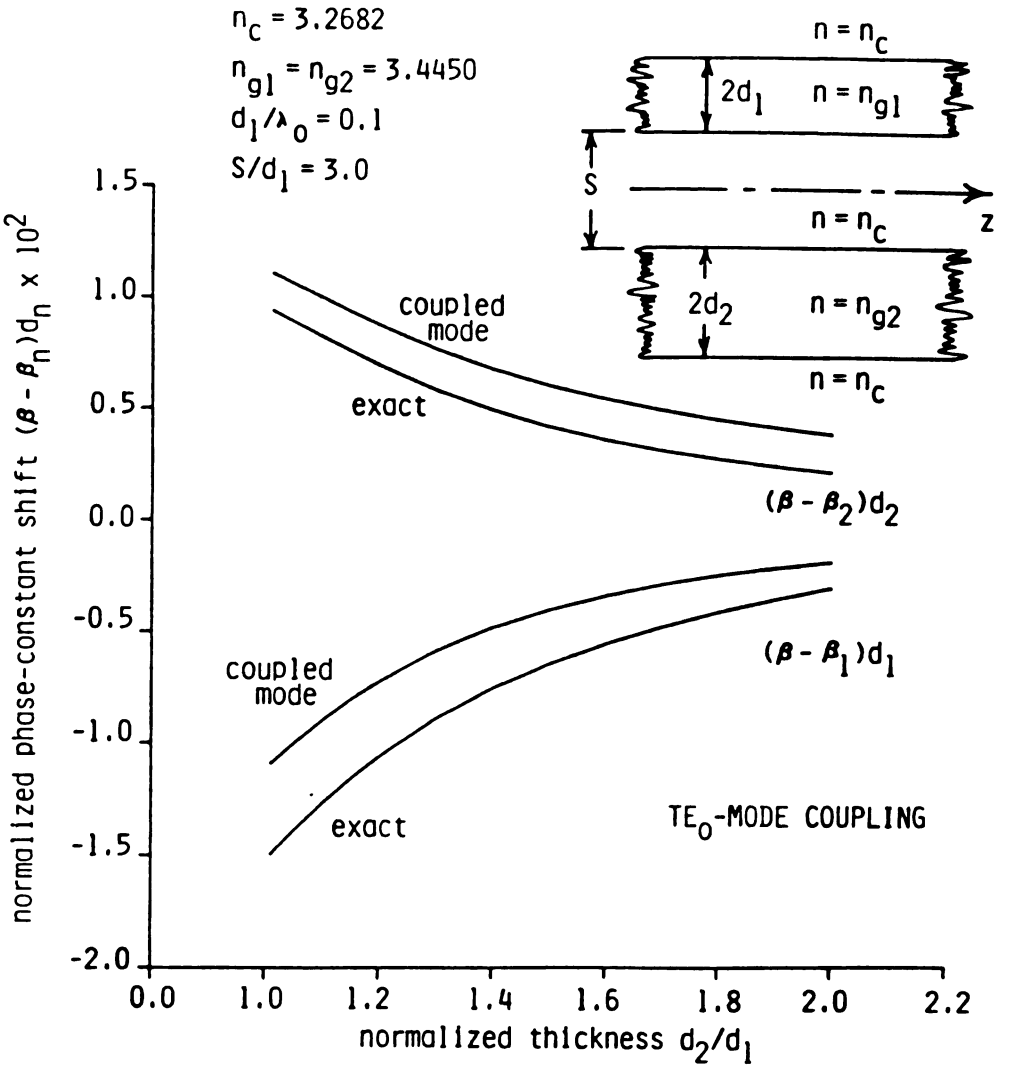

Figure 5.14 Results of integral-operator-based, coupled-mode perturbation solution for non-degenerate TE_0-mode coupling between differing slab waveguides; phase-constant shifts (exact and coupled-mode) for variable thickness d_2/d_1.

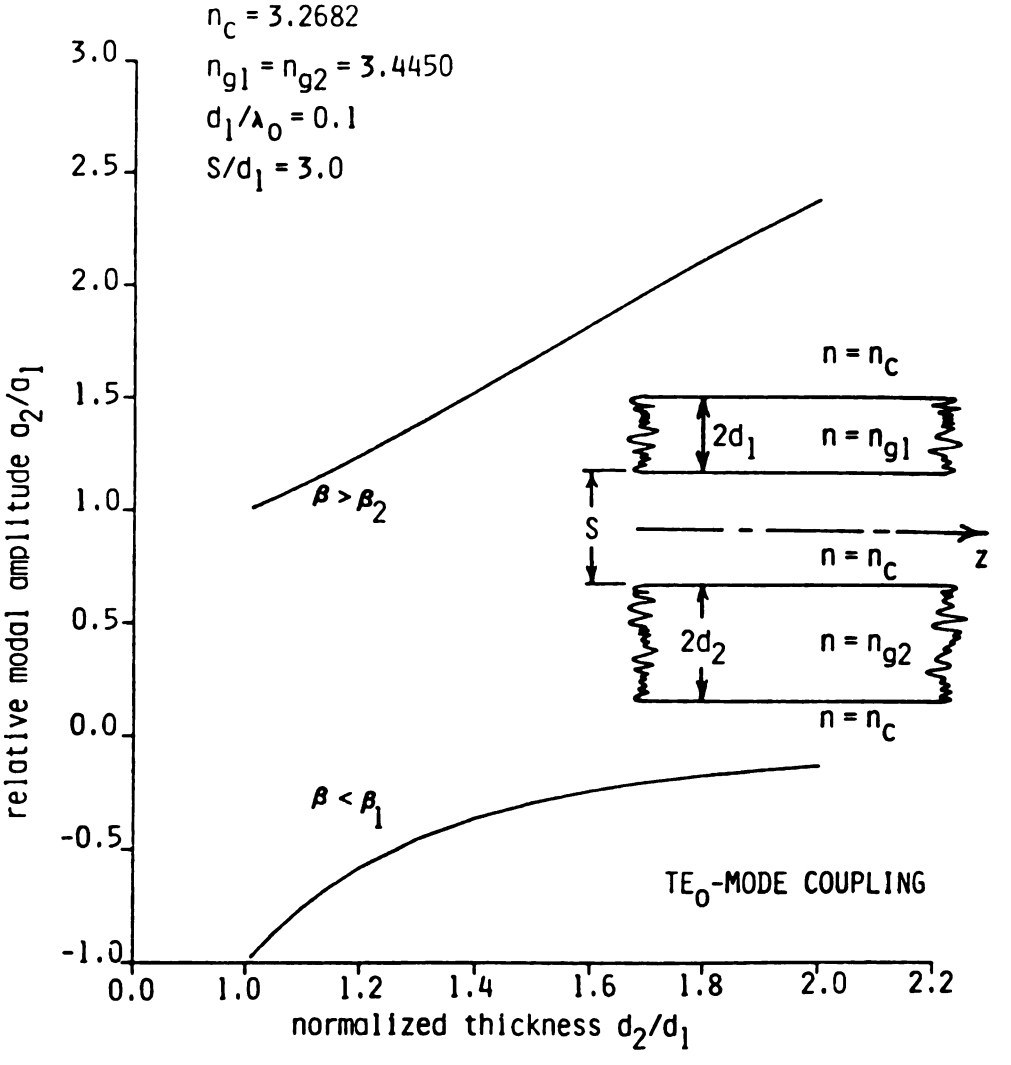

Figure 5.15 Results of integral-operator-based, coupled-mode perturbation solution for non-degenerate TE_0-mode coupling between differing slab waveguides; modal amplitude ratio for variable thickness d_2/d_1.

CHAPTER VI

CONCLUSION

An integral-operator technique, representing an alternative to conventional boundary-value analysis, has been applied to two classes of problems for EM wave propagation along open-boundary dielectric waveguides. First, the scattering of surface-wave modes by a discontinuity along the waveguide. Second, the coupling of surface-wave modes in a multi-waveguide system.

In the construction of a volume electric field integral equation, equivalent polarization current is essential to its formulation. Identification of this current for the device discontinuity region results from the index contrast between the discontinuity and the unperturbed background waveguide; it is this current which maintains the scattered field. Using this scattered field in conjunction with the incident field, the unknown total field is cast into an integral equation and numerical solutions are subsequently sought. For the coupling problem, a system of N coupled waveguides is replaced by equivalent polarization sources which arise from the index contrast between each core and its surround cladding. This current then radiates into unbounded space in the presence of other sources. Coupling

phenomena are the consequence of the total contributions of all the fields maintained by these N coupled polarization sources.

Solutions to the resulting EFIEs' are demonstrated through the application to slab waveguides. In the treatment of scattering by dielectric-slice obstacles, neglecting the contribution from radiation spectrum for small discontinuies, a Fourier transform method yields the limiting reflection and transmission coefficients which are further confirmed by the Moment Method numerical calculation. Other results, including the contributions from the radiation spectrum, are also computed by MoM solution and an approximate solution assuming fields in the slice region have the axial propagation constant obtained in the radiationless case. In the coupling treatment, again, a Fourier transform approach recovers the familiar eigenvalue equation for a two-slab system. Together with the above treatment for scattering, this demonstrates the versatility of the transform technique. Subsequent coupled-mode perturbation analysis yields the exact results which can be obtained from the conventional differential-operator approximation. This new coupled-mode theory is applicable to relatively general waveguide systems, since it requires approximation of only the waveguide core fields.

In short, the contributions of this dissertation research are that the applicability of Integral-Operator analysis is clearly demonstrated and the correctness of the

obtained results are verified. This method, when considering the abundance of unsolved problems associated with the open-boundary waveguide structures in both the optical and millimeter regions, provides an invaluable tool for future research in these areas. To further emphasize this point, it was recently pointed out by Oliner, et al. [30,37] that the approximate treatments [12,60] of surface-wave modes supported by integrated dielectric waveguides neglect, due to an inadequate account for coupling between TE and TM components of the hybrid modes, important physical phenomena. Those new physical effects include both leakage and sharp resonance phenomena not predicted by the conventional approximate methods. It is clear that the integral-operator analysis described in this research provides an exact description of the hybrid propagation modes; it will therefore expose the same new effects for a more general class of graded-index dielectric waveguide systems having cores of any cross-section shape.

Future research in the extention and application of this powerful analysis should consider the complex configurations of practical integrated waveguide systems i.e., isolated, or coupled systems of integrated guides as indicated in Figure 6.1. In that Figure, waveguide cores are deposited upon a uniform thin-film layer of index n_f and the waveguides are covered by a uniform cladding overlay of index n_c while the film layer is deposited upon a uniform substrate of index n_s. Recommended investigations of the

resulting rib or strip structures from such a configuration include: i) surface-wave propagation modes supported by the graded-index rib waveguide, by approximate perturbation, and numerical methods, ii) study of system-mode surface waves supported by coupled systems (both parallel and non-parallel) of graded strip, channel and rib waveguides using quasi-closed-form exact and approximate coupled-mode approaches, iii) description of propagation modes supported by electrooptic integrated dielectric waveguides, iv) analysis on the coupling of radiation to and from integrated dielectric waveguide systems, including quantification of continuous-spectrum radiation modes on rib-related waveguide structures as forced solutions to the appropriate EFIE's and v) experimental confirmation of selected analytical predictions.

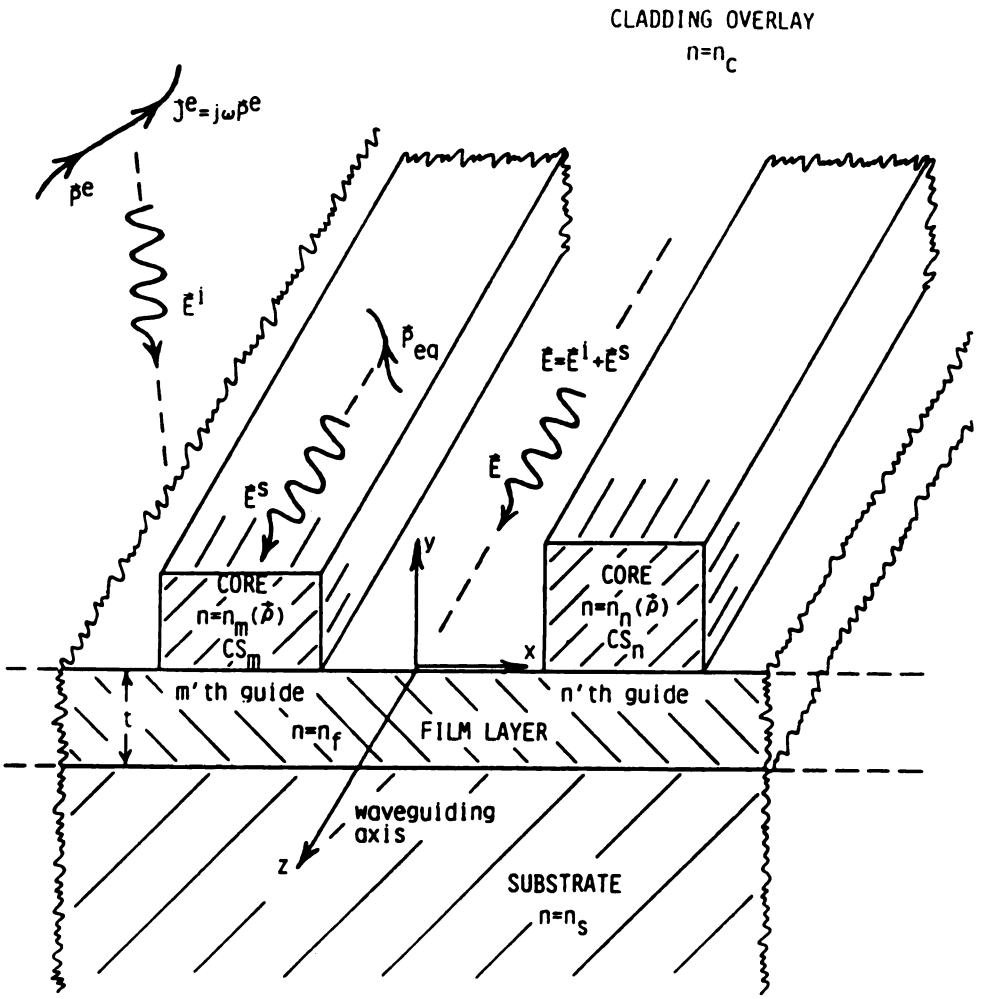

Figure 6.1 Configuration of integrated, open-boundary, dielectric-waveguide system consisting of arbitrary-shaped, graded-index core regions adjacent to the film/overlay interface deposited upon a uniform substrate.

LIST OF REFERENCES

LIST OF REFERENCES

[1] D. Hondros, and P. Debye, "Elektromagnetische Wellen in dielektrischen Drähten." Ann. Physik, vol. 32, pp. 456-476, 1910.

[2] S.E. Miller, "Integrated Optics: An introduction." BSTJ, vol. 48, pp. 2059-2069, 1969.

[3] N.S. Kapany, Fiber Optics, New York: Academic Press, 1967.

[4] H. Kogelnik, "Limits in Integrated Optics," Proc. IEEE, vol. 69, no. 2, pp. 232-238, Feb. 1981.

[5] R.M. Knox, "Dielectric Waveguide Microwave Integrated Circuits-An Overview," IEEE MTT-s Trans., vol. MTT-24, no. 11, pp. 806-814, Nov. 1976.

[6] H.R. Taylor and A. Yariv, "Guided Wave Optics," Proc. IEEE, vol. 62, no. 8, pp. 1044-1060, August 1974.

[7] R.C. Pate and E.F. Kuester, "Fundamental Propagation Modes on a Dielectric Waveguide of Arbitrary Cross Section," Sci. Rpt. no. 45, U.S. Army Research Office, Contract no. DAAG29-78-C-0173, Electromagnetics Laboratory, University of Colorado, Boulder, Colorado, Feb. 1979.

[8] C. Yeh, "Optical Waveguide Theory," Digest of North American Radio Science (URSI) Meeting, Laval University, Quebec, Canada, p. 78, June 1980.

[9] R.E. Collin, Field Theory of Guided Waves, New York: McGraw-Hill, 1960, pp. 453-508.

[10] N.S. Kapany and J.J. Burke, Optical Waveguides, New York: Academic Press, 1972.

[11] D. Marcuse, Theory of Dielectric Optical Waveguides, New York: Academic Press, 1974.

[12] E.A.J. Marcatili, "Dielectric Rectangular Waveguide and Directional Coupler for Integrated Optics," BSTJ, vol. 48, no. 9, pp. 2071-2102, Sept. 1969.

[13] J.E. Goell, "A Circular-Harmonic Computer Analysis of Rectangular Dielectric Waveguides," BSTJ, vol. 48, no. 9, pp. 2133-2160, Sept. 1969.

[14] D.R. Johnson and D.P. Nyquist, "Integral-Operator Analysis of Dielectric Optical Waveguides - Theory and Application," Digest of Radio Science (URSI) Meeting, University of Colorado, Boulder, Colorado, p. 104, Nov. 1978.

[15] S.V. Hsu and D.P. Nyquist, "Integral-Operator Analysis of Coupled Dielectric Waveguide System - Theory and Application," Digest of Radio Science (URSI) Meeting, University of Washington, Seattle, Washington, June 1979.

[16] D.R. Johnson and D.P. Nyquist, "Numerical Solution of Integral-Operator Equation for Natural Modes along Heterogeneous Optical Waveguides," Digest of National Radio Science (URSI) Metting, University of Colorado, Boulder, Colorado, p. 156, Jan. 1981.

[17] B.Z. Katsenelenbaum, "On the Propagation of Electromagnetic Waves along an Infinite Dielectric Cylinder at Low Frequencies," Dokl. Akad. Nauk. SSSR, vol. 58, no. 7, 1947 (in Russian).

[18] S.V. Hsu and D.P. Nyquist, "Integral-Operator Formulation for scattering from Obstacles in Dielectric Optical Waveguides," USNC/URSI Meeting, University of Colorado, Boulder, Colorado, digest p. 90, Nov. 1979.

[19] S.V. Hsu and D.P. Nyquist, "Integral-Equation Formulation for Mode Conversion and Radiation from Discontinuity in Open-Boundary Waveguide," Digest of North American Radio Science (URSI) Meeting, Laval University, Quebec, Canada, p. 62, June 1980.

[20] D. Marcuse, "Radiation Losses of Tapered Dielectric Slab Waveguide," BSTJ, vol. 49, no. 2, p. 273, Feb. 1970.

[21] S.F. Mahmoud and J.C. Beal, "Scattering of Surface Waves at a Dielectric Discontinuity on a Planar Waveguide," IEEE MTT-s Trans., vol. MTT-23, no. 2, p. 193, Feb. 1975.

[22] B. Rulf, "Discontinuity Radiation in Surface Waveguides," JOSA, vol. 65, no. 11, p. 1248, Nov. 1975.

[23] K. Morishita, S.I. Inagaki, and N. Kumagai, "Analysis of Discontinuities in Dielectric Waveguides by the Least Squares Boundary Residual Method," IEEE MTT-s Trans., vol. MTT-27, no. 4, pp. 310-315, April 1979.

[24] L. Lewin, "A Method for the Calculation of the Radiation Pattern and Mode-Conversion Properties of a Solid-State Heterojunction Laser," IEEE MTT-s Trans., vol. MTT-23, no. 7, pp. 576-585, July 1975.

[25] R.W. Davis and J.N. Walpole, "Output Coupling for closely confined $pb_{1-x}Sn_xTe$ Double Heterostructure Lasers," IEEE J. Quant. Elect., vol. QE-12, no. 5, pp. 291-303, May 1976.

[26] C.C. Ghizoni, J.M. Ballantyne and C.L. Tang, "Theory of Optical Waveguide Distributed Feedback Lasers: A Green's Function Approach," IEEE J. Quant. Elect., vol. QE-13, no. 10, pp. 843-848, Oct. 1977.

[27] T.E. Rozzi and G.H. In't Veld, "Field and Network Analysis of Interacting Step Discontinuities in Planar Dielectric Waveguides," IEEE MTT-s Trans., vol. MTT-27, no. 4, pp. 303-309, April 1979.

[28] T.E. Rozzi, "Rigorous Analysis of the Step Discontinuity in a Planar Dielectric Waveguide," IEEE MTT-s Trans., vol. MTT-26, no. 10, pp. 738-346, Oct. 1978.

[29] C.Vassallo, "On a rigorous Calculation of the Efficiency for Coupling Light Power into Optical Waveguides," IEEE J. Quant. Elect., vol. QE-13, no. 4, pp. 165-173, April 1977.

[30] S-T Peng and A. A. Oliner, "Guidance and Leakage Properties of a Class of Open Dielectric Waveguides: Part I--Mathematical Formulations," IEEE MTT-s Trans., vol. MTT-29, no. 9, pp. 843-855, Sept. 1981.

[31] D. Marcuse, "The Coupling of Degenerate Modes in Two Parallel Dielectric Waveguides," BSTJ, vol. 50, no. 6, pp. 1791-1816, July-August 1971.

[32] L.O. Wilson and F.K. Reinhart, "Coupling of Nearly Degenerate Modes in Parallel Asymmetrical Dielectric Waveguides," BSTJ, vol. 53, no. 4, pp. 717-739, April 1974.

[33] E.F. Kuester and D.C. Chang, "Nondegenerate Surface Wave Mode Coupling between Dielectric Waveguides," IEEE MTT-s Trans., vol. MTT-23, no. 11, pp. 877-882, Nov. 1975.

[34] S.E. Miller, "Coupled Wave Theory and Waveguide Applications," BSTJ, vol. 33, no. 3, pp. 661-719, May 1954.

[35] A.W. Snyder, "Coupled-mode theory for Optical Fibers," JOSA, vol. 62, pp. 1267-1277, 1972.

[36] J.A. Arnaud, "Transverse Coupling in Fiber Optics-Part I: Coupling between Trapped Modes," BSTJ, vol. 53, 217-224, 1974.

[37] A.A. Oliner, S-T Peng, T-I Hsu, and A. Sanchez, "Guidance and Leakage Properties of a Class of Open Dielectric Waveguides: Part II--New Physical Effects," IEEE MTT-s Trans., vol. MTT-29, no. 9, pp. 855-869, Sept. 1981.

[38] R.F. Harrington, Time Harmonic Electromagnetic Fields, New York: McGraw-Hill, p. 347, 1961.

[39] A.L. Jones, "Wave Propagation in Optical Fibers," Ph.D. dissertation, Ann Arbor, Michigan: University Microfilms, 1964.

[40] Y. Rahmat-Sami, "On the Question of Computation of the Dyadic Green's Function at the Source Region in Waveguides and Cavities," IEEE MTT-s Trans., vol. MTT-23, no. 9, pp. 762-765, Sept. 1975.

[41] V.V. Shevchenko, Continuous Transition in Open Waveguides, Boulder, Colorado: Golem Press, pp. 22-48 and 93-116, 1971.

[42] D. Marcuse, Light Transmission Optics, Princenton: Van Nostrand Reinhold, 1972, Chapter 8.

[43] D.P. Nyquist, D.R. Johnson and S.V. Hsu, "Orthogonality and Amplitude Spectrum of Radiation Modes along Open-Boundary Waveguides," JOSA, vol. 71, no. 1, pp. 49-54, Jan. 1981.

[44] D. Marcuse, "Radiation Losses of Dominant Mode in Round Dielectric Waveguides," BSTJ, vol. 49, no. 8, pp. 1665-1693, Oct. 1970.

[45] R.F. Harrington, Time Harmonic Electromagnetic Fields, New York: McGraw-Hill, 1961, pp. 125-128.

[46] R.H.T. Bates and F.L. Ng, "Polarization-Source Formulation of Electromagnetism and Dielectric-loaded Waveguides," Proc. Inst. Elec. Eng., vol. 119, pp. 1568-1574, Nov. 1972.

[47] J. Van Bladel, "Some Remarks On Green's Dyadic for Infinite Space," IEEE AP-S Trans., vol. AP-9, no. 6, pp. 563-566, Nov. 1961.

[48] A.D. Yaghjian, "Electric Dyadic Green's Function in the Source Region," Proc. IEEE, vol. 68, no. 2, pp. 248-263, Feb. 1980.

[49] K.M. Chen, "A Simple Physical Picture of Tensor Green's Function in Source Region," Proc. IEEE, vol. 65, no. 8, pp. 1202-1204, Aug. 1977.

[50] R.F. Harrington, Field Computation by Moment Methods, New York: MacMillan, Chapter 1 and 7, 1968.

[51] R. Courant and D. Hilbert, Method of Methematical Physics, vol. 1, New York: Interscience Publishers, Chapter III, 1953.

[52] R.E. Collin, Field Theory of Guided Waves, New York: McGraw-Hill, pp. 25-27, 1960.

[53] R.F. Harrington, Time Harmonic Electromagnetic Fields, New York: McGraw-Hill, pp. 113, 1961.

[54] R.E. Collin and F.J. Zucker, Antenna Theory-Part I, New York: McGraw-Hill, pp. 41-43, 1969.

[55] I.S. Gradshteyn and I.M. Ryzhik, Table of Integral Series and Products, New York: Academic Press, 1965.

[56] J.A. Arnaud, Beam and Fiber Optics, New York: Academic Press, Chapter 3, 1976.

[57] D.R. Johnson, Integral-Operator Analysis of Open-Boundary Dielectric Waveguides, Ph.D. Dissertation, Michigan State University, p. 23, 1980.

[58] R.E. Collin, Field Theory of Guided Waves, New York: McGraw-Hill, p. 62, 1960.

[59] C.C. Johnson, Field and Wave Electrodynamics, New York: McGraw-Hill, p. 8, 1965.

[60] W.V. McLevige, T. Itoh, and R. Mittra, "New Waveguide Structures for Millimeter-Wave and Optical Integrated Circuits," IEEE MTT-s Trans., vol. MTT-23, no. 10, pp. 788-794, Oct. 1975.

APPENDICES

APPENDIX A

SLAB2 SOURCE LISTING

```
0001  FTN4
0002        PROGRAM SLAB2
0003        REAL N1,N2,N3,K0D,KPND,KPD
0004        COMPLEX RN,TN,DUMMY
0005        COMPLEX B0PD,C,BMB,BPB,RF,C4,AP,AM,R0,T0,ME,DIAG,DET,EY
0006        DIMENSION XN(32),ZN(32),ME(32,33),EY(35)
0007        DIMENSION GMND(2),KPND(2),BND(2),RN(2),TN(2)
0008        COMMON/NATEL/XN,ZN,KPD,B0D,N1,N2,N3,K0D,GMD,DXN,C2,DZN,E0,PI,NP,NX
0009       1,NZ,NPP1
0010        COMMON/SCAT0/Z0,Z0OD
0011        COMMON/SMODE/RN,TN,GMND,KPND,BND,MMOD
0012        COMMON ME
0013        PI=3.1415926536
0014        Z0=120.0*PI
0015        DPR=180.0/PI
0016  C ***************************************************************************
0017  C READ FIRST DATA CARD FOR REFRACTIVE INDICES (N1,N2,N3) OF CORE, CLADDING, AN
0018  C DISCONTINUITY REGIONS, RESPECTIVELY.
0019  C ***************************************************************************
0020        WRITE(1,61)
0021     61 FORMAT(10X,13HREAD N1,N2,N3)
0022        READ(1,*) N1,N2,N3
0023      1 FORMAT(3F10.3)
0024  C ***************************************************************************
0025  C READ SECOND DATA CARD FOR NORMALIZED SLAB THICKNESS DOL0 AND NORMALIZED
0026  C EIGENVALUE PARAMETERS (GMD,KPD,B0D) OF THE UNPERTURBED SLAB WAVEGUIDE.
0027  C ***************************************************************************
0028        WRITE(1,62)
0029     62 FORMAT(10X,21HREAD DOL0,GMD,KPD,B0D)
0030        READ(1,*) DOL0,GMD,KPD,B0D
0031      2 FORMAT(F15.2,3E15.8)
0032        K0D=2.0*PI*DOL0
0033  C ***************************************************************************
0034  C READ THIRD DATA CARD FOR NORMALIZED LENGTH Z0OD OF DISCONTINUITY REGION AND
0035  C AMPLITUDE E0 OF INCIDENT WAVE.
0036  C ***************************************************************************
0037        WRITE(1,63)
0038     63 FORMAT(10X,17HREAD Z0OD,E0,MMOD)
0039        READ(1,*) Z0OD,E0,MMOD
0040     3  FORMAT(F10.2,F10.1,I1)
0041  C ***************************************************************************
0042  C READ FOURTH DATA CARD FOR NUMBERS OF PARTITIONS (NX,NZ) ALONG X AND Z
0043  C DIRECTIONS, RESPECTIVELY.
0044  C ***************************************************************************
0045        WRITE(1,64)
0046     64 FORMAT(10X,10HREAD NX,NZ)
0047        READ(1,*) NX,NZ
0048      4 FORMAT(I2,3X,I2)
0049        NP=NX*NZ
0050        NPP1=NP+1
0051        DO 44 N=1,MMOD
0052        WRITE(1,65)
0053     65 FORMAT(10X,27HREAD GMND(N),KPND(N),BND(N))
0054        READ(1,*)  GMND(N),KPND(N),BND(N)
0055     41 FORMAT(3E15.8)
```

```
0056      44 CONTINUE
0057   C ********************************************************************************
0058   C PRINT ESSENTIAL INPUT DATA.
0059   C ********************************************************************************
0060         WRITE(6,5)
0061       5 FORMAT(1H1,//,10X,21HESSENTIAL INPUT DATA.,//)
0062         WRITE(6,6) N1,N2,N3
0063       6 FORMAT(1H0,///,10X,4HN1= ,F4.1,2X,23H(SLAB REFRACTIVE INDEX),/,10X
0064        1,4HN2= ,F4.1,2X,27H(CLADDING REFRACTIVE INDEX),/,10X,4HN3= ,F4.1,2
0065        2X,32H(DISCONTINUITY REFRACTIVE INDEX))
0066         WRITE(6,7) DOL0,GMD,KPD,B0D
0067       7 FORMAT(1H0,/,10X,6HD/L0= ,F5.2,2X,32H(NORMALIZED SLAB HALF THICKNE
0068        1SS),//,10X,5HGMD= ,E14.8,2X,38H(NORMALIZED CLADDING DECAY EIGENVAL
0069        2UE),/,10X,5HKPD= ,E14.8,2X,28H(NORMALIZED SLAB EIGENVALUE),/,10X,5
0070        3HB0D= ,E14.8,2X,38H(NORMALIZED PHASE-CONSTANT EIGENVALUE))
0071         WRITE(6,8) Z0OD,E0,MMOD
0072       8 FORMAT(1H0,/,10X,6HZ0/D= ,F5.2,2X,31H(RELATIVE DISCONTINUITY LENGT
0073        1H),//,10X,4HE0= ,F4.1,2X,5H(V/M),2X,25H(INCIDENT WAVE AMPLITUDE)//
0074        ,,10X,5HMMOD=,I1,2X,23H(NUMBER OF MODES EXIST))
0075         WRITE(6,9) NX,NZ
0076       9 FORMAT(1H0,/,10X,4HNX= ,I3,2X,20H(PARTITIONS ALONG X),/,10X,4HNZ=
0077        1,I3,2X,20H(PARTITIONS ALONG Z))
0078         DO 99 N=1,MMOD
0079         WRITE(6,91) N,GMND(N),KPND(N),BND(N)
0080      91 FORMAT(1H0,/,10X,2HN=,I1,2X,5HGMND=,F15.8,2X,5HKPND=,F15.8,2X,4HBN
0081        DD=,F15.8)
0082      99 CONTINUE
0083   C ********************************************************************************
0084   C CALCULATE AND PRINT THE APPROXIMATE, RADIATIONLESS SLAB FIELD AND REFLECTION
0085   C AND TRANSMISSION COEFFICIENTS.
0086   C ********************************************************************************
0087         C1=KPD+0.5*SIN(2.0*KPD)
0088         C2=(KPD/GMD)*(COS(KPD))**2+C1
0089         C3=B0D*B0D+(N3*N3-N1*N1)*K0D*K0D*C1/C2
0090         IF(C3) 10,11,11
0091      10 B0PD=CMPLX(0.0,-SQRT(-C3))
0092         GO TO 12
0093      11 B0PD=CMPLX(SQRT(C3),0.0)
0094      12 C=0.5*(N3*N3-N1*N1)*CMPLX(0.0,K0D*K0D/B0D)*C1/C2
0095         BMB=B0PD-B0D
0096         BPB=B0PD+B0D
0097         RF=BMB/BPB
0098         C4=1.0-RF*RF*CEXP(CMPLX(0.0,-4.0)*B0PD*Z0OD)
0099         AP=CMPLX(0.0,1.0)*BMB*E0*CEXP(CMPLX(0.0,-1.0)*BMB*Z0OD)/(C*C4)
0100         AM=AP*RF*CEXP(CMPLX(0.0,-2.0)*B0PD*Z0OD)
0101         R0=CMPLX(0.0,-2.0)*RF*CEXP(CMPLX(0.0,-1.0)*BPB*Z0OD)*(CSIN(BPB*Z0O
0102        1D)+CEXP(CMPLX(0.0,-2.0)*B0PD*Z0OD)*CSIN(BMB*Z0OD))/C4
0103         T0=(1.0-CMPLX(0.0,2.0)*CEXP(CMPLX(0.0,-1.0)*BMB*Z0OD)*(CSIN(BMB*Z0
0104        1OD)+RF*RF*CEXP(CMPLX(0.0,-2.0)*B0PD*Z0OD)*CSIN(BPB*Z0OD))/C4)*CEXP
0105        2(CMPLX(0.0,-2.0)*B0D*Z0OD)
0106         WRITE(6,13)
0107      13 FORMAT(1H1,/////,10X,89HRESULTS OF APPROXIMATE RADIATIONLESS SOLUT
0108        1ION FOR SLAB FIELD AND SCATTERING COEFFICIENTS.)
0109         WRITE(6,14) B0PD
0110      14 FORMAT(1H0,/////,20X,6HB0PD=(,E10.4,1H,,E10.4,1H))
```

```
0111          APM=CABS(AP)
0112          APP=DPR*ATAN2(AIMAG(AP),REAL(AP))
0113          AMM=CABS(AM)
0114          AMP=DPR*ATAN2(AIMAG(AM),REAL(AM))
0115          WRITE(6,15) APM,APP,AMM,AMP
0116       15 FORMAT(1H0,///,20X,3HAP=,E10.4,6HEXP(J*,E10.4,1H),//,20X,3HAM=,E10
0117         1.4,6HEXP(J*,E10.4,1H))
0118          R0M=CABS(R0)
0119          R0P=DPR*ATAN2(AIMAG(R0),REAL(R0))
0120          T0M=CABS(T0)
0121          T0P=DPR*ATAN2(AIMAG(T0),REAL(T0))
0122          WRITE(6,16) R0M,R0P,T0M,T0P
0123       16 FORMAT(1H0,///,20X,3HR0=,E10.4,6HEXP(J*,E10.4,1H),//,20X,3HT0=,E10
0124         1.4,6HEXP(J*,E10.4,1H))
0125     C ***************************************************************************
0126     C PARTITION THE DISCONTINUITY REGION USING NORMALIZED COORDINATE VARIABLES.
0127     C ***************************************************************************
0128          DXN=1.0/NX
0129          DZN=2.0*Z00D/NZ
0130          DO 17 I=1,NX,1
0131          XN(I)=(I-0.5)*DXN
0132       17 CONTINUE
0133          DO 18 J=1,NZ,1
0134          ZN(J)=-Z00D+(J-0.5)*DZN
0135       18 CONTINUE
0136     C ***************************************************************************
0137     C GENERATE THE ELEMENTS OF MOM MATRIX ME(M,N).
0138     C ***************************************************************************
0139          CALL MATEL(ME)
0140     C     WRITE (6,68) ME
0141     C  68 FORMAT(1H1,1X,7HME(M,N),/,163(13E10.3,/))
0142          DO 19 M=1,NP,1
0143          DIAG=ME(M,M)
0144     C     WRITE(6,71) M,M,DIAG
0145     C  71 FORMAT(1X,3HME(,I2,1H,,I2,2H)=,2E15.4)
0146          DO 19 N=1,NPP1,1
0147     C     WRITE(6,77) M,N,ME(M,N),M,M,DIAG
0148     C  77 FORMAT(1X,3HME(,I2,1H,,I2,2H)=,2E15.4,5X,5HDIAG(,I2,1H,,I2,2H)=,
0149     C    C2E15.4,/)
0150          DUMMY=ME(M,N)
0151          ME(M,N)=DUMMY/DIAG
0152     C     WRITE(6,78) ME(M,N)
0153     C  78 FORMAT(1X, 8HME/DIAG=,2E15.4,//)
0154       19 CONTINUE
0155     C     WRITE(6,69) ME
0156     C  69 FORMAT(1H1,1X,7HME/DIAG,/,163(13E10.3,/))
0157     C ***************************************************************************
0158     C SOLVE THE MATRIX EQUATION FOR THE EY(N) AND PRINT THE RESULTS.
0159     C ***************************************************************************
0160          CALL CMATP(-1,ME,NP,1,DET,1.0E-35)
0161     C     WRITE(6,70) ME
0162     C  70 FORMAT(1H1,1X,7HME(INV),/,163(13E10.3,/))
0163          DO 20 N=1,NP,1
0164          EY(N)=ME(N,NPP1)
0165       20 CONTINUE
```

```
0166          EYMAX=CABS(EY(1))
0167          DO 202 N=1,NP,1
0168          IF(CABS(EY(N))-EYMAX) 202,202,201
0169      201 EYMAX=CABS(EY(N))
0170      202 CONTINUE
0171          WRITE(6,21)
0172       21 FORMAT(1H1,/////,10X,77HRESULTS OF NUMERICAL MOM SOLUTION FOR SLAB
0173         1 FIELD AND SCATTERING COEFFICIENTS.)
0174          WRITE(6,211)
0175      211 FORMAT(1H0, 9X,46HPROGRAM WITH SYMMETRY AND MULTIMODE SCATTERING)
0176          WRITE(6,22)
0177       22 FORMAT(1H0,////,10X,50HINDUCED FIELD EY(X,Z) IN THE DISCONTINUITY
0178         1REGION.,/////,6X,1HI,6X,1HJ,6X,5HXN(I),6X,5HZN(J),6X,1HN,17X,5HEY(
0179         1N),19X,6HEYA(N),7X,6HEYP(N),//)
0180          DO 24 L=1,NZ,1
0181          DO 24 K=1,NX,1
0182          N=K+(L-1)*NX
0183          EYA=CABS(EY(N))/EYMAX
0184          REY=REAL(EY(N))
0185          AEY=AIMAG(EY(N))
0186          EYP=DPR*ATAN2(AEY,REY)
0187          WRITE(6,23) K,L,XN(K),ZN(L),N,EY(N),EYA,EYP
0188       23 FORMAT(5X,I2,5X,I2,5X,F6.3,5X,F6.3,5X,I3,5X,1H(,E11.5,1X,1H,,1X,E1
0189         11.5,1H),5X,E11.5,5X,F6.1)
0190       24 CONTINUE
0191      C ***************************************************************************
0192      C CALCULATE AND PRINT THE SCATTERING COEFFICIENTS RN AND TN.
0193      C ***************************************************************************
0194          WRITE(6,25)
0195       25 FORMAT(1H1,/////,10X,86HSCATTERING (REFLECTION AND TRANSMISSION) C
0196         1OEFFICIENTS DESCRIBING DISCONTINUITY REGION.)
0197          CALL SCATC(EY,RN,TN)
0198          DO 999 N=1,MMOD
0199          RNM=CABS(RN(N))
0200          ARN=AIMAG(RN(N))
0201          RRN=REAL(RN(N))
0202          RNP=DPR*ATAN2(ARN,RRN)
0203          TNM=CABS(TN(N))
0204          RTN=REAL(TN(N))
0205          ATN=AIMAG(TN(N))
0206          TNP=DPR*ATAN2(ATN,RTN)
0207          WRITE(6,26) N,RNM,RNP,TNM,TNP
0208       26 FORMAT(1H0,////,20X,2HN=,I1,2X,3HRN=,E10.4,6HEXP(J*,E10.4,1H),//,
0209         X25X,3HTN=,E10.4,6HEXP(J*,E10.4,1H))
0210      999 CONTINUE
0211          STOP
0212          END
```

```
FTN4 COMPILER: HP92060-16092 REV. 1901 (781201)

**  NO WARNINGS **  NO ERRORS **   PROGRAM = 02711       COMMON = 04224
```

```
0213          SUBROUTINE MATEL(ME)
0214          REAL N1,N2,N3,K0D,KPND,K2D,K2DME,K2DPE,K2DSQ,KPD
0215          COMPLEX ME,C6,C7,MED,MER,XCEXP,XMED,XMER
0216          DIMENSION ME(32,33),XN(32),ZN(32)
0217          COMMON/NATEL/XN,ZN,KPD,B0D,N1,N2,N3,K0D,GMD,DXN,C2,DZN,E0,PI,NP,NX
0218         1,NZ,NPP1
0219          COMMON/NER/K2D,VN,EPS,C8,K2DME,K2DPE,RHONM
0220          COMMON/FMATL/HDXN,HDZN,K2DSQ,VNSQ
0221          K2D=N2*K0D
0222          VN=SQRT(N1*N1-N2*N2)*K0D
0223          DZM=ZN(NZ)-ZN(1)
0224          EPS=K2D/10.0
0225          K2DME=K2D-EPS
0226          K2DPE=K2D+EPS
0227          RHONM=10.0*K2D
0228          C8=4.0*(N3*N3-N1*N1)*K0D*K0D/PI
0229          HDXN=DXN/2.0
0230          HDZN=DZN/2.0
0231          K2DSQ=K2D*K2D
0232          VNSQ=VN*VN
0233          DO 1 M=1,NP,1
0234          DO 1 N=1,NPP1,1
0235          ME(M,N)=CMPLX(0.0,0.0)
0236        1 CONTINUE
0237          DO 4 J=1,NZ,1
0238          DO 4 I=1,NX,1
0239          M=I+(J-1)*NX
0240          XNI=XN(I)
0241          ZNJ=ZN(J)
0242          XEY0=EY0(XNI,1)
0243          XCEXP=CEXP(CMPLX(0.0,-B0D*ZNJ))
0244          ME(M,NPP1)=E0*XEY0*XCEXP
0245          DO 4 L=1,NZ,1
0246          DO 4 K=1,NX,1
0247          N=K+(L-1)*NX
0248          XMED=MED(I,J,K,L)
0249          XMER=MER(I,J,K,L)
0250  C       GO TO 3
0251          IF(M-N) 3,2,3
0252        2 ME(M,N)=1.0+XMED+XMER
0253          GO TO 4
0254        3 ME(M,N)=XMED+XMER
0255        4 CONTINUE
0256          RETURN
0257          END

 FTN4 COMPILER: HP92060-16092 REV. 1901 (781201)

 **  NO WARNINGS **  NO ERRORS **   PROGRAM = 00371       COMMON = 00000
```

```
0258          COMPLEX FUNCTION MED(I,J,K,L)
0259          REAL N1,N2,N3,KPND,KPD,K0D
0260          COMPLEX RN,TN,C6,C7
0261          DIMENSION GMND(2),KPND(2),BND(2),RN(2),TN(2)
0262          DIMENSION XN(32),ZN(32)
0263          COMMON/NATEL/XN,ZN,KPD,B0D,N1,N2,N3,K0D,GMD,DXN,C2,DZN,E0,PI,NP,NX
0264         1,NZ,NPP1
0265          COMMON/SMODE/RN,TN,GMND,KPND,BND,MMOD
0266          MED=CMPLX(0.0,0.0)
0267          DO 99 N=1,MMOD
0268          XX=KPND(N)
0269          C1=XX+0.5*SIN(2.0*XX)
0270          C2=(XX/GMND(N))*(COS(XX))**2  +C1
0271          C5=4.0*(N3*N3-N1*N1)*(K0D*K0D/(BND(N)*BND(N)))*SIN(XX*DXN/2.0
0272         C)/C2
0273          C6=CMPLX(0.0,SIN(BND(N)*DZN/2.0))
0274          C7=1.0-CEXP(CMPLX(0.0,-BND(N)*DZN/2.0))
0275          XNI=XN(I)
0276          XNK=XN(K)
0277          ZNJ=ZN(J)
0278          ZNL=ZN(L)
0279          IF(J-L) 2,1,2
0280        1 MED=MED+C5*COS(XX*XNI)*COS(XX*XNK)*C7
0281          GO TO 99
0282        2 MED=MED+C5*COS(XX*XNI)*COS(XX*XNK)*C6*CEXP(CMPLX(0.0
0283         *,-BND(N)*ABS(ZNJ-ZNL)))
0284       99 CONTINUE
0285          RETURN
0286          END


 FTN4 COMPILER: HP92060-16092 REV. 1901 (781201)

 **  NO WARNINGS **  NO ERRORS **   PROGRAM = 00380      COMMON = 00000
```

```
0287          COMPLEX FUNCTION MER(I,J,K,L)
0288          REAL N1,N2,N3,K0D,KPD,K2D,K2DME,K2DPE,K2DSQ
0289          COMPLEX C10,I1,I2,I3
0290          DIMENSION XN(32),ZN(32)
0291          COMMON/NATEL/XN,ZN,KPD,B0D,N1,N2,N3,K0D,GMD,DXN,C2,DZN,E0,PI,NP,NX
0292         1,NZ,NPP1
0293          COMMON/FMATL/HDXN,HDZN,K2DSQ,VNSQ
0294          COMMON/NER/K2D,VN,EPS,C8,K2DME,K2DPE,RHONM
0295          COMMON/FMER/DZNJL,II,JJ,KK,LL
0296  C       MER=CMPLX(0.0,0.0)
0297  C       GO TO 10
0298       12 II=I
0299          JJ=J
0300          KK=K
0301          LL=L
0302          RHON=K2D
0303          SIGN=SQRT(VN*VN+RHON*RHON)
0304          C9=COS(SIGN*XN(I))*COS(SIGN*XN(K))*SIN(SIGN*HDXN)/((1.0+(VNSQ/(RHO
0305         1N*RHON))*SIN(SIGN)**2)*SIGN)
0306          C9X=(K2D-EPS)/(SQRT((K2D)**2-(K2D-EPS)**2))
0307          C10=PI/2.0-ATAN(C9X)+CMPLX(0.0,ACOSH(1.0+EPS/K2D))
0308          I2=CMPLX(0.0,HDZN)*C9*C10
0309          DZNJL=ABS(ZN(J)-ZN(L))
0310          CALL CSIMC(1,0.0,K2DME,0.10,20,I1,NOI1,R1)
0311          CALL CSIMC(1,K2DPE,RHONM,0.10,20,I3,NOI2,R2)
0312          MER=C8*(I1+I2+I3)
0313       10 RETURN
0314          END


 FTN4 COMPILER: HP92060-16092 REV. 1901 (781201)

 **  NO WARNINGS **  NO ERRORS **   PROGRAM = 00328      COMMON = 00000
```

```
0315          COMPLEX FUNCTION F(INDEX,RHON)
0316          REAL KPD,K2D,K2DSQ
0317          COMPLEX BTN,C11
0318          DIMENSION XN(32),ZN(32)
0319          COMMON/NATEL/XN,ZN,KPD,BOD
0320          COMMON/NER/K2D,VN
0321          COMMON/FMATL/HDXN,HDZN,K2DSQ,VNSQ
0322          COMMON/FMER/DZNJL,II,JJ,KK,LL
0323          IF(INDEX-1) 7,1,7
0324        1 RHONSQ=RHON*RHON
0325          SIGN=SQRT(VNSQ+RHONSQ)
0326          IF(RHON-K2D) 2,3,3
0327        2 BTN=CMPLX(SQRT(K2DSQ-RHONSQ),0.0)
0328          GO TO 4
0329        3 BTN=CMPLX(0.0,-SQRT(RHONSQ-K2DSQ))
0330        4 C11=RHONSQ*COS(SIGN*XN(II))*COS(SIGN*XN(KK))*SIN(SIGN*HDXN)/((RHON
0331         1SQ+VNSQ*SIN(SIGN)**2)*BTN*BTN*SIGN)
0332          IF(JJ-LL) 6,5,6
0333        5 F=C11*(1.0-CEXP(CMPLX(0.0,-1.0)*BTN*HDZN))
0334          GO TO 7
0335        6 F=C11*CMPLX(0.0,1.0)*CEXP(CMPLX(0.0,-1.0)*BTN*DZNJL)*CSIN(BTN*HDZN
0336         1)
0337        7 RETURN
0338          END


  FTN4 COMPILER: HP92060-16092 REV. 1901 (781201)

  **  NO WARNINGS **  NO ERRORS **   PROGRAM = 00322      COMMON = 00000
```

```
0339          SUBROUTINE SCATO(EY,RN,TN)
0340          REAL N1,N2,N3,K0D,KPND,EPD
0341          COMPLEX EY,RN,TN,EYSB,EYSF,XCEXP,YCEXP
0342          COMPLEX RR,TT
0343          COMPLEX RX,TX
0344          DIMENSION RX(2),TX(2)
0345          DIMENSION EY(35),XN(32),ZN(32)
0346          DIMENSION GMND(2),KPND(2),BND(2),RN(2),TN(2)
0347          COMMON/NATEL/XN,ZN,KPD,B0D,N1,N2,N3,K0D,GMD,DXN,DZN,E0,PI,NP,NX
0348         1,NZ,NPP1
0349          COMMON/SCATO/Z0,Z00D
0350          COMMON/SMODE/RX,TX,GMND,KPND,BND,MMOD
0351          DSN=DXN*DZN
0352          DO 99 J=1,MMOD
0353          XX=KPND(J)
0354          CC1=XX+.5*SIN(2.0*XX)
0355          CC2=(XX/GMND(J))*(COS(XX))**2+CC1
0356          BB=BND(J)
0357          AJ=SQRT(K0D*Z0*XX/(2.0*BB*CC2))
0358          IF(J.NE.1) GO TO 300
0359          A1=AJ
0360      300 CONTINUE
0361          EYSB=CMPLX(0.0,0.0)
0362          EYSF=CMPLX(0.0,0.0)
0363          DO 1 L=1,NZ,1
0364          DO 1 K=1,NX,1
0365          N=K+(L-1)*NX
0366          XEY0=EY0(XN(K),J)
0367          XCEXP=CEXP(CMPLX(0.0,-BND(J)*ZN(L)))
0368          EYSB=EYSB+EY(N)*XEY0*XCEXP*DSN
0369          YCEXP=CEXP(CMPLX(0.0,BND(J)*ZN(L)))
0370          EYSF=EYSF+EY(N)*XEY0*YCEXP*DSN
0371        1 CONTINUE
0372          EYSB=EYSB*2.0
0373          EYSF=EYSF*2.0
0374          C8=(N3*N3-N1*N1)*K0D/(Z0*E0)
0375          RR=CMPLX(0.0,-1.0)*C8*CEXP(CMPLX(0.0,-1.0*(B0D+BND(J))*Z00D))*EYSB
0376          RN(J)=RR*AJ/A1
0377          IF(J.NE.1) GO TO 100
0378          TT=CEXP(CMPLX(0.0,-1.0*(B0D+BND(J))*Z00D))*(1.0-CMPLX(0.0,1.0)*C8*
0379         *EYSF)
0380          GO TO 200
0381      100 TT=CEXP(CMPLX(0.0,-1.0*(B0D+BND(J))*Z00D))*(0.0-CMPLX(0.0,1.0)*C8*
0382         *EYSF)
0383      200 CONTINUE
0384          TN(J)=TT*AJ/A1
0385       99 CONTINUE
0386          RETURN
0387          END


 FTN4 COMPILER: HP92060-16092 REV. 1901 (781201)
```

```
0388          FUNCTION EY0(X,N)
0389          REAL N1,N2,N3,KPND,KPD,K0D,K2D,K2DME,K2DPE,K2DSQ
0390          COMPLEX RN,TN
0391          DIMENSION GMND(2),KPND(2),BND(2),RN(2),TN(2),XN(32),ZN(32)
0392          COMMON/SMODE/RN,TN,GMND,KPND,BND,MMOD
0393          COMMON/NATEL/XN,ZN,KPD,B0D,N1,N2,N3,K0D,GMD,DXN,CC,DZN,E0,PI,NP,NX
0394         1,NZ,NPP1
0395          COMMON/SCATO/Z0,Z00D
0396          XX=KPND(N)
0397          C1=XX+0.5*SIN(2.0*XX)
0398          C2=(XX/GMND(N))*(COS(XX))**2+C1
0399          B=BND(N)
0400          A=SQRT(K0D*Z0*XX/(2.0*B*C2))
0401          EY0=A*COS(XX*X)
0402          RETURN
0403          END
```

```
0404          FUNCTION ACOSH(X)
0405          ACOSH=ALOG(X+SQRT(X*X-1))
0406          RETURN
0407          END
```

```
  FTN4 COMPILER: HP92060-16092 REV. 1901 (781201)

  **  NO WARNINGS **  NO ERRORS **   PROGRAM = 00030       COMMON = 00000
```

```
0408          SUBROUTINE CMATP(IJOB,A,N,M,DET,EP)
0409          COMPLEX A,R,DET,CONST,S,CNST,Z,U,X
0410          DIMENSION A(32,33)
0411       30 FORMAT(1X,42HTHE DETERMINANT OF THE SYSTEM EQUALS ZERO./
0412         11X,36HTHE PROGRAM CANNOT HANDLE THIS CASE.//)
0413          DET=1.
0414          NP1=N+1
0415          NPM=N+M
0416          NM1=N-1
0417          IF(IJOB) 2,1,2
0418        1 DO 3 I=1,N
0419          NPI=N+I
0420          A(I,NPI)=1.
0421          IP1=I+1
0422          DO 3 J=IP1,N
0423          NPJ=N+J
0424          A(I,NPJ)=0.
0425        3 A(J,NPI)=0.
0426        2 DO 4 J=1,NM1
0427          C=CABS(A(J,J))
0428          JP1=J+1
0429          DO 5 I=JP1,N
0430          D=CABS(A(I,J))
0431          IF(C-D) 6,5,5
0432        6 DET=-DET
0433          DO 7 K=J,NPM
0434          B=A(I,K)
0435          A(I,K)=A(J,K)
0436        7 A(J,K)=B
0437          C=D
0438        5 CONTINUE
0439          IF(CABS(A(J,J))-EP) 14,15,15
0440       15 DO 4 I=JP1,N
0441          CONST=A(I,J)/A(J,J)
0442          DO 4 K=JP1,NPM
0443          CNST=CONST*A(J,K)
0444        4 A(I,K)=A(I,K)-CNST
0445          IF(CABS(A(N,N))-EP) 14,18,18
0446       14 DET=0.
0447          IF(IJOB) 16,16,17
0448   16     WRITE(6,30)
0449       17 RETURN
0450       18 DO 11 I=1,N
0451       11 DET=DET*A(I,I)
0452          IF(IJOB) 10,10,17
0453       10 DO 12 I=1,N
0454          K=N-I+1
0455          KP1=K+1
0456          DO 12 L=NP1,NPM
0457          S=0.
0458          IF(N-KP1) 22,19,19
0459       19 DO 13 J=KP1,N
0460          Z=S
0461       13 S=Z+A(K,J)*A(J,L)
0462    C  22 U=A(K,L)-S
0463    C     X=U/A(K,K)
0464    C     A(K,L)=X
0465       22 U=A(K,L)
0466          A(K,L)=(U-S)/A(K,K)
0467       12 CONTINUE
0468          RETURN
0469          END
```

FTN4 COMPILER: HP92060-16092 REV. 1901 (781201)

```
0470          SUBROUTINE CSIMC(INDEX,X1,XEND,TEST,LIM,AREA,NOI,R)
0471          COMPLEX ODD,EVEN,AREA1,ENDS,F,AREA
0472          NOI=0
0473          ODD=CMPLX(0.0,0.0)
0474          INT=1
0475          V=1.0
0476          EVEN=CMPLX(0.0,0.0)
0477          AREA1=CMPLX(0.0,0.0)
0478          ENDS=F(INDEX,X1)+F(INDEX,XEND)
0479        2 H=(XEND-X1)/V
0480          ODD=EVEN+ODD
0481          X=X1+H/2.
0482          EVEN=CMPLX(0.0,0.0)
0483          DO 3 I=1,INT
0484          EVEN=EVEN+F(INDEX,X)
0485          X=X+H
0486        3 CONTINUE
0487          AREA=(ENDS+4.0*EVEN+2.0*ODD)*H/6.0
0488          NOI=NOI+1
0489          R=CABS((AREA1-AREA)/AREA)
0490          IF(NOI-LIM) 31,32,32
0491       31 IF(R-TEST) 32,32,4
0492       32 RETURN
0493        4 AREA1=AREA
0494          INT=2*INT
0495          V=2.0*V
0496          GO TO 2
0497          END


0498          BLOCK DATA NATEL,SCATO,SMODE,NER,FMATL,FMER
0499          REAL N1,N2,N3,KPND,KPD,K0D,K2D,K2DME,K2DPE,K2DSQ
0500          COMPLEX RN,TN
0501          DIMENSION XN(32),ZN(32)
0502          DIMENSION GMND(2),KPND(2),BND(2),RN(2),TN(2)
0503          COMMON/NATEL/XN,ZN,KPD,B0D,N1,N2,N3,K0D,GMD,DXN,C2,DZN,E0,PI,NP,NX
0504         1,NZ,NPP1
0505          COMMON/SCATO/Z0,Z00D
0506          COMMON/SMODE/RN,TN,GMND,KPND,BND,MMOD
0507          COMMON/NER/K2D,VN,EPS,C8,K2DME,K2DPE,RHONM
0508          COMMON/FMATL/HDXN,HDZN,K2DSQ,VNSQ
0509          COMMON/FMER/DZNJL,II,JJ,KK,LL
0510          END

 FTN4 COMPILER: HP92060-16092 REV. 1901 (7B1201)

 **  NO WARNINGS **  NO ERRORS **

BLOCK COMMON NATEL   SIZE =  00156

BLOCK COMMON SCATO   SIZE =  00004

BLOCK COMMON SMODE   SIZE =  00029

BLOCK COMMON NER     SIZE =  00014

BLOCK COMMON FMATL   SIZE =  00008

BLOCK COMMON FMER    SIZE =  00006
```

```
FTN4,L
      SUBROUTINE PLOT(DATX,NS,KURVS,XSTART,XSTEP,XMAX,ISYM,MAN,XDATA,MV,
     *NPTS,INCRMT)
C*****************************************************************************
C*****************************************************************************
C*                                                                           *
C*                     X-Y PLOT SUBROUTINE                                   *
C*                                                                           *
C*****************************************************************************
C*****************************************************************************
C*                                                                           *
C*                                                                           *
C*                                                                           *
C*                                                                           *
C*                                                                           *
C*         SOURCE: SPLT2                                                     *
C*         RELOCATABLE: RPLT2                                                *
C*                                                                           *
C*    THIS IS A STANDARD FORTRAN X-Y PLOTTING SUBROUTINE. IT CAN             *
C*    SIMULTANEOUSLY PLOT 12 DIFFERENT CURVES (ONE IS A BLANK). THE          *
C*    X-AXIS CAN BE STARTED OR STOPPED AT ANY VALUE & INCREMENTED            *
C*    BY ANY AMOUNT. THE USER CAN ALSO SPECIFY WHAT INCREMENT THE            *
C*    X-AXIS VALUES ARE TO BE PRINTED. THE X-AXIS CAN BE SCALED BY           *
C*    ANY FUNCTION THE USER DESIRES, SUCH AS A LOG FUNCTION. X-AXIS          *
C*    SCALING IS DETERMINED BY THE MINIMUM AND MAXIMUM DATA VALUES OF        *
C*    THE FIRST CURVE TO BE PLOTTED. THE Y-AXIS CAN BE SCALED LARGER         *
C*    THAN THE MAXIMUM VALUE BY FILLING THE FIRST ARRAY WITH LARGE           *
C*    VALUES & PRINTING IT WITH BLANKS. IF THE X VALUE EQUALS THE Y          *
C*    VALUE THEN A $ SYMBOL IS PRINTED.                                      *
C*                                                                           *
C*****************************************************************************
C*                                                 *          *             *
C*                                                 * PRINTOUT * INTEGER     *
C*            ARGUMENT DEFINITION                  *  SYMBOL  *  DESIG.     *
C*                                                 *          *             *
C*****************************************************************************
C*                                                 *          *             *
C*    ARG1: ARRAY NAME WHERE CURVE DATA IS         *    0     *     1       *
C*          STORED                                 *          *             *
C*    ARG2: M DIMENSION OF ARRAY                   *    *     *     2       *
C*    ARG3: NUMBER OF CURVES TO BE PLOTTED         *    X     *     3       *
C*    ARG4: STARTING POINT OF THE X-AXIS           *    +     *     4       *
C*    ARG5: AMOUNT X SHOULD BE INCREMENTED         *    .     *     5       *
C*    ARG6: FINAL VALUE OF X                       *    A     *     6       *
C*    ARG7: ARRAY NAME IN WHICH SYMBOL DATA        *    D     *     7       *
C*          IS STORED IN                           *          *             *
C*    ARG8: INTEGER INDICATOR--0 TELLS PROGRAM     *    4     *     8       *
C*          TO GENERATE LINEAR X-AXIS, 1 TELLS     *          *             *
C*          PROGRAM THAT USER IS GENERATING        *          *             *
C*          THE AXIS                               *          *             *
C*    ARG9: ARRAY NAME WHERE USERS X-AXIS          *    0     *     9       *
C*          IS STORED (USE 0 IF ARG8=0)            *          *             *
C*    ARG10:VALUE TO WHICH ARG9 IS DIMENSIONED     *    #     *    10       *
C*          (USE 1 IF ARG8=0)                      *          *             *
C*    ARG11:NO. DATA POINTS TO BE PLOTTED IF       *    $     *    11       *
C*          ARG8=1, OTHERWISE 0                    *          *             *
C*    ARG12:INCREMENT IN WHICH X-AXIS VALUES       *  BLANK   *    12       *
C*          ARE TO BE PRINTED                      *          *             *
C*                                                 *          *             *
C*****************************************************************************
```

```
C*************************************************************************
      DIMENSION LINEA(101),LINEB(101),DATX(2,1),ISMBL(12),ISYM(12),IY(12
     *),XDATA(1)
      DATA IBLNK/1H /,IDT/1HI/,ISMBL/1HO,1H*,1HX,1H+,1H.,1HA,1HD,1H4,
     *1HQ,1H#,1H$,1H /,IABAR/1H:/
       DATA CENTR1/1.5/,CENTR2/51.5/,LINES/101*1H-/
      KOUNT=65
      WRITE(6,9)
      CALL EXEC(3,1106B,65)
      IAXIS=0
      AMAX = 0.0
      AMIN = 0.0
      XVAL = XSTART
      NO = 1
      IN = INCRMT + 1
      DO 6 N=1,12
6     IY(N) = 0
      LINEB(1) = IABAR
      LINEB(26) = IABAR
      LINEB(51) = IABAR
      LINEB(76) = IABAR
      LINEB(101) = IABAR
      DO 10 I=1,101
10    LINEA(I) = IBLNK
      NSTEPS = 1.0 + ((XMAX - XSTART) / XSTEP)
      IF(MAN.EQ.1) NSTEPS = NPTS
      DO 20 K=1,NSTEPS
      IF(DATX(1,K).GT.AMAX) AMAX = DATX(1,K)
      IF(DATX(1,K).LT.AMIN) AMIN = DATX(1,K)
20    CONTINUE
      IF(AMIN.LT.0.0) GO TO 30
      SCALE = 100./AMAX
      CENTR = CENTR1
      T1 = AMAX
      T2 = 0.75 * AMAX
      T3 = 0.5 * AMAX
      T4 = 0.25 * AMAX
      T5 = 0.0
      GO TO 60
30    AIMIN = -AMIN
      IF(AMAX.GT.AIMIN) GO TO 40
      IF(AMAX.EQ.0.0) GO TO 35
      SCALE = 50./AIMIN
      T1 = AIMIN
      T2 = 0.5 * AIMIN
      T3 = 0.0
      T4 = 0.5 * AMIN
      T5 = AMIN
      GO TO 50
35    SCALE = 100./AIMIN
      CENTR = 101.5
      T1 = 0.0
      T2 = 0.25 * AMIN
      T3 = 0.5  * AMIN
      T4 = 0.75 * AMIN
      T5 = AMIN
      GO TO 60
40    SCALE = 50./AMAX
      T1 = AMAX
      T2 = 0.5 * AMAX
```

```
      T3 = 0.0
      T4 = 0.5 * (-AMAX)
      T5 = -AMAX
50    CENTR = CENTR2
60    VARX = XSTART
      ICNTR = CENTR
      DO 110 J=1,NSTEPS
      KOUNT=KOUNT+1
      IAX=0
      IF(MAN.EQ.1)VARX=XDATA(J)
      LINEA(ICNTR) = IDT
      Y = -XSTEP
      IF(KOUNT.NE.66)GO TO 80
75    IAX=1
      IF(KOUNT.EQ.66)KOUNT=0
      IAX=1
5     FORMAT("*",4X,F10.2,4(15X,F10.2))
      DO 70 M=1,101
70    LINEA(M) = LINEB(M)
80    DO 81 L=1,KURVS
      IY(L)  = (DATX(L,J)*SCALE)+CENTR
      LINEA(IY(L)) = ISMBL(ISYM(L))
81    CONTINUE
      DO 83 M=1,KURVS
      DO 82 N=1,KURVS
82    IF(((IY(M).EQ.IY(N)).AND.(M.NE.N)).AND.( .NOT.((ISYM(N).EQ.12)
     *.OR.(ISYM(M).EQ.12)))) LINEA(IY(M)) = ISMBL(11)
83    CONTINUE
      IF(NO.EQ.1) GO TO 95
      WRITE(6,7) LINEA
      IF(IAX.EQ.1)WRITE(6,5)T5,T4,T3,T2,T1
7     FORMAT(10X,101A1)
4     FORMAT(10X,101A1,5X,F15.4)
95    IF(MAN.EQ.1)XVAL=XDATA(J)
      IF(MAN.NE.1) VARX = VARX + XSTEP
      IF(NO.NE.1) GO TO 105
      WRITE(6,4) LINEA,XVAL
      IF(IAX.EQ.1)WRITE(6,5)T5,T4,T3,T2,T1
105   NO = NO + 1
      IF((VARX.GT.(XSTEP*0.25)).OR.(VARX.LT.(Y*.25)))GO TO 106
106   IF(NO.EQ.IN)NO=1
      IF(MAN.NE.1) XVAL = XVAL + XSTEP
      DO 90 M=1,101
90    LINEA(M) = IBLNK
110   CONTINUE
      DO 107 M=1,101
107   LINEA(M)=LINEB(M)
      WRITE(6,4)LINEA
      WRITE(6,5)T5,T4,T3,T2,T1
120   WRITE(6,9)
9     FORMAT("1")
      CALL EXEC(3,11068,64)
130   RETURN
      END
      END$
```

APPENDIX B

SLAB2 OUTPUT SAMPLE

```
ESSENTIAL INPUT DATA.


N1= 1.6  (SLAB REFRACTIVE INDEX)
N2= 1.0  (CLADDING REFRACTIVE INDEX)
N3= 3.0  (DISCONTINUITY REFRACTIVE INDEX)

D/L0=  .50  (NORMALIZED SLAB HALF THICKNESS)

GMD= .37203240E+01  (NORMALIZED CLADDING DECAY EIGENVALUE)
KPD= .12473061E+01  (NORMALIZED SLAB EIGENVALUE)
B0D= .48693342E+01  (NORMALIZED PHASE-CONSTANT EIGENVALUE)

Z0/D=  .08  (RELATIVE DISCONTINUITY LENGTH)

E0= 1.0  (V/M)  (INCIDENT WAVE AMPLITUDE)

MMOD=2  (NUMBER OF MODES EXIST)

NX=  4  (PARTITIONS ALONG X)
NZ=  8  (PARTITIONS ALONG Z)

N=1  GMND=    3.72032400  KPND=    1.24730610  BND=    4.86933420

N=2  GMND=    1.62902900  KPND=    3.56971310  BND=    3.53883310
```

RESULTS OF APPROXIMATE RADIATIONLESS SOLUTION FOR SLAB FIELD AND SCATTERING COEFFICIENTS.

BOPD=(.9269E+01, .0000E+00)

AP= .6313E+00EXP(J*-.2070E+02)

AM= .1964E+00EXP(J*-.1004E+03)

RO= .5611E+00EXP(J*-.1715E+03)

TO= .8277E+00EXP(J*-.8146E+02)

RESULTS OF NUMERICAL MOM SOLUTION FOR SLAB FIELD AND SCATTERING COEFFICIENTS.

PROGRAM WITH SYMMETRY AND MULTIMODE SCATTERING

INDUCED FIELD EY(X,Z) IN THE DISCONTINUITY REGION.

I	J	XN(I)	ZN(J)	N	EY(N)	EYA(N)	EYP(N)
1	1	.125	-.066	1	(.55812E+01 , .14754E+01)	.71878E+00	14.8
2	1	.375	-.066	2	(.30470E+01 , -.12984E+01)	.41239E+00	-23.1
3	1	.625	-.066	3	(.21479E+01 , -.11598E+01)	.30392E+00	-28.4
4	1	.875	-.066	4	(.29957E+01 , .18170E+01)	.43623E+00	31.2
1	2	.125	-.047	5	(.60585E+01 , .30208E+00)	.75527E+00	2.9
2	2	.375	-.047	6	(.33614E+01 , -.25116E+01)	.52245E+00	-36.8
3	2	.625	-.047	7	(.23911E+01 , -.21229E+01)	.39812E+00	-41.6
4	2	.875	-.047	8	(.32602E+01 , .13477E+01)	.43924E+00	22.5
1	3	.125	-.028	9	(.63681E+01 , -.85719E+00)	.80003E+00	-7.7
2	3	.375	-.028	10	(.35512E+01 , -.36653E+01)	.63543E+00	-45.9
3	3	.625	-.028	11	(.25461E+01 , -.30431E+01)	.49402E+00	-50.1
4	3	.875	-.028	12	(.34382E+01 , .84815E+00)	.44092E+00	13.9
1	4	.125	-.009	13	(.65715E+01 , -.20382E+01)	.85667E+00	-17.2
2	4	.375	-.009	14	(.36328E+01 , -.47465E+01)	.74421E+00	-52.6
3	4	.625	-.009	15	(.26078E+01 , -.38931E+01)	.58342E+00	-56.2
4	4	.875	-.009	16	(.36511E+01 , .19691E+00)	.45526E+00	3.1
1	5	.125	.009	17	(.65197E+01 , -.30952E+01)	.89860E+00	-25.4
2	5	.375	.009	18	(.35867E+01 , -.57050E+01)	.83904E+00	-57.8
3	5	.625	.009	19	(.25728E+01 , -.46482E+01)	.66148E+00	-61.0
4	5	.875	.009	20	(.36289E+01 , -.30868E+00)	.45346E+00	-4.9
1	6	.125	.028	21	(.62106E+01 , -.40789E+01)	.92513E+00	-33.3
2	6	.375	.028	22	(.34143E+01 , -.65113E+01)	.91541E+00	-62.3
3	6	.625	.028	23	(.24422E+01 , -.52854E+01)	.72494E+00	-65.2
4	6	.875	.028	24	(.33644E+01 , -.81147E+00)	.43091E+00	-13.6
1	7	.125	.047	25	(.58055E+01 , -.48630E+01)	.94292E+00	-40.0
2	7	.375	.047	26	(.31390E+01 , -.71356E+01)	.97861E+00	-66.3
3	7	.625	.047	27	(.22213E+01 , -.57864E+01)	.77172E+00	-69.0
4	7	.875	.047	28	(.31475E+01 , -.12040E+01)	.41958E+00	-20.9
1	8	.125	.066	29	(.52403E+01 , -.54785E+01)	.94393E+00	-46.3
2	8	.375	.066	30	(.27464E+01 , -.75474E+01)	.10000E+01	-70.0
3	8	.625	.066	31	(.19173E+01 , -.61364E+01)	.80046E+00	-72.6
4	8	.875	.066	32	(.28481E+01 , -.15337E+01)	.40277E+00	-28.3

SCATTERING (REFLECTION AND TRANSMISSION) COEFFICIENTS DESCRIBING DISCONTINUITY REGION.

N=1 RN= .5562E+00EXP(J*-.1728E+03)

TN= .8149E+00EXP(J*-.8109E+02)

N=2 RN= .6860E-01EXP(J*-.1559E+03)

TN= .7356E-01EXP(J*-.1540E+03)

APPENDIX C

OSWDSC SOURCE LISTING

```
1=C################################################################
2=C# THIS PROGRAM CALCULATE DISCONTINUITY FIELD BY ITERATIVE SOLUTION  #
3=C################################################################
4=      PROGRAM OSWDSC(TAPE1,INPUT,OUTPUT,TAPE5=INPUT,TAPE2=OUTPUT)
5=      REAL N1,N2,N3,KOD,KPD,K2D,K2DSQ,K2DME,K2DPE
6=      COMPLEX A1,C,D,I1,I2,I3,EL,EL1,EI,GEL
7=      DIMENSION C(4096),D(4096),EL1(8,8),EL(8,8),EI(8,8)
8=      DIMENSION ERR(8,8)
9=      DIMENSION XM(8),ZN(8),XI(8),ZJ(8)
10=      COMMON/F/C1K2,VNSQ,KPD,K2D,K2DSQ,XM,ZN,XI,ZJ,M,N,I,J
11=
12=C ##############################################################
13=C READ FIRST DATA LINE FOR REFRACTIVE INDICES (N1,N2,N3) OF CORE, CLADDI
14=C DISCONTINUITY REGIONS, RESPECTIVELY.
15=C ##############################################################
16=      READ (1,1) N1,N2,N3
17=    1 FORMAT(3F10.3)
18=C ##############################################################
19=C READ SECOND DATA LINE FOR NORMALIZED SLAB THICKNESS DOLO AND NORMALIZE
20=C EIGENVALUE PARAMETERS (GMD,KPD,BOD) OF THE UNPERTURBED SLAB WAVEGUIDE.
21=C ##############################################################
22=      READ (1,2) DOLO,GMD,KPD,BOD
23=    2 FORMAT(F15.2,3E15.8)
24=C ##############################################################
25=C READ THIRD DATA LINE FOR NORMALIZED LENGTH ZOOD OF DISCONTINUITY REGIO
26=C AMPLITUDE E0 OF INCIDENT WAVE.
27=C ##############################################################
28=      READ (1,3) ZOOD,E0
29=    3 FORMAT(F10.2,F10.1)
30=C ##############################################################
31=C READ FOURTH DATA LINE FOR NUMBERS OF PARTITIONS (NX,NZ) ALONG X AND Z
32=C DIRECTIONS, RESPECTIVELY.
33=C ##############################################################
34=      READ (1,4) NX,NZ
35=    4 FORMAT(I2,3X,I2)
36=C ##############################################################
37=C PRINT ESSENTIAL INPUT DATA.
38=C ##############################################################
39=      WRITE(2,5)
40=    5 FORMAT(1H1,//,10X,21HESSENTIAL INPUT DATA.,//)
41=      WRITE(2,6) N1,N2,N3
42=    6 FORMAT(1HO,///,10X,4HN1= ,F4.1,2X,23H(SLAB REFRACTIVE INDEX),/,10X
43=     1,4HN2= ,F4.1,2X,27H(CLADDING REFRACTIVE INDEX),/,10X,4HN3= ,F4.1,2
44=     2X,32H(DISCONTINUITY REFRACTIVE INDEX))
45=      WRITE(2,7) DOLO,GMD,KPD,BOD
46=    7 FORMAT(1HO,/,10X,6HD/LO= ,F5.2,2X,32H(NORMALIZED SLAB HALF THICKNE
47=     +SS),//,10X,5HGMD= ,E14.8,2X,38H(NORMALIZED CLADDING DECAY EIGENVAL
```

```
48=     2UE),/,10X,5HKPD= ,E14.8,2X,28H(NORMALIZED SLAB EIGENVALUE),/,10X,5
49=     3HBOD= ,E14.8,2X,38H(NORMALIZED PHASE-CONSTANT EIGENVALUE))
50=      WRITE(2,8) ZOOD,E0
51=    8 FORMAT(1H0,/,10X,6HZO/D= ,F5.2,2X,31H(RELATIVE DISCONTINUITY LENGT
52=     1H),//,10X,4HE0= ,F4.1,2X,5H(V/M),2X,25H(INCIDENT WAVE AMPLITUDE))
53=      WRITE(2,9) NX,NZ
54=    9 FORMAT(1H0,/,10X,4HNX= ,I3,2X,20H(PARTITIONS ALONG X),/,10X,4HNZ=
55=     1,I3,2X,20H(PARTITIONS ALONG Z))
56=C ##########################################################
57=C PARTITION THE DISCONTINUITY REGION USING NORMALIZED COORDINATE VARIABL
58=C ##########################################################
59=16    CONTINUE
60=      PI=3.1415926536
61=      ZO=120.0*PI
62=      KOD=2.0*PI*DOLO
63=      NXH=NX/2
64=      DXN=2.0/NX
65=      DZN=2.0*ZOOD/NZ
66=      DO 17 N=1,NX,1
67=      XN(N)=-1.0+(N-0.5)*DXN
69=      I=N
69=      XI(I)=XN(N)
70=   17 CONTINUE
71=      DO 18 N=1,NZ,1
72=      ZN(N)=-ZOOD+(N-0.5)*DZN
73=      J=N
74=      ZJ(J)=ZN(N)
75=   18 CONTINUE
76=C ######################################################
77=C        DEFINE FREQUENTLY USED CONSTANTS                #
78=C ######################################################
79=      DNSQ=N1**2-N2**2
80=      K2D=N2*KOD
81=      K2DSQ=K2D**2
82=      VNSQ=DNSQ*KOD**2
83=      SGMN=SQRT(VNSQ+K2DSQ)
84=      RHONM=10.0*K2D
85=      EPS=K2D/10.0
86=      K2DME=K2D-EPS
87=      K2DPE=K2D+EPS
88=      TER=0.0
89=      L=0
90=C ######################################################
91=C        DEFINE CONSTANT COEFFICIENTS                    #
92=C ######################################################
93=      A=COS(KPD)*COS(KPD)/6ND+SIN(2*KPD)/(2*KPD)+1
94=      A=A*2*BOD
95=      A=SQRT(KOD*ZO/A)
96=      A1=CMPLX(0.0,-1.0)*(KOD/ZO)*A**2*DNSQ*DXN*DZN
97=      C1K2=1+(VNSQ/K2DSQ)*(SIN(SGMN))**2
```

```
98=C ##################################################
99=C       CALCULATE GREEN'S FUNCTION FOR ALL CELLS      #
100=C ##################################################
101=      DO 60 M=1,MX
102=      DO 60 N=1,MZ
103=      DO 50 I=1,MX
104=      DO 50 J=1,MZ
105=      L=L+1
106=C ##################################
107=C  CALCULATE DISCRETE CONTRIBUTIONS  #
108=C ##################################
109=      B(L)=A1*COS(KPB*XI(I))*CEXP(CMPLX(0.0,-1.0)*BOB*ABS(ZN(N)-
110=     -ZJ(J)))
111=C ##################################
112=C  CALCULATE CONTINUOUS CONTRIBUTIONS #
113=C ##################################
114=      CALL CSIMCON(1,0.0,K2BME,0.10,20,I1,MOI1,R1)
115=      CALL CSIMCON(1,K2BPE,RHOMM,0.10,20,I3,MOI3,R3)
116=      I2=COS(SGMM*XI(I))*COS(SGMM*XN(M))/C1K2
117=      I2=I2*(PI/2.0-ASIN(1-EPS/K2B)+CMPLX(0.0,1.0)*ACOSH(1+EPS/K2B)-
118=     +2*CMPLX(0.0,1.0)*ABS(ZN(N)-ZJ(J))*EPS)
119=      C(L)=CMPLX(0.0,-1.0)*(KOB/(2*PI))*BMSQ*(I1+I2+I3)*BXM*BZM*KOB
120=50    CONTINUE
121=      EI(M,N)=EQ*A*COS(KPB*XN(N))*CEXP(CMPLX(0.0,-1.0)*BOB*ZN(N))
122=      EL(M,N)=CMPLX(.657,-.46)*CEXP(CMPLX(.0,-2.423*ZN(N)))
123=      EL(M,N)=EL(M,N)+CMPLX(-.4,.02)*CEXP(CMPLX(.0,2.423*ZN(N)))
124=C ##########################################################
125=C#      USE APPROXIMATED FIELD EL(M,N) AS 0TH ITERATIVE TOTAL FIELD
126=C##########################################################
127=C     EL(M,N)=EI(M,N)
128=60    CONTINUE
129=      PRINT *,' '
130=      PRINT *,' '
131=      PRINT *,'          SUCCESSIVE ITERATION ERRORS: '
132=      K=0
133=70    K=K+1
134=      TER=0.0
135=      TELMM=0.0
136=      L=0
137=      DO 110 M=1,MX
138=      DO 110 N=1,MZ
139=      GEL=CMPLX(0.0,0.0)
140=      DO 100 I=1,MX
141=      DO 100 J=1,MZ
142=      L=L+1
143=      GEL=GEL+(B(L)+C(L))*EL(I,J)
144=
145=100   CONTINUE
146=      EL1(M,N)=EI(M,N)+GEL
147=      ERR(M,N)=(CABS(EL1(M,N)))**2-(CABS(EL(M,N)))**2
148=      ERR(M,N)=ABS(ERR(M,N))
149=      ERR(M,N)=SQRT(ERR(M,N))
150=      TELMM=TELMM+CABS(EL(M,N))
```

```
150=      TELMN=TELMN+CABS(EL(M,N))
151=      TER=TER+ERR(M,N)
152=      PCHG=TER*100/TELMN
153=      EL(M,N)=EL1(M,N)
154=110   CONTINUE
155=
156=      IF (K.GT.2) GO TO 115
157=      PRINT *, ' '
158=      PRINT *,'          ',K,' TH ITERATION ERROR = ',TER
159=      PRINT *,'          PERCENTAGE ERROR IS: ',PCHG
160=115   CONTINUE
161=      IF (PCHG -1.0) 120,120,70
162=120   PRINT *, ' '
163=      PRINT *, '          CONVERGE TO .01 ERROR AFTER ',K,' ITERATIONS.'
164=      PRINT *,' '
165=      PRINT *,'          CONVERGED DISCONTINUITY FIELDS: '
166=      PRINT *,' '
167=      EYMAX=CABS(EL(1,1))
168=      DO 124 M=1,MXM
169=      DO 124 N=1,MZ
170=      IF (CABS(EL(M,N))-EYMAX) 124,124,122
171=122   EYMAX=CABS(EL(M,N))
172=124   CONTINUE
173=      DO 128 M=1,MXM
174=      DO 128 N=1,MZ
175=      EY=CABS(EL(M,N))/EYMAX
176=      WRITE(2,22) M,N,EY
177=22    FORMAT(1HO,10X,3HEY(,I1,1H,,I1,3H)= ,F7.4)
178=128   CONTINUE
179=C*****************************************************************
180=C*       INTERACTIVE ITERATION INPUTS                             *
181=C*****************************************************************
182=      PRINT *,' '
183=      PRINT *,'DOLO=?,ZOOD=?,QUIT=0 OR CONTINUE=1....  '
184=      READ (5,*)  DOL,ZOOD,KK
185=      IF(KK.EQ.0) GO TO 200
186=      IF(DOL.EQ.DOLO) GO TO 130
187=      DOLO=DOL
188=      PRINT *,'GMD=?,KPD=?,BOD=?'
189=      PRINT *,' '
190=      READ (5,*) GMD,KPD,BOD
191=      PRINT *,'          GMD=',GMD
192=      PRINT *,'          KPD=',KPD
193=      PRINT *,'          BOD=',BOD
194=130   CONTINUE
195=      PRINT *,' '
196=      PRINT *,'          DOLO=',DOLO
197=      PRINT *,'          ZOOD=',ZOOD
198=      GO TO 16
199=200   END
```

```
      COMPLEX FUNCTION F(INDEX,RHON)
      TYPE REAL KPD,K2D,K2DSQ
      TYPE COMPLEX BTN
      DIMENSION XN(8),ZN(8),XI(8),ZJ(8)
      COMMON/F/C1K2,VNSQ,KPD,K2D,K2DSQ,XN,ZN,XI,ZJ,M,N,I,J
      IF(INDEX-1) 7,1,7
    1 RHONSQ=RHON*RHON
      SIGN=SQRT(VNSQ+RHONSQ)
      C1=RHONSQ+VNSQ*(SIN(SIGN))**2
      C1=RHONSQ/C1
      IF(RHON-K2D) 2,3,3
    2 BTN=CMPLX(SQRT(K2DSQ-RHONSQ),0.0)
      GO TO 4
    3 BTN=CMPLX(0.0,-SQRT(RHONSQ-K2DSQ))
    4 F=COS(SIGN*XI(I))*COS(SIGN*XN(N))
      F=F*CEXP(CMPLX(0.0,-1.0)*BTN*ABS(ZN(N)-ZJ(J)))/(BTN)
      F=F*C1
    7 RETURN
      END

      FUNCTION ACOSH(X)
      ACOSH=ALOG(X+SQRT(X*X-1))
      RETURN
      END

      SUBROUTINE CSIMCON(INDEX,X1,XEND,TEST,LIM,AREA,NOI,R)
      TYPE COMPLEX ODD,EVEN,AREA1,ENDS,F,AREA
      NOI=0
      ODD=CMPLX(0.0,0.0)
      INT=1
      V=1.0
      EVEN=CMPLX(0.0,0.0)
      AREA1=CMPLX(0.0,0.0)
      ENDS=F(INDEX,X1)+F(INDEX,XEND)
    2 H=(XEND-X1)/V
      ODD=EVEN+ODD
      X=X1+H/2.
      EVEN=CMPLX(0.0,0.0)
      DO 3 I=1,INT
      EVEN=EVEN+F(INDEX,X)
      X=X+H
    3 CONTINUE
      AREA=(ENDS+4.0*EVEN+2.0*ODD)*H/6.0
      NOI=NOI+1
      R=CABS((AREA1-AREA)/AREA)
      IF(NOI-LIM) 31,32,32
   31 IF(R-TEST) 32,32,4
   32 RETURN
    4 AREA1=AREA
      INT=2*INT
      V=2.0*V
      GO TO 2
      END
```

APPENDIX D OSWDSC SAMPLE OUTPUT

```
ESSENTIAL INPUT DATA.
N1= 1.6  (SLAB REFRACTIVE INDEX)
N2= 1.0  (CLADDING REFRACTIVE INDEX)
N3= 3.0  (DISCONTINUITY REFRACTIVE INDEX)

D/LO=  .15  (NORMALIZED SLAB HALF THICKNESS)

GND= .85349900E+00  (NORMALIZED CLADDING DECAY EIGENVALUE)
KPD= .81069800E+00  (NORMALIZED SLAB EIGENVALUE)


BOD= .12715050E+01  (NORMALIZED PHASE-CONSTANT EIGENVALUE)

ZO/D=  .10  (RELATIVE DISCONTINUITY LENGTH)

EO= 1.0  (V/M)  (INCIDENT WAVE AMPLITUDE)

NX=  4  (PARTITIONS ALONG X)
NZ=  8  (PARTITIONS ALONG Z)


 SUCCESSIVE ITERATION ERRORS:

 1 TH ITERATION ERROR = 231.7218972309
 PERCENTAGE ERROR IS: 1386.83584294

 2 TH ITERATION ERROR = 28.75023329532
 PERCENTAGE ERROR IS: 12.37396458678

 CONVERGE TO .01 ERROR AFTER 4 ITERATIONS.

 CONVERGED DISCONTINUITY FIELDS:

 EY(1,1)=  .8021
 EY(1,2)=  .8077
 EY(1,3)=  .8124
 EY(1,4)=  .8164
 EY(1,5)=  .8193
 EY(1,6)=  .8212
 EY(1,7)=  .8223
 EY(1,8)=  .8225
 EY(2,1)=  .9775
 EY(2,2)=  .9834
 EY(2,3)=  .9884
 EY(2,4)=  .9926
 EY(2,5)=  .9959
 EY(2,6)=  .9981
 EY(2,7)=  .9995
 EY(2,8)= 1.0000

DOLO=?,ZOOD=?,QUIT=0 OR CONTINUE=1....0.,0.,0
```